ADVANCED ANIONIC DOPANTS FOR POLYPYRROLE BASED ELECTROCHEMICAL SUPERCAPACITORS

By

Yeling Zhu, B. Eng.

A Thesis

Submitted to the School of Graduate Studies

In Partial Fulfillment of the Requirements

For the Degree

Master of Applied Science

McMaster University

MASTER OF APPLIED SCIENCE (2014) McMaster University

(Materials Science and Engineering) Hamilton, Ontario

TITLE: Advanced Anionic Dopants for Polypyrrole Based Electrochemical Supercapacitors

AUTHOR: Yeling Zhu, B, Eng. (Zhejiang University, China)

SUPERVISOR: Dr. Igor Zhitomirsky

NUMBER OF PAGES: XIII, 120

Abstract

Electrochemical Supercapacitors (ES), also known as Supercapacitor or Ultracapacitor, has been regarded as an advanced electrical energy storage device for decades. Fabrication of advanced electrode materials is of critical importance for advanced ES. Among various materials used for ES electrode, polypyrrole (PPy) is found to be a promising material due to high specific capacitance, good electrical conductivity, low cost and ease of processing. The use of advanced anionic dopants and addition of multiwall carbon nanotube (MWCNT) have been proved an .effective approach towards advanced PPy based ES with improved electrochemical behaviors.

In this research, chemical polymerization of PPy powders and PPy/MWCNT composite materials have been successfully accomplished in presence of advanced anionic dopants, including chromotrope families, amaranth, pyrocatechol violet, eriochrome cyanine R and acid fuchsin. The influence of polyaromatic dopants with different molecular size, charges and charge to mass ratios on the microstructure and electrochemical characteristics has been discussed. PPy coated MWCNT with uniform microstructures was successfully achieved in simple chemical methods.

The results showed PPy powders with enhanced microstructures and electrochemical behaviors can be obtained by using such advanced anionic dopants. Multi-charged polyaromatic dopants with larger molecular size benefitted PPy powders with smaller particle size, improved specific capacitance, and enhanced cycling stability, at high electrode mass loadings. Moreover, advanced aromatic dispersant and chemical synthesis was proved a simple and effective method for fabrication of PPy/MWCNT composite materials at different PPy/MWCNT mass ratio, among which the powder with PPy/MWCNT mass ratio of 7:3 showed optimum electrochemical

performance. Last but not the least, the use of advanced high porosity current collector (Ni foam) allowed high electrode mass loading and good electric conductivity. As a result, advanced PPy/MWCNT composite materials which allows improved electrochemical behaviors, especially at high mass loading, are promising electrode materials for ES.

Acknowledgement

I hereby express my deepest gratitude to Professor Igor Zhitomirsky for his intellectual guidance and continuous encouragement. I have most appreciated the stimulating and enthusiastic environment Professor Zhitomirsky provides in my way towards the nature of science. I hope Professor Zhitomirsky continue with great success in the future.

I am grateful to my committee members for their constructive criticism which helps form ideas for further investigations.

I thank Yaohui Wang and Yanchao Sun, who have offered me great help in the electrochemical supercapacitor technologies at the beginning of my research.

To my group mates, Yisong Su, Shilei Chen, Mustafa Ata, Kaiyuan Shi and Yangshuai Liu, I extend my thanks for all your help and support. It is fortunate for me to share the unforgettable two years with you all.

I am grateful for all the help received from the Canadian Centre for Electron Microscopy. I would not have completed this research without the excellent support of the faculty and technical staff.

Finally, I thank my parents for instilling in me the pleasure of discovery for the arts of life and science.

Table of Contents

List of Figures

List of Tables

1 Introduction

Electrochemical Supercapcitor (ES), often called Supercapacitor or Ultracapacitor [1], has been investigated as an advanced energy storage device for decades. The energy storage in ES arises from an electric double layer or reversible redox reaction at the electrode/electrolyte interface. Because of high surface area of specific materials and electric double layer, ES has high power density and high energy density. Compared to normal batteries, the relatively unchanged electrode of ES in charge/discharge cycle (C-D cycle) gives excellent effective cycle life. Electrochemical properties of ES are determined by electrode, electrolyte, etc., with the electrode as the key factor. Various types of materials have been studied for electrode, including conducting polymers and their composite materials with high surface area materials.

Polypyrrole (PPy) based ES has been attracting significant interest due to high specific capacitance (SC), high electrical conductivity, low cost, and easy fabrication of PPy[2]. Electrochemical polymerization of PPy has been widely regarded for long time as the approach to obtain PPy-based ES. However, it is limited in practical application for its low efficiency in production and low loading of active material (<1 mg cm^{-2}). In comparison, chemical polymerization of PPy can achieve industrially valuable PPy based ES. It is therefore employed in this study. It has advantage in mass production, high loading of active materials (up to 40 mg cm^{-2} achieved in this work) and high mass percentage of active materials in electrode. In addition, a high-porous Nickel foam (>95 % porosity) is used as the current collector. It allows high mass loading of PPy and decreases interface contact

resistance, which improve the capacitive properties of ES.

Anionic dopants play a vital role in charging & discharging of PPy, which corresponds to storing & releasing energy of ES. In this study, we use Chromotrope (CHR) families, Amaranth, Eriochrome Cyanine R (ECR), etc. This represents an original and comprehensive research conducted to mechanistically investigate the effects of dopant structures on physical and electrochemical characteristics of PPy. Furthermore, it aims at exploring and developing the general principles in selection of good dopants for PPy based ES.

A major factor that limits the application of PPy based ES is the degradation of bulky materials due to swelling and shrinkage during C-D cycles. The loss in mass and decrease in mechanical properties of PPy are attributed to absorption and infiltration of the electrolyte, as well as ion flow in the bulky PPy matrix during C-D cycles. Another factor that prevents PPy based ES far from use is the relatively low electrical conductivity of chemical-synthesized PPy bulky powders, although PPy is a good conducting polymer. To overcome poor stability and to further increase electrical conductivity of the active material, multi-walled carbon nanotubes (MWCNT) was introduced to fabricate the PPy/MWCNT composite materials. The factors that determine morphologies and capacitive behaviors of the composite material were the use of dopant, the selection of MWCNT dispersing agent, and the PPy/MWCNT mass ratio. The PPy/MWCNT composite electrode showed improved morphologies and enhanced electrochemical characteristics from the pure PPy electrode.

2 Literature Review

2.1 History of Supercapacitor

In 1957, H.I. Becker from General Electric designed the first ES (U.S. Patent 2,800,616). The ES was based on a porous carbon electrode immersed in electrolyte. This was the first electrical device using the type of double layer charge storage theories - energy arising from non-Faradaic charge separation at electrode/electrolyte interface. Later in 1962, R.A. Rightmire from Standard Oil Company of Ohio (SOHIO) invented the device (U.S. Patent 3,288,641) in a format, which is now commonly used. Rightmire's work was further developed in 1970 by another researcher from SOHIO, D.L. Boos, with his patent (U.S. Patent 3,536,963) forming the foundation for many thousands of patents and journal articles in subsequent developments, covering all the aspects of ES. In 1975, Conway developed another type of double layer charge storage theories – energy arising from Faradaic adsorption/desorption of H or some base metals (Pb, Bi, and Cu) at noble current collectors. In this theory, a series of ES based on oxides of variable valence metal ions or metal sulfide were developed, i.e. RuO_2 membrane in aqueous sulfuric acid solution, which showed an ideal electrochemical stability with up to 10^5 effective C-D cycles.

The first commercial production of ES was realized by Nippon Electric in 1978, under SOHIO's patent. Once commercialized, ES was treated as a back-up power devices for volatile chips and complementary metal-oxide-semiconductor (CMOS) memories in computer. Other applications were investigated and commercialized in the following 30

years, i.e. portable wireless communications, high-efficiency energy storage device for electric vehicles (EVs) and hybrid electric vehicles (HEVs)[3], etc. A number of companies were involved in the 30 years of explosive development, i.e. SOHIO, NEC, ECOND, Panasonic, ELIT, ELNA, Maxwell, ESMA, Cap-XX, NCC, NessCap, etc.[4] In 2001, the market for ES was estimated to reach100 million US dollars, while in 2010 the worldwide sales of ES reached 400 million US dollars[5]. It was a continued boost. For ES device, the current trend is the cells having devices from milli-farad to hundreds of thousands of farad (produced by ESMA), with an applicable operating potential of 1,500 V (produced by ELIT)[4]. In summary, the ES technology has experienced a breakthrough in the past 30 year and it still has miles to go to meet practical applicability.

2.2 Energy Storage Devices

Since the Industrial Revolution of England in 1770s, fossil fuels like coal, petroleum and natural gas have provided continuous support to the development of our industries and societies. However, the ecological disasters and environmental pollutions brought by fossil fuels, such as global warming (mainly due to CO_2emission)[6], pollutants sulfur dioxide[7] and nitrogen oxide[8], along with their non-renewable properties, limit their further development and utilization in traditional ways. Filling the gap between decreasing availability of fossil fuels and increasing energy consumption in the modern society has become a significant global issue.

Green and renewable energy supplies[9, 10], like solar energy[11], wind power[12], hydro power[13], biogas [14]and even nuclear energy[15], have attracted great attentions

over the past decades. However, considerable disadvantages, like instable support (solar & wind energy), low efficiency (solar), limited life cycle of device (solar), geographic restrictions (wind & hydro power), and potential risks (nuclear energy), become obstacles [16-18]for vast applications of these energy forms.

To solve reliability issue of the green energy supplies, energy storage systems play an important role. Such systems store and release energy whenever needed to satisfy industrial and social demands. Typically, there are mainly four types of energy storage devices - conventional capacitors, batteries, fuel cells and ES [3]. Conventional capacitors[19] store and retrieve energy by achieving non-Faradaic accumulation and releasing opposite charges electrostatically on the surfaces of two electrodes separated by vacuum space or dielectric layer. The C-D cycle is highly reversible. Batteries [20] provide (or "provide/restore" for rechargeable batteries) energy by outputting (or "outputting/inputting")Faradaic current, generated by reduction or oxidation of some chemical substrates at electrodes with phase change. Fuel cells[21] convert chemical energy directly to electrical energy by reduction of oxidant and oxidation of fuel through internal electrolyte, usually with help of high-efficient catalyst (Pt). To some degree, it is more precise to use "energy generator" to describe fuel cells, rather than "energy storage device". ES[22], as described above in 2.1, stores and releases energy by achieving non-Faradaic charge adsorption and desorption at the electrode/electrolyte interface (double-layer capacitors), or fast and highly reversible Faradaic reaction inside the bulky electrode (pseudo-capacitors)[19], or combination of the above two (hybrid capacitors)[23].

Ragone Plot[24] (also called Ragone Chart) is named after D.V. Ragone. It is a chart,

first designed for performance comparison of batteries and later used to describe and compare any energy storage devices. In this chart, the horizontal axis represents energy density while the vertical axis represents power density. Energy density is the energy stored per unit mass (or per unit volume), that is, "how much" energy is available. Power density is the amount of energy delivered per time, that is, "how quickly" the energy can be delivered. The energy density W_m (mass normalized) and average power density $\overline{P_m}$ (mass normalized) of any energy storage devices could be expressed as:

$$W_m = \frac{1}{m}\int_{t_1}^{t_2} Vidt \cdots\cdots (2\text{-}1)$$

$$\overline{P_m} = \frac{1}{m(t_2-t_1)}\int_{t_1}^{t_2} Vidt \cdots\cdots (2\text{-}2)$$

Where m is the mass; t_1 and t_2 correspond to the start and end times for energy store or release; V is the voltage; i is the current.

For an ideal ES, with a constant current charge or discharge, the two equations[25] can be expressed as:

$$W_m = \frac{1}{2m} C V_m^2 \cdots\cdots (2\text{-}3)$$

$$\overline{P_m} = \frac{1}{2m} i V_m \cdots\cdots (2\text{-}4)$$

Where $V_m$is the maximum voltage. The maximum power delivery P_{max}[25],

$$P_{max} = \frac{1}{4R_s} V_m^2 = 2\overline{P_m} \cdots\cdots (2\text{-}5)$$

Where R_s is the equivalent series resistance (ESR).

The energy density and power density of ES canthus be calculated and compared to other energy storage devices in Ragone Plot. As shown in Figure 2-1, it can be clearly seen

that conventional capacitors have ultra-high power density (~10^5W kg^{-1}) and can store and release energy in a very short period of time. However, they are limited in the capacity (~10^{-2} Wh kg^{-1}) in energy storage and the C-D process within 3.6 ms. In contrast, batteries and fuel cells (not shown in the Figure) exhibit high energy density (~10^1 - 10^2 Wh kg^{-1}), as the storage form of chemical energy in the battery electrode or fuel. They are undoubtedly higher in density than electrostatic energy of the conventional capacitors. Nevertheless, in terms of the mechanisms of batteries and fuel cells, the transformation between chemical energy and electric energy at the electrode/electrolyte interface involves essential processes of ion (or metal) diffusion in electrolyte. These diffusion processes can act as a limiting factor in determining the speed of C-D cycles, resulting in the relatively low power density (~10^2W kg^{-1}) of the cells.

The ES combines the high energy capacity of batteries and fuel cells with the high power input/output rate of conventional capacitors. As shown in Figure 2-1, the energy density and power density of ES are at the levels of ~10^0- 10^1Wh kg^{-1} and ~10^3 - 10^4 W kg^{-1}. The electric double layer at electrode/electrolyte interface of ES, where energy is stored, is much smaller in size than the dielectric of conventional capacitors. ES enjoys an energy density of two to three orders of magnitude higher than the others, because of its much larger surface area. For industrial application, an ideal ES should have high energy density, high power density, high effective cycle life (> 10^6 cycles), high efficiency (> 95 %), easy processability, ecological friendliness and relatively low cost [1, 19, 26].

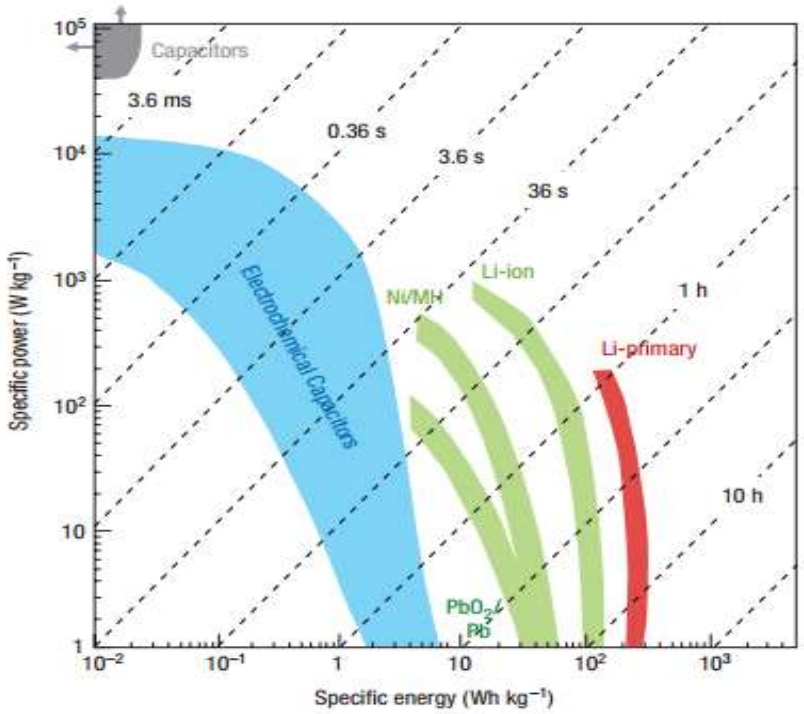

Figure 2-1 Ragone Plot of the common energy storage devices[27]

2.3 Applications of Electrochemical Supercapacitors and Limiting Factors

Because of the high energy and power density properties, ES has attracted great attention in industrial and commercial applications over the past 30 years. As shown in Figure 2-2, the application includes small portable electronics[28], large industrial equipment[29, 30], high-efficiency energy storage device for electric vehicles (EVs)[31] and hybrid electric vehicles (HEVs)[32], etc.

Due its advantages in effective cycle life and fast C-D cycle, ES device is regarded as promising small portable electronics with applications in digital camera flash, mobile phone, uninterruptible power supply (UPS)[33] for desktop, laptop, etc. Especially for its small size, high energy storage and high power output of device, ES becomes one of the

few choices in fabrication of Micro/Nano Electro Mechanical systems (MEMs/NEMs),which are used in micro sensors and actuators[34, 35].

Electrochemical supercapacitor (ES)

Figure 2-2 Application of ES devices: (First row) ES device, solar cell source with ES energy storage, ES based LED driver and corresponding cell phone; (Second row) ES based electric bus at 2010 Shanghai EXPO, Green Cargo from Bombardier Transportation.

Fast and highly reversible storage and release of large amount of energy makes ES an ideal secondary energy source in EVs and HEVs [36]. The pulse power output of ES provides the essential power and energy for starting and accelerating vehicles. ES can also collect the wasted kinetic energy in deceleration and braking of the vehicle[37]. The efficiency of primary energy (gasoline or diesel) utilization in HEVs is thus greatly

improved. The requirement for the output of combustion engine is "smoothed" within the use time, allowing the primary engine work under an optimized condition [38].A similar situation applies to EVs. The pulse output of ES partially replaces battery in providing huge power in a limited period of time. The primary battery is freed from supplying the unusual huge output and thus its effective life can be greatly prolonged. Furthermore, ES has an excellent temperature reliability from -35 to 60 ℃, better than batteries (mostly from -10 to 40 ℃) and fuel cells (usually used at high temperature).

In spite of its advantages discussed above, ES is still far from full commercial exploitation and industrial utilization[3]. Among the vital limiting factors is the high capital cost of the materials such as RuO_2 and the other transition metal oxides. The energy density also makes ES difficult in competing with batteries and fuel cells under specific circumstances. Another issue could be the difficulty in recycling used ES, even though some ES devices have long life time up to 10^6 effective cycles. Electrode is the key factor that determines physical and electrochemical properties of ES. Therefore, developing new materials of reduced cost and enhanced energy density for ES electrode represents an important research area nowadays, as pointed out in a review paper[4], "*The unique attributes of ECs (ESs) often complement the weaknesses of other power sources like batteries and fuel cells*".

2.4 Energy Storage Mechanism of Electrochemical Supercapacitors

ES has a history of more than 30 years by now[4].However, it failed to attract good attention at the beginning because of its low energy capacity and relatively high cost[1]. Big breakthroughs occurred in the last decade. New energy storage theories were developed

for ES. Inventions of low-cost ES materials and designs for high-performance ES electrodes were followed, with products gradually seen in the market place.

ES devices can be divided into three categories based on their differences in energy storage mechanisms and active materials used. They are (1) electrochemical double-layer capacitors (EDLSs), (2) pseudo-capacitors (or redox capacitors) and (3) hybrid capacitors[39].

2.4.1 Electrochemical Double Layer Supercapacitors

EDLSs are ESs that store and release energy with non-Faradaic charge adsorption and desorption at the double layer of electrode/electrolyte interface. The double layer, also termed as electric double layer (EDL), refers to two parallel layers of opposite charges adjacent to electrode surfaces. Many theories[22] were proposed to describe the structure of EDL and to quantitatively calculate related parameters such as those by H. Helmholtz, L.G. Gouy and D.L. Chapman, O. Stern, D.C. Grahame, J.O. Bockris and M.A.V. Devanthan and K.A. Müller, etc.

EDL was first theorized as early as 1853, using Helmholtz's model. It was regarded as a simple molecular dielectric with opposite charges stored electrostatically on the two sides, which formed the foundation for the theory of interface. In 1910s, L.G. Gouy and D.L. Chapman observed that the capacitance of EDLSs was dependent not only on the applied potential but also on the ionic concentration of electrolyte. A new model was then proposed, in which a diffuse model was introduced to replace the rigid molecular dielectric. The charge distribution of ions was expressed as a function of distance from the

electrode/electrolyte interface following the *Maxwell-Boltzmann* statistics. While the Gouy-Chapman model was sophisticated, it could not provide a convincing explanation to the highly charged EDL. In 1924, O. Stern combined Gouy-Chapman's model and Helmholtz's work and proposed a composite theory. As asserted, some ions adhere to the electrode and form the so-called "Stern layer", while other ions form a diffuse layer next to the Stern layer. The diffusion layer decays in a non-linear potential fashion with distance[40].

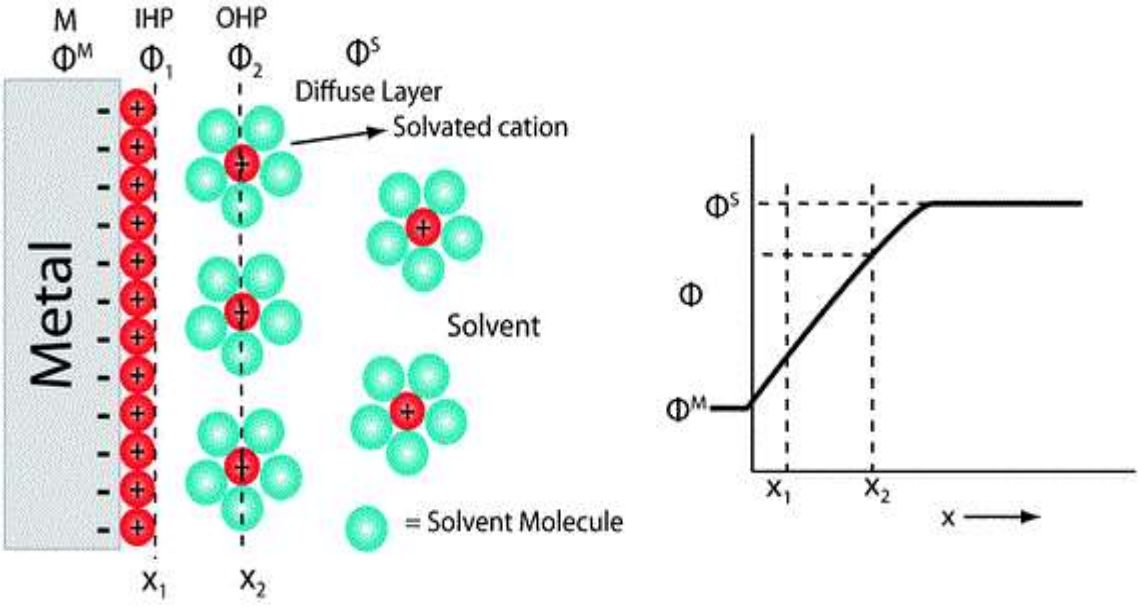

Figure 2-3 Illustration showing the double layer formation of a typical EDLC electrode with IHP and OHP standing for the inner Helmholtz plane and outer Helmholtz plane, respectively.[41]

In 1947, D.C. Grahame suggested that some ionic or uncharged species penetrate the Stern layer, dividing it into two sections. One is the inner Helmholtz plane (IHP), where the ions are directly adsorbed to the electrode without a solvated coat. The other is the

outer Helmholtz plane (OHP), in which the solvated ions are at their closest distance from the electrode. Grahame's model was further modified by J.O. Bockris, M.A.V. Devanthan and K.A. Müller in 1963, by taking the distribution and action of interfacial solvent molecules into consideration. This modification resulted in the BDM model, which is most commonly used today. The BDM model, shown in Figure 2-3, suggests that solvent molecules form a major portion of the first layer adjacent to the electrode surface and isolated ions. This first layer of solvent can orientate to electric field depending on the charge. Solvated ions are outside the IHP but are close to the electrode, that is, in the OHP. The IHP and OHP contribute to most of the potential drop (purple line). The diffuse layer is further outside the OHP and gives the non-linear potential drop.

The Helmholtz layer, or the Stern layer, forms the major part of the whole capacitance. It is analogous to a parallel plate capacitor. Its capacitance can be expressed as[25]:

$$C_{dl} = \frac{1}{d}\varepsilon_r\varepsilon_0 A \cdots\cdots (2\text{-}6)$$

Where ε_r and $\varepsilon_0$are the relative dielectric constant of double layer and the permittivity of vacuum; A and d correspond to the surface area and thickness of the double layer, respectively. In a system where solvent molecules firmly adhere to electrode surface with few charges transferring across the interface, EDLS collects and releases energy in a non-Faradaic process. In other words, the ions at OHP determine the quantity and contribute to a majority of the capacitance. Such characteristics lead to a highly reversibility of C-D cycle and a good effective cycle life of EDLS devices.

The double layer thickness d is in the order of ion diameter (3-8Å) [22]. It is far smaller than the distance between the plates in conventional capacitors. Improvement in

capacitance can also be achieved by increasing surface area *A* with porous materials having high specific surface area (SSA) and excellent electric conductivity. Hence, reduced thickness and increased surface area of the double layer dramatically improved the capacitance of EDLS (~10^0-10^1 F) from the conventional capacitors (typically ~10^{-9}-10^{-6} F).

It should be pointed out that although the structure of EDLS consisting of two electrodes dipped in electrolyte appears somewhat similar to conventional capacitors or batteries. Each electrode in EDLS is an individual capacitor and one EDLS cell can be considered as two capacitors connected in series. The total capacitance of an EDCL cell is thus[25],

$$C_{cell} = \left(\frac{1}{C_1} + \frac{1}{C_2}\right)^{-1} \quad \text{(2-7)}$$

Where C_1 and C_2 are the capacitances of the two capacitors. For a symmetrical ES (two similar electrodes), $C_{cell} = C_{single}/2$.

2.4.2 Pseudo-Supercapacitors

There were significant improvements in the mechanistic theories of pseudo-supercapacitors in 1970s to 1980s, based on the extensive fundamental work[42] on RuO_2 by B.E. Conway, as well as that of the Nobel Prize winner R.A. Marcus's. The latter explains the basics of electron charge transfer in the absence of chemical bonds. Different from EDLS, of which capacitance arises from non-Faradaic electrostatic adsorption or desorption, pseudo-supercapacitor (PS), also named pseudo-capacitor, achieves energy

storage by Faradaic charge transfer at the surface or in the bulk near solid electrode surface.

Three Faradaic charge transfer models have been proposed to describe the interfacial structure and energy storage mechanism of PS. The first model is based on surface adsorption of ions from electrolyte (Figure 2-4 (a))[43]. Different from OHP, ions in PS are directly adsorbed to the electrode surface without solvated molecules.

The second model is based on Faradaic current generated from compound formation via redox reaction in the bulk electrode material close to its surface (Figure 2-4 (b))[39, 44]. Since the adsorption and redox reaction occur at the electrode/electrolyte interface, the processes strongly depend on the SSA of electrode. The first two models are normally used to describe performance of the devices having metal oxides as the active materials.

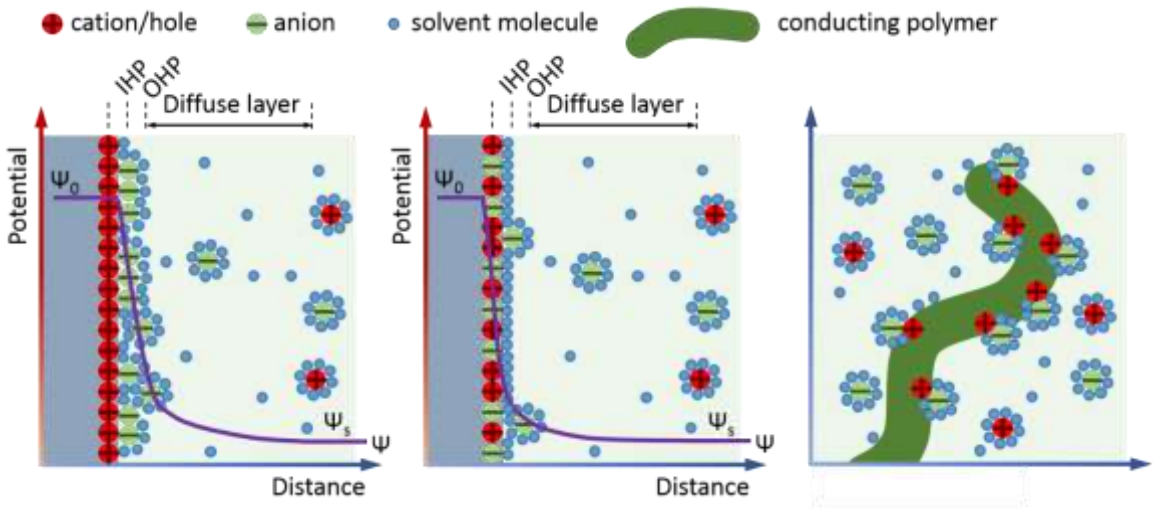

(a) IHP adsorption (b) redox reaction (c) doping/dedoping

Figure 2-4 Schematic diagrams (only show positively charged electrode) of PS

The third model is to specifically describe the mechanism of conducting polymer (CP)-based PS (Figure 2-4(c))[45]. With applied potential or current density, CP-based PS device can store and release energy from the doping/de-doping process occurred in the whole bulk of electrode. Different from metal oxide-based PS, the CP-based PS is not so dramatically affected by SSA of the bulk materials. Its performance is related to the permeability of electrolyte infiltration into bulky electrode and the electric conductivity of CPs.

It should be pointed out that it is difficult to classify an ES system into either pure non-Faradaic or pure Faradaic process because both storage mechanisms often coexist. In some systems, one process contributes up to 95%-98% of the capacitance. Table 2-1 gives more information of the comparisons between EDLS and PS.

Table 2-1 Additional information of EDLS and PS comparison[46]

	EDLS	PS
Capacitance density	20-50 μF cm^{-2}	200-2000 μF cm^{-2}
Capacitance variation vs. potential	Fairly constant, except for point of zero charge (p.z.c.)	Obvious maxima observed for single-state process
Reversibility	Excellent	Quite good

2.4.3 Hybrid Supercapacitors

According to Equation 2-3 & 2-5, the energy density and power density are proportional to the voltage square. Increase in the voltage window results in a large increase in stored energy and power output. However, traditional ES device consists of two electrodes of the same materials, that is, symmetrical ES. The open circuit voltage of

symmetrical ES equals to the voltage window of single electrode[19].

Hybrid supercapacitor (HS)[47, 48]was then proposed. It is based on the application of EDLS capacitor and the use of different PS materials for electrodes asymmetrically in a single cell. HS has attracted great attention in the recent years. HS devices have one electrode of EDLS type charged and discharged in the non-Faradaic process, and the other electrode of PS type charged and discharged in the Faradaic process. These capacitors combine the features of electrolytic and redox capacitors. When the electrode materials are carefully selected with a certain voltage window, the optimized HS devices have an enhanced open circuit voltage higher than the sum of the two [49, 50], as illustrated in Figure 2-5.

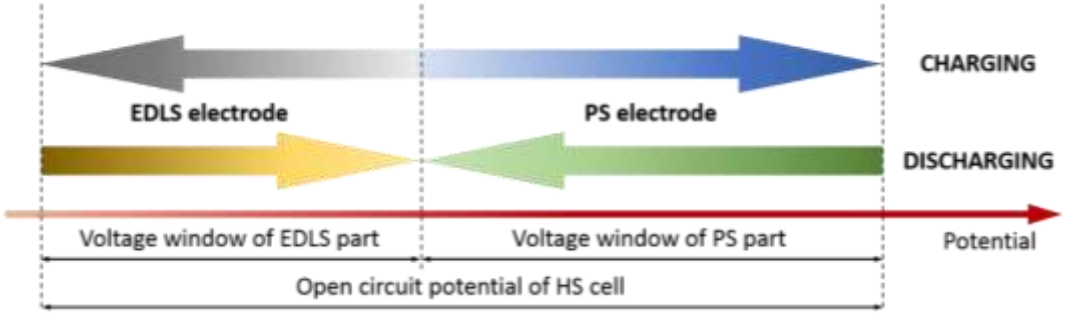

Figure 2-5 Schematic voltage window of HS, arised from EDLS electrode and PS electrode

D.A. Evans[51] designed the first HS device in 1994, using the anode of 200V tantalum electrolytic capacitor and the cathode of RuO_2 pseudo-supercapacitor. The device gave an energy density of five times higher than the same size tantalum electrolytic capacitor.

Although HS gives excellent performance, it is limited in applications due to high costs in manufacturing.

2.5 Materials for Electrodes of Supercapacitors

Based on ES mechanisms, electrode materials can be classified into three types: (1) high specific surface area materials (for EDLSs), (2) redox pseudo-capacitive materials (for PSs) and (3) materials for hybrid capacitors [27, 40].

2.5.1 High Specific Surface Area Carbon Materials

According to Equation 2-6, ultrahigh capacitance can be realized by employing ES materials of high SSA and excellent electric conductivity. The surface area and electric conductivity are the two key parameters determining performance of ES devices[25].Also important for high-performance ES are a number of other properties, including wide temperature adaptability, longtime physical and chemical stability, easy processability, etc.

Since the first ES device in 1957, carbon in various forms has been considered as good candidates as advanced ES materials[52]. Activated carbon (AC), activated carbon fiber (ACF), carbide derived carbon (CDC), carbon nanotubes (CNTs), graphene and carbon aerogel (CA) have been all investigated and found to meet the requirements [39, 43].

Since electrolytic ions travel through pores, pore size and size distribution of the carbon materials play important roles. In 2008, P. Simon and A. Burke[53] theorized the pore size network in activated carbon grain. The theory is applicable to various carbon forms and other potential EDLS materials, as shown in Figure 2-6. The closed pores (dead

pores; not shown in the Figure 2-6) are those stable void spaces totally surrounded by active materials. These pores are unavailable for electrolyte and do not contribute to energy storage. On the other side, the open pores (active pores) are accessible for electrolyte. These pores form the electrode/electrolyte interface for energy storage. The pore sizes can be further divided into three groups: (1) micropores (<2 nm), (2) mesopores (2-50 nm) and (3) macropores (>50 nm)[53].

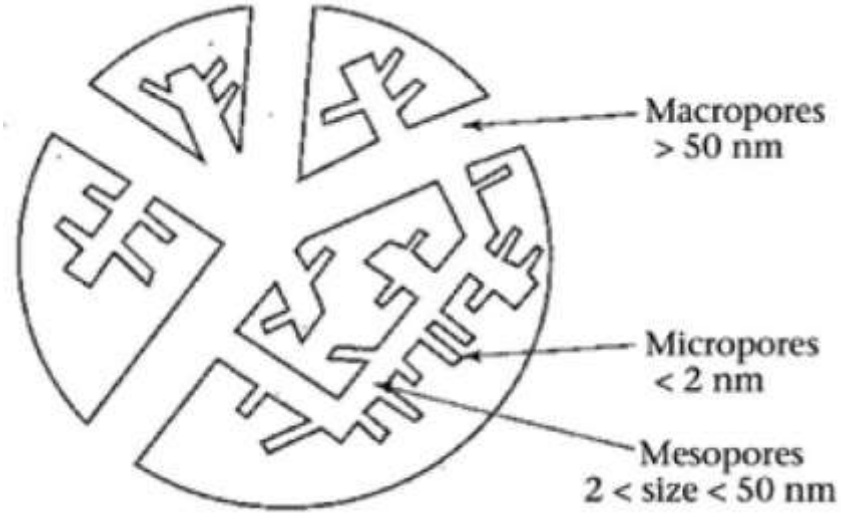

Figure 2-6 Schematic network for pore size distribution in active material grain[53]

It was long believed that among the three types of pores, micropores make little contribution to formation of EDL and charge storage, because they are smaller than solvated electrolytic ions and are not accessible for the latter. However, recent researches[53] on electrochemical properties of well controlled pore size carbon materials revealed that ultrahigh capacitance can be achieved by micropores, as shown in Figure 2-7. With pore sizes in 1.5~4 nm, the free space for electrolyte infiltration is reduced, restricting motions of electrolytic ions and thus reducing capacitance. With pores <1.5 nm,

solvated ions distort or even lose part of their solvation shells for entering the narrow spaces[53]. The reduced space force ions closer to the electrode surface and enhanced the capacitance via Faradaic process in electrode materials (see Equation 2-6) [54] .

Besides SSA and pore size, the other key parameter that determines ES performance is the electric conductivity of bulk carbon [25, 55]. It is well known that sp^3- and sp^2-hybridization are most commonly observed in carbon materials. In sp^3-hybridization, four stable σ-orbits are formed in one carbon atom. In sp^2-hybridization, three σ-orbits are formed and one electron is left in the remaining p-orbit, forming π-bond when its electron cloud approaches and overlaps with nearby p-orbits. The p-orbit electron is delocalized in the whole π cloud region, providing the essential charge transfer route for electric conductivity. A high ratio of sp^2-hybridization carbon is vitally important for high electric conductivity.

Activated carbon (AC)[56] is an extremely porous form of carbon and is attractive for fabrication of EDLS with high SSA (1000-3000 $m^2 g^{-1}$). AC is of low cost and sufficient resource. It can be mass produced from carbon-rich sources, such as wood and coal, carbonized in an inert atmosphere at high temperature and activated with selective oxidation[57]. The porous AC is usually pressed into a desired shape, called consolidated amorphous carbon (CAC) that is widely used in ES manufacturing. According to Table 2-1, if the capacitance density of EDLS, 10 μF cm^{-2}, multiplied by a typical SSA of 1000 m^2g^{-1}, we can theoretically achieve ES device with specific capacitance of 100 F g^{-1}. Factors such carbon selection, surface functionality of AC, and working temperature have great impact on the electrochemical properties of AC-based ES devices[43]. In most cases, AC

electrodes display predominantly the EDLS type of charge storage, with PS type as the minor contributor. The micropores are accessible to electrolytic ions with distortion and/or loss of solvation shell, allowing Faradaic reactions with electrode for the PS part[25].

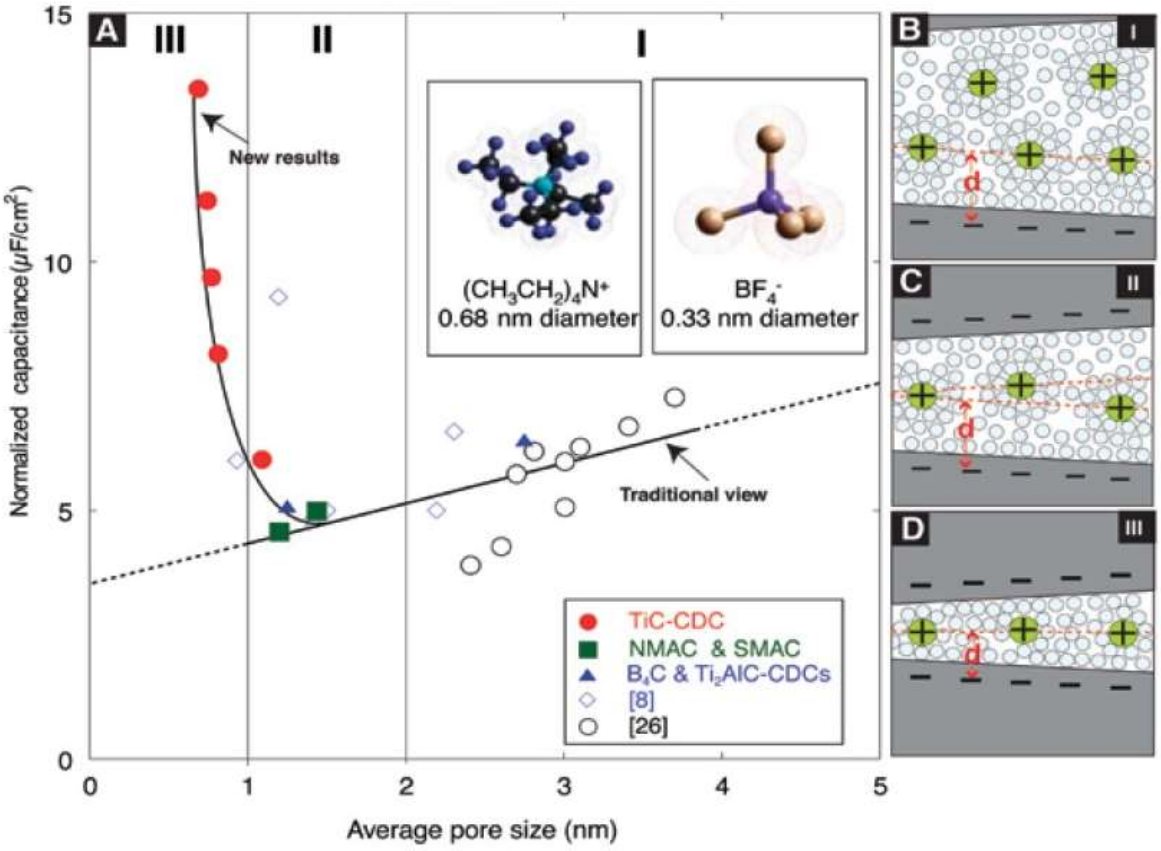

Figure 2-7 Normalized capacitance vs. average pore size for TiC-CDC and other comparable data in the same electrolytes[53]

Polymer materials such as phenolic and acetone-furfuryl resins have also been used as carbon sources. The products of high temperature carbonization (>1200 ℃), termed as glassy carbon (GC), allow excellent mechanical properties and processability. They have a

perfect electric conductivity for 100% sp^2-hybridization and two-dimensional structure of carbon, similar to graphite and far better than amorphous AC[43]. GC has unique specifications such as high hardness and low friction. It has been widely used in ES applications as the current collector but not as the bulky electrode until activation processes were developed to increase the permeability to electrolyte [54].

Activated carbon fibers (ACFs) [43] are produced from activated carbon and have typical diameters about 10 μm. The one dimensional structure of ACF allows low electrical resistance along fiber axis and fabrication of textile cloth. The micropores of ACF have a relatively narrow pore size distribution that can be controlled. The surface area of ACF woven is up to about 2500 m^2g^{-1}[58], which is comparable to AC. Furthermore, the capacitance with ACF electrodes is mainly from EDLS, with small amount of PS due to the presence of micropores, which is quite similar to AC.

Carbide derived carbon (CDC) [43], also named tunable nanoporous carbon (TNC), is carbonized from carbide precursors, such as binary carbides TiC/SiC, ternary carbides Ti_2AlC, and polymer-derived ceramics Si-O-C/Si-N-C. CDC has SSA of > 3000 m^2 g^{-1}, which is the highest value ever reported. Nearly all the forms of carbon structures, including micro/meso/macropores, two-dimensional CNTs, graphite/graphene and three-dimensional nanocrystalline diamond, could be detected in CDC. The micropores contribute to the majority of SSA. The pore size distribution and bulk porosity of CDC vary with the type of carbon precursor and carbonization conditions. Many research groups reported the application of CDC in ES fabrications. J. Eskusson[59] worked on Mo_2C derived carbon, C.R. Pérez[60] on TiC derived carbon, and F. Liu[61] on SiC derived carbon.

Carbon nanotubes (CNTs)[43] are produced by catalytic decomposition of certain hydrocarbons. They are carbon molecules having cylinder nanostructure. Similar to ACF, the one-dimensional and long-ranged structure of CNTs gives good electric conductivity. Depending on the number of graphene-structured layers in each tube, CNTs are generally categorized as single-walled CNT (SWCNT) and multi-walled CNT (MWCNT), where in the latter case the CNT has thicker coaxial walls with a space distance of 0.34 nm[62]. The wettability on the CNT surface is comparably higher than that of AC, due to its regular pattern. It can also be enhanced by surface functionalization or activation [63]. Hence, although the SSAs of SWCNT (theoretically 1315 $m^2 g^{-1}$) and MWCNT (100-500 $m^2 g^{-1}$, determined by degree of nesting) are much lower than those of AC and CDC, SWCNT and MWCNT achieved capacitance of~180 F $g^{-1}$and ~100 F g^{-1}, respectively[43]. CNTs and derivatives, such as nitrogen-doped CNTs and graphenated CNTs, have good potential for ES applications due to their high physical properties, good electric conductivity, excellent electrolyte accessibility, and high thermal stability[64, 65].

Graphene [66, 67] can be regarded as one-atom thick of graphite. It is a two-dimensional crystalline of carbon (~100% sp^2-hybridization). However, not until the recent decade did graphene receive in-depth investigation[68]. Graphene has an ultrahigh SSA (2630 $m^2 g^{-1}$) and a theoretical capacitance of 550 F g^{-1}.It also has superb electric conductivity (> 1700 S m^{-1}), surpassing AC (~10-100 S m^{-1}), making it promising for ES application[69]. As most carbon materials are fragile and amorphous, certain current collectors are usually occupied in fabricating ES devices. In 2012, M.F El-Kady [70] reported the fabrication of pure graphene electrode without other current collectors and

obtained a high capacitance of 276 F g^{-1}.

Table 2-2 Summary of properties of various carbon materials [71]

Carbon materials	SSA (m^2 g^{-1})	Hybridization status of C	Capacitance (F g^{-1})		Charge storage
			Aqueous electrolyte	Organic Electrolyte	
AC	1000-3000	Mixed	<200	<100	EDLS dominating, with a small amount of PS due to micropores
ACF	1000-3000	Mixed	120-370	80-200	
CDC	>3000	Mixed	170-220	100-120	
CNTs	100-500 (MWCNT) ~1300 (SWCNT)	~100% sp^2	50-100 (MWCNT)	<60	
Graphene	Theoretical 2630	~100% sp^2	100-200	120	
CA	400-1000	Mixed	100-125	<80	

Carbon aerogel (CA) [43] is usually produced by carbonization of polymer aerogels such as resorcinol-formaldehyde resin precursor. It was first developed in the late 1980's. CA is considered as a type of promising materials for ES fabrication due to the high SSA (400-1000 m^2 g^{-1}), high porosity and good electric conductivity [35].With its ultralow volumetric density (0.16 mg cm^{-3} was achieved for graphene aerogel), CA can act as current collector and be fabricated into composite electrode with high capacitance PS materials. A summary of physical and electrochemical properties of various carbon materials is given in Table 2-2.

2.5.2 Redox Pseudo-Capacitive Materials

Although capacitance from PS via Faradaic charge transfer is always present in carbon-based ES, it is little in amount and can be neglected. ES electrodes based on metal oxides, metal nitrides and conducting polymers show sufficient Faradaic processes and have mainly the pseudo-capacitive type of charge storage[19]. Due to highly reversible redox reaction at electrode/electrolyte interface or bulky electrode near the surface, redox pseudo-capacitive materials give capacitance densities one or two orders of magnitude higher than the high SSA carbon materials, as shown in Table 2-1.

2.5.2.1 Metal Oxides

Various transition metal oxides[72] have long been investigated as ES materials for the charge transfer in bulky redox reactions, such as RuO_2, IrO_2, Fe_3O_4, MoO_3, MnO_2, NiO, V_2O_5, etc. A typical redox reaction of PS materials during C-D cycles can be written as[25]:

$$M_mO_n + xH^+ + xe^- \leftrightarrow M_mO_{n-x}(OH)_x \cdots\cdots\cdots\cdots \text{(2-8)}$$

Where $M_mO_n$is the oxide of metal with a valence of $+\left(\frac{2n}{m}\right)$.

In some cases, electrolytic cations (A^+=K^+, Na^+, Li^+…)are involved in the redox reaction, so the expression may be rewritten as[25]:

$$M_mO_n + xH^+ + yA^+ + (x+y)e^- \leftrightarrow A_yM_mO_{n-x}(OH)_x \cdots\cdots\cdots \text{(2-9)}$$

Since these reactions occur at electrode/electrolyte interface, it is particularly beneficial to increase SSA of metal oxides for enhancing the interface-related charge storage[39]. This can be achieved through decreasing particle size, increasing porosity (especially the ratio of micropores), and fabricating metal oxides having certain structures

(nanorod/nanofiber/hollow) via template methods[63].An ideal morphologic design of electrode is a bi-continuous network of metal oxide and void space (including macro/meso/micropores).In this type of designs, all the essential properties of ES become available, high SSA (high capacitance), high charge transfer rate (high power input/output), good mechanical strength (structure/performance stability) and low metal oxides/electrolyte resistance[43].

RuO_2 [73, 74]has been long investigated as a type of PS materials for its high capacitance, good electrochemical reversibility, good electric conductivity with support, and acceptable cycle life. The redox reaction of RuO_2 as pseudo-capacitive materials in aqueous electrolyte follows Equation 2-8, where m=1, n=2 and x varies from 0 to 2, corresponding to the valence variation of Ru from (IV) to (II) in the ternary compound. Enhancement in capacitance could be achieved by a fine grained process such as annealing, deposited on high-porous current collector or fabricated into composite materials [75-77]. I.H. Kim[78] vapor grew carbon fibers from (VGCF)/RuO_2xH_2O composite materials using a thermal decomposition method. The product gave capacitance of 1017 F g^{-1} higher than the pure RuO_2 xH_2O powder of 410 F g^{-1}. In another work of the same researcher[79], a type of three dimensional CNT/RuO_2 composite materials was prepared by electrochemical deposition, and it gave an ultrahigh capacitance of 1170 F g^{-1} and high capacitance retention at an increased current density. Besides, IrO_2square nanotube has relatively high SSA and good electrochemical reversibility. D.S. Tsai[80] reported the fabrication of IrO_2 nanotube/CNT composite materials for enhanced capacitance retention (vs. the number of C-D cycles) with an initial value of 69 F g^{-1}.

Unfortunately, though attractive capacitance and perfect processability for composite materials, the limited resource and high price of Ru and Ir elements limit their extensive applications[39].The demand for low-cost metal oxide-based PS materials remains. A typical example is the oxide of manganese [81, 82]. It is attractive for high capacitance and inexpensive pristine materials. The charge storage mechanism is proposed to follow Equation 2-9, where m=1 and n=2.Electrolytic cations, except for hydrogen ions, are involved in charge storage due to adsorption. Electrochemical deposition[83, 84], chemical synthesis[85], sol-gel[86] and pulsed laser deposition[87, 88] methods are commonly used in preparation of manganese oxide for ES application. C.K. Lin[89] reported that the specific capacitance of manganese oxide electrodes, prepared via sol-gel method, was 53.2, 230.5, 185.6 and 189.9 F g^{-1} after heat treating at 250, 300, 350 and 400 ℃, respectively. There existed a maximum capacitance as a function of temperature. S.Y. Lu[90]prepared Mn_3O_4/carbon aerogel composite materials and reported high capacitance of 503 F g^{-1} at scan rate of 25 mV s^{-1}. Good capacitance retention was evident in cycling tests. Other metal oxides, such as cobalt oxide[91], iron oxide[92] and nickel oxide[93]have also been researched as inexpensive pseudo-capacitive materials.

Besides the binary metal-oxygen systems, ternary metal-metal-oxygen systems[94]have also attracted attention recently, as promising electrode materials. D. Yang[88] researched Vanadium-doped MnO_2 materials and revealed higher capacitance of 95 F g^{-1}, at doping level of 9.7 atm. % and high scan rate of 100 mV s^{-1}. As a reference, the capacitance of undoped MnO_2was64 F g^{-1}. T. Wang [95] fabricated $NiCo_2O_4$ nanowire and $CoMoO_4$ nanoplate via a facial hydrothermal method. A highest area normalized

capacitance of 14.67 F cm^{-2} was achieved. This was attributed to the high capacitance of metal oxides, large SSA due to nanostructured materials, and easy diffusion of electrolyte due to ordered growing $NiCo_2O_4$-$CoMoO_4$ composite material of core-shell structure. A summary of the electrochemical properties of common metal oxides for PS is given in Table 2-3.

Table 2-3 Pseudo-capacitance and conductivity of selected metal oxides [96]

Metal oxides	Electrolyte (aqueous)	Theoretical capacitance (F g^{-1})	Conductivity (S cm^{-1})
MnO_2	Na_2SO_4	1380 (0.9 V)	10^{-5}-10^{-6}
NiO	KOH, NaOH	2584 (0.5 V)	0.01-0.32
Co_3O_4	KOH, NaOH	3560 (0.45 V)	10^{-4}-10^{-2}
V_2O_5	NaCl, Na_2SO_4	2120 (1 V)	10^{-4}-10^{-2}
RuO_2 xH_2O	H_2SO_4, Na_2SO_4	1200-2200 (1.23 V)	10^3 for polycrystalline ~1 for amorphous

2.5.2.2 Metal Nitrides/Sulfides

Metal nitrides (VN, TiN, etc.)[97, 98] are another type of promising materials for the fabrication of high performance ES. They have such outstanding features as high specific capacitance and excellent electrical conductivity (4,000-55,500 S cm^{-1} for TiN)[25].D.W. Choi and P.N, Kumta [98, 99] investigated the nanostructured VN as electrode materials. They prepared the materials through two-step ammonolysis reaction of metal halides and

achieved an impressive capacitance of 1340 and 554 F g^{-1} at the scan rate of 2 mV s^{-1} and 100 mV s^{-1}, respectively. G. Cui [100] reported the fabrication of TiN-VN core-shell nanostructured composite materials for ES use and obtained 247.5 F g^{-1} with improved retention with increasing the voltage variation rate. Most recently, Y. Li [101] researched TiN electrode having thin carbon shell and found an incredibly high capacitance retention of 88.4% after 15000 cycles, compared to 8.5 % retention of the pristine TiN electrode. The carbon shell coating was believed to provide good protection for TiN from irreversible oxidation by water and/or oxygen, as shown in Equation 2-10 and 2-11[101].

$$TiN + 2H_2O \rightarrow TiO_2 + 0.5N_2 + 4H^+ + 4e^- \cdots\cdots\cdots\cdots\cdots\cdots (2\text{-}10)$$

$$TiN + O_2 \rightarrow TiO_2 + 0.5N_2 \cdots\cdots\cdots\cdots\cdots\cdots\cdots\cdots\cdots\cdots\cdots\cdots\cdots\cdots (2\text{-}11)$$

Metal sulfides (CoS, ZnS, etc.)[102, 103] have also attracted a wide attention in the recent years. They have good stability and ultrahigh capacitance. Carbon materials of high electric conductivity are often incorporated into metal sulfides to fabricate composite materials for enhanced electrochemical characteristics, especially for high capacitance retention at high potential variation rate. H. Chang[102] reported high capacitance of 2140 ± 90 F g^{-1} for CoS/CNT composite materials. This capacitance is an order of magnitude higher than EDLS carbon materials. The results suggested that the incorporation of CNT yield high capacitance retention at increasing potential variation rate or current density. B.P.C. Ragupathy[103] reported the synthesis of nano-dispersed CoS and CoS/graphene composite materials, and achieved electrochemical capacitance of 2100.8 F g^{-1} and 2423.3 F g^{-1}, respectively.

2.5.2.3 Conducting Polymers

Since the synthesis polyacetylene[104]in 1970's, conducting polymers (CPs) have experienced a rapid development for various applications over the past 40 years because of uniqueness of their physical and chemical properties[45, 105]. Many CPs have been extensively studied as potential materials for ES utilization, i.e. polypyrrole (PPy)[106], polyaniline (PAn)[107], polythiophene (PTh)[108], poly(3,4-ethylenedioxythiophene) (PEDOT)[109], as shown in Table 2-4.

Table 2-4 Electrochemical properties of common CPs for ES application [45]

Conducting polymers	Molecular weight ($g\ L^{-1}$)	Potential range (V)	Theoretical SC ($F\ g^{-1}$)	Measured SC ($F\ g^{-1}$)
PAni	93	0.7	750	240
PPy	67	0.8	620	530
PTh	84	0.8	485	-
PEDOT	142	1.2	210	92

A common specification of CPs is the delocalized π-conjugated backbone of polymer chains, which can be ultra-conductive after certain redox or doping processes[39]. Depending on the polarity of dopant chemicals or the redox type, the CPs van have p-doped or n-doped state (Figure 2-8)[19]. The former corresponds to the oxidized CPs with anion dopants, while the latter is the reduced CPs with cation dopants. It was reported that p-doped CPs have higher stability than n-doped CPs[19]. Compared to n-doped CPs, p-Doped CPs have been extensively studied in ES applications.

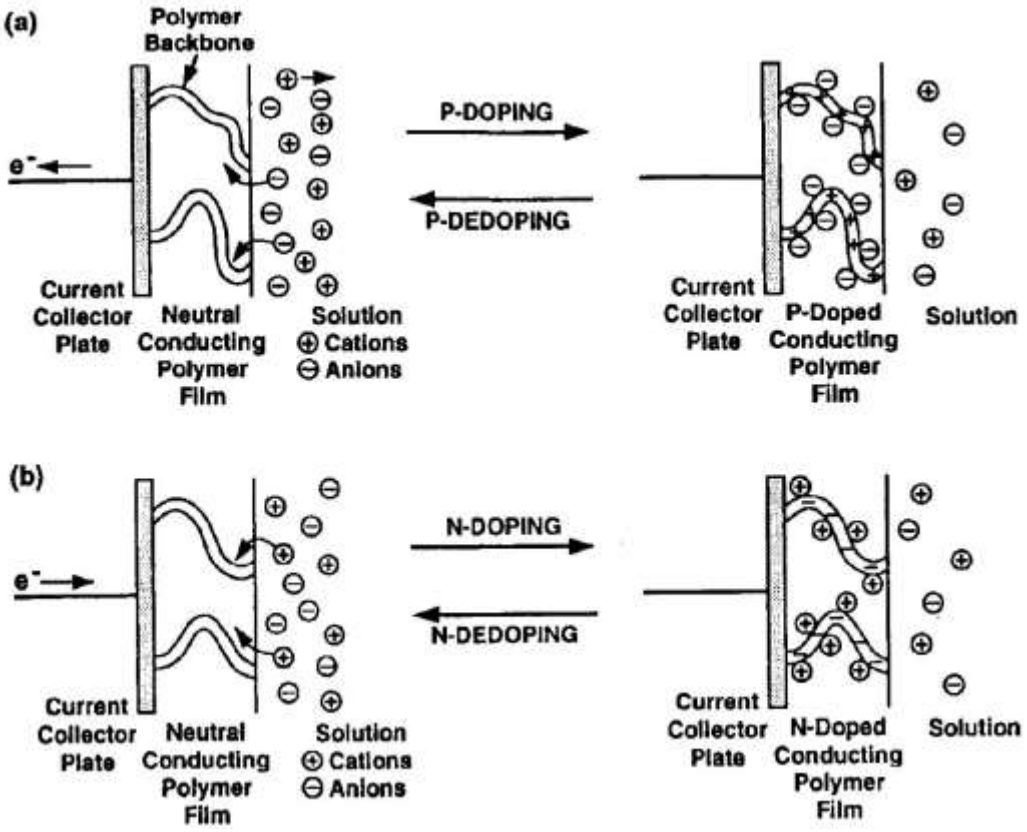

Figure 2-8 Schematic diagram of charging-discharging state for (a) p-type and (b) n-type CP electrodes[19]

Compared to other carbon materials, CPs have better specific capacitance (see Table 2-4) and relatively lower SSA requirement used for capacitance due to fast and reversible reaction of doping-dedoping in bulk instead of in an interface area. CPs are more electric conductive, more environmental friendly, and less costly than metal oxides. Many factors, including selection of monomer, electrolyte and substrate, nano-morphology and dopant utilization, have important effects on the electrochemical applications of CPs. Dopant molecules greatly affect morphology and capacitance of CPs[45].

2.5.3 Composite Materials

Composite materials are fabricated when materials from two or more categories (carbon materials, metal oxides/nitrides/sulfides and CPs) are incorporated in preparation of active materials[39]. Because of certain advantages and disadvantages of individual material (Table 2-5), it is of great importance to integrate the advantages of pure species via hybridization and achieve high performance composite materials.

Table 2-5 Typical advantages/disadvantages of ES materials (summarized from [39, 40, 58])

Materials	Advantages	Disadvantages
Carbon materials	High electric conductivity High electrochemical stability	Low specific capacitance
Metal oxides	Ultrahigh specific capacitance	Low electric conductivity High cost (for part species) Low stability during cycle
Metal nitrides/sulfides	Ultrahigh specific capacitance High electric conductivity	Low stability in aqueous High toxicity
CPs	**High specific capacitance** **Environmental friendliness (comparably)** **Low cost, High flexibility**	**Low stability during cycle**

Great research efforts have been made to overcome disadvantages of the individual materials listed in Table 2-5, in preparation of high quality composite materials. Various types of hybridization have been tried[110]. Typical examples are summarized and given in Table 2-6. Pristine CPs are capable to gain stability and enhanced electric conductivity

when incorporated with carbon based reinforcements, which are important for the practical application of CPs as shown in Table 2-5.

Table 2-6 Recent developments in the composite materials for ES application

Hybridization*	Typical example	Capacitance	Reference
C + MO	MnO_2 coated MWCNTs	246 F g^{-1} at 1000 mV s^{-1} with good stability	[111]
C + MN	Carbon coated VN	124.5 F g^{-1} at 5 A g^{-1} with excellent cyclic stability	[101]
C + MS	NiS embedded graphene	800 F g^{-1} at 1 A g^{-1} with small decay vs. cycle	[112]
C + CPs	Polyaniline (PAn) coated porous carbon	1600 F g^{-1} at 1.98 A $g^{-1}$with good stability	[113]
MO + CPs	MnO_2 embedded polypyrrole	620 F g^{-1} at 5 mV s^{-1}	[114]
C + MO + CPs	CNT/Polypyrrole/hydrous MnO_2 ternary composite	281 F g^{-1} at 20 mV $s^{-1}$with good retention vs. frequency	[115]

*:C – carbon materials; MO/MN/MS – metal oxides/nitrides/sulfides.

2.6 Electrolytes for Supercapacitors

The electrolytes are essential for the fabrication of any ES cells and play a significant role in the performance of the latter[22]. Electrolytes provide ions for charge transfer and formation of EDL, or redox reaction to achieve charge storage.

The conductivity of electrolytes[19] is mainly determined by solubility of the electrolytic ions, mobility of the free/dissociated ions, solvation of the free ions, dielectric constant of the bulk solvent, and viscosity of solvent. A transmission-like model[19] for a single pore is shown in Figure 2-9, where R_e and R_s are the ohmic resistance of electrolyte and solid electrode material, respectively, Z_f is the electrode Faradaic impedance and C_{dl} is

the double-layer capacitance.

Three different types of liquid electrolytes have been widely investigated: (1) aqueous electrolyte, (2) organic electrolyte and (3) ionic liquid (including polyelectrolyte). More recently, solid electrolyte or gel electrolyte were obtained by incorporation of polyvinyl alcohol [49, 116], which attracted great attentions for their importance in the fabrication of solid state ES.

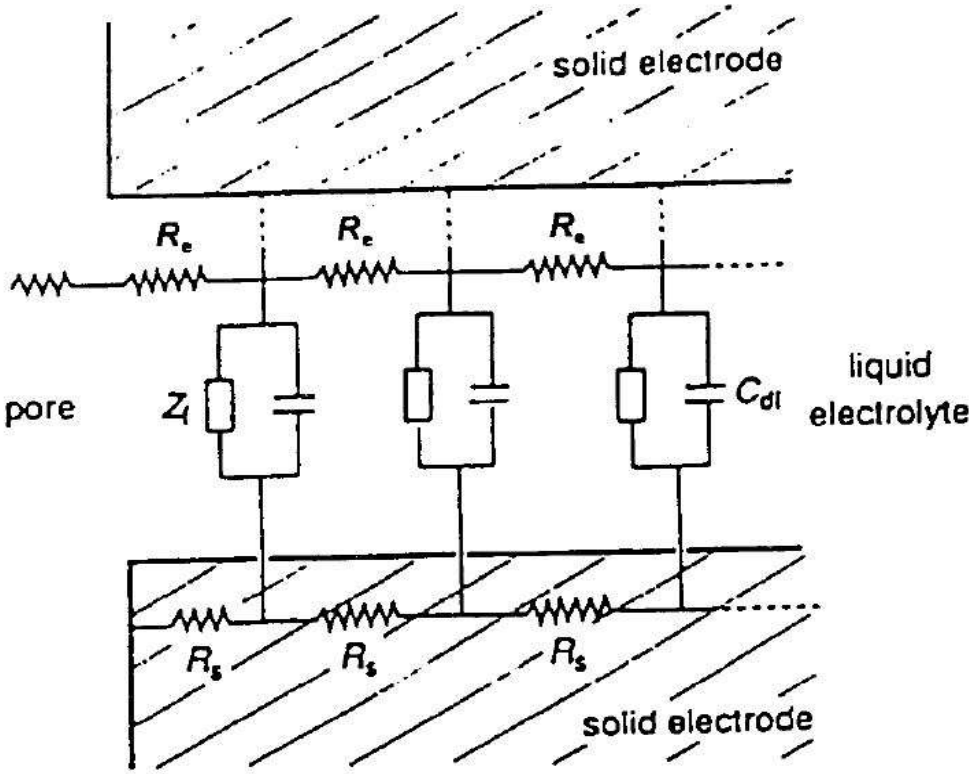

Figure 2-9 Transmission-line model for a single pore[19]

2.6.1 Aqueous Electrolytes

Aqueous electrolytes for ES devices can be acid solution (H_2SO_4, HCl, etc.)[117], alkaline solution (KOH, NaOH, etc.)[118] and neutral salt solution ($LiClO_4$, Na_2SO_4, KCl,

etc.)[119]. Normally, aqueous electrolytes show features such as low equivalent series resistance (ESR),high ion density (compared to organic electrolytes) and low cost[19]. Besides, it is worthy to note that strong acidic solutions are much more corrosive than strong basic solutions (e.g., KOH or NaOH) and the latter may thus be preferred for some cases. Aqueous electrolytes without heavy metal ions are promising for ES fabrication as green materials. However, the thermodynamic decomposition voltage of water is 1.23 V and it severely restricts the energy density according to Equation 2-3, compared to organic electrolyte.

2.6.2 Organic Electrolytes

In principle, the organic electrolytes such as acetonitrile (AN)[120, 121] and dimethoxy ethane (DME)[122]used for ES fabrication give higher operating potentials due to their higher decomposition limitations. Hence, higher energy densities can be achieved by organic electrolytes than aqueous electrolytes according to Equation 2-3. For instance, with suitable solvents, R_4N^+ electrolytic ions yields an operating potential as high as 4.0 V in some cases [19, 123]. Nevertheless, most organic electrolytes have higher electric resistance (usually at least 20 times higher than aqueous electrolytes), smaller power capability (due to low solubility of ions in organic solvents), more complex production conditions (due to high requirement for dryness), higher cost, flammability and toxicity, which limits their wide application.

2.6.3 Ionic Liquids

Ionic liquids (ILs) [66, 71] are a class of organic salts of low melting point because of

no volatile organic solvent involved. Common ILs, including $AlCl_4^-$ and trifluoromethylsulfonate (triflate), require high temperature (usually > 60 ℃) to generate enough electric conductivity[19]. Other advantages of ILs are high thermal stability, high electrochemical stability over a large range of operating potentials, non-toxicity, non-flammability. The operating potentials are determined by the electrochemical stability of salts. However, ILs have similar limitations as organic electrolytes such as relatively low conductivity and power density.

2.7 Fabrication of Conducting Polymer Electrodes

A series of CPs have been extensively studied as potential materials for ES application, and the most widely investigated are polypyrrole (PPy), polyaniline (PAn) and polythiophene (PTh), as well as their derivatives[45]. The low ESR, high specific capacitance and low cost are major reasons for CPs to become promising candidates as advanced ES active materials.

2.7.1 Electrochemical Properties of Conducting Polymers

CPs have various physical and electrochemical properties depending on different chemical compositions and synthesis methods. Typical CPs for ES application are presented in Figure 2-10.

The doping (oxidation/reduction in some cases) of the CPs can result in the formation of p-typed or n-typed CPs with good electric conductivity[19], illustrated in Figure 2-8. Currently, three categories of CPs have been investigated: (1) linear type polymers

(e.g.Polyacetylene (PA)); (2) polyaromatic polymers (e.g. poly(*p*-phenylene) (PPP) and poly(p-phenylenevinylene) (PPV)); (3) polyheterocyclic polymers (e.g. polypyrrole (PPy) and polythiophene (PTh)).

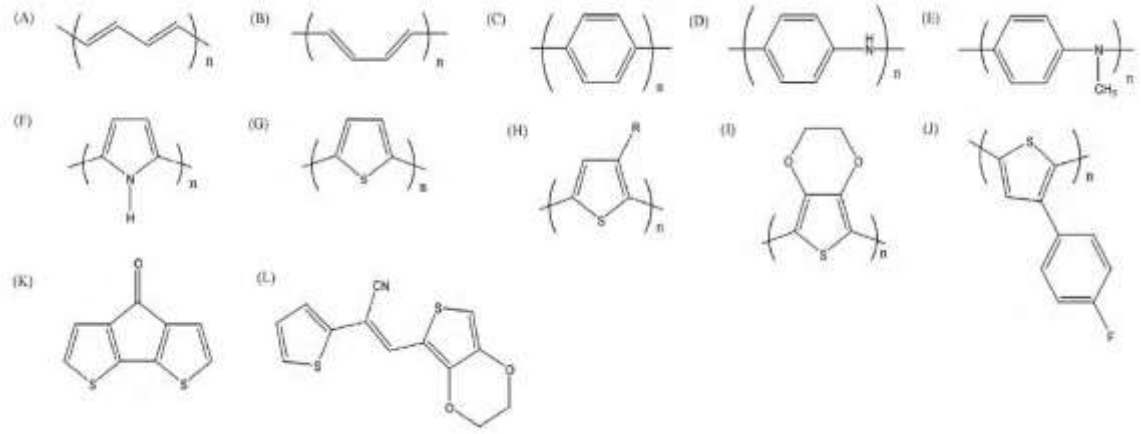

Figure 2-10 Common CPs or monomers. (A) *trans*- and (B) *cis*-poly(acetylene), (C) poly(p-phenylene), (D) polyaniline (PAn), (E) poly(n-methylaniline), (F) polypyrrole, (G) polythiophene, (H) 3-substituted polythiophene, (I) poly(3,4-ethylenedioxylthiophene), (J) poly(3-(4-fluorophenyl)thiophene), (K) poly(cyclopenta[2,1-b;3,4-b'-dithiphen-4-one]), (L) 1-cyano-2-(2-[3,4-ethylenedioxylthienyl]-1-(2-thienyl)vinylene).[45]

The conductivity of typical CPs is given in Table 2-7. The conductivity of CPs is dependent on doping density, mobility of electrons and/or other charge carriers (solitons, polarons and bipolarons), chemical environment (in bulk or in solvent) and doping temperature. For example, polyacetylene (PA) has relatively low electric conductivities of 10^{-10}-10^{-8} S cm^{-1}, while heavily iodine-doped PA reaches 10^{4} S cm^{-1}[124], higher than liquid mercury.

Table 2-7 Conductivity and doping type of typical CPs[125]

polymer	maximum conductivity	type of doping
polyacetylene	200-1000	n, p
polyparaphenylene	500	n, p
polyparaphenylene sulfide	3-300	p
polyparaphenylene vinylene	1-1000	p
polypyrrole	40-200	p
polythiophene	10-100	p
polyisothianaphthene	1-50	p

Since early 1980's, several mechanisms[125-129] have been proposed to elaborate the intra-/inter-molecular charge transfers, which are extremely vital in understanding the formation of electric conductivity of CPs. Currently, it is widely accepted that the structural defects such as solitons (single radical), polarons (single cation/anion with one charge) and bipolarons (two separated polarons) are the main sources of charge carriers in delocalized π-conjugated systems in the CP molecules (usually along chain backbones)[129]. These defects can transfer between inter-molecules via electron hopping. The CP molecules of the ground state produce the structural defects in the polymer backbone. The defects can then move along π-conjugated system via rearrangement of electron cloud, causing alternating change in single and double bonds. The possible structures of PPy in the ground state ((a) aromatic and (b) quinoid) and the charge carrier defects ((c, left) soliton, (c, right) polaron, (d) bipolaron) are shown in Figure 2-11.The charge carrier defects can move along PPy backbone. Figure 2-12 shows a typical charge carrier defect (polaron) moving along backbone, with corresponding energy shiftof polymer segment rearrangement between two thermodynamic stability states (α & γ)[125].

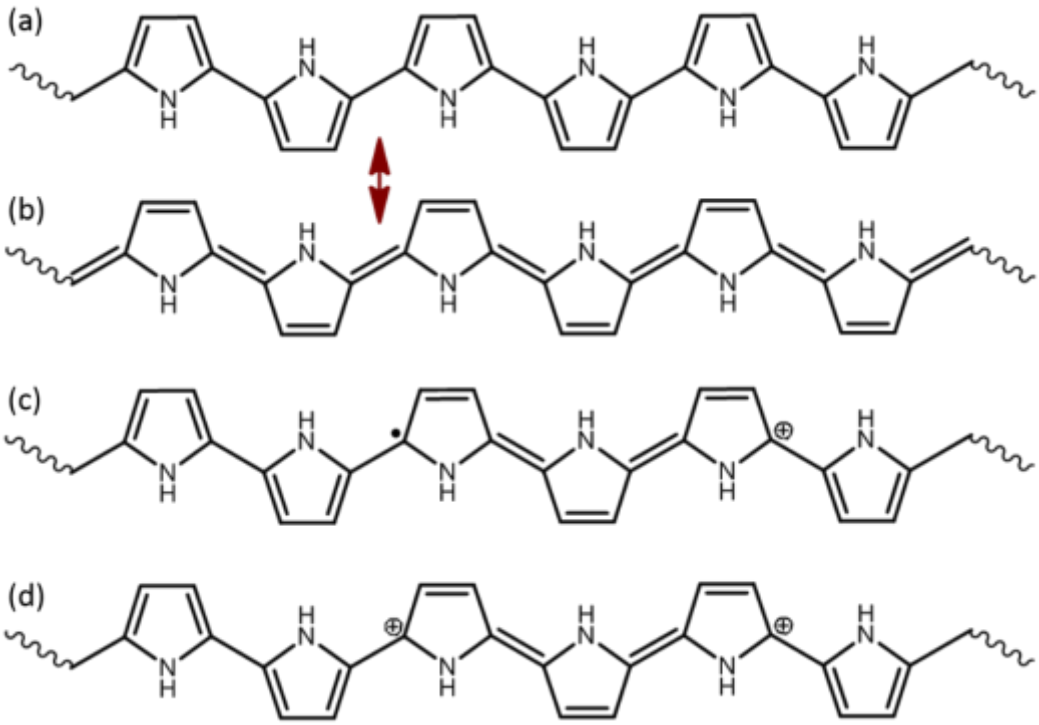

Figure 2-11 Chemical structures of PPy at ground state. (a) aromatic and (b) quinoid) and with charge carrier defects ((c) soliton & polaron and (d) bipolaron.[125, 129, 130]

Since the electric conductivity of CPs comes from charge carriers moving along π-conjugated systems, breakdowns of such systems (termed degradation) will definitely result in reduced conductivity. Such degradation in the backbone of CPs may be originated from two factors [131, 132]. Extrinsic degradation is caused by external environmental oxidants such as oxygen and water attacking charged sites of the polymer segment by nucleophilic or electrophilic mechanism. Intrinsic degradation is related to thermodynamic stability of pristine CPs. Polyheterocyclic CPs such as PPy have enhanced stabilities in the extrinsic degradation, because oxidants react preferentially at the nitrogen atoms on PPy without breaking the π-conjugation. In air, PTh has similar properties as PPy. However, in

the presence of water, PTh experiences apparent loss in capacitance because of breaking down of conjugation caused by irreversible reactions[131].Besides, PPy chains have better stability against intrinsic degradation than linear type polymers due to its relatively strong intermolecular π-π stacking.

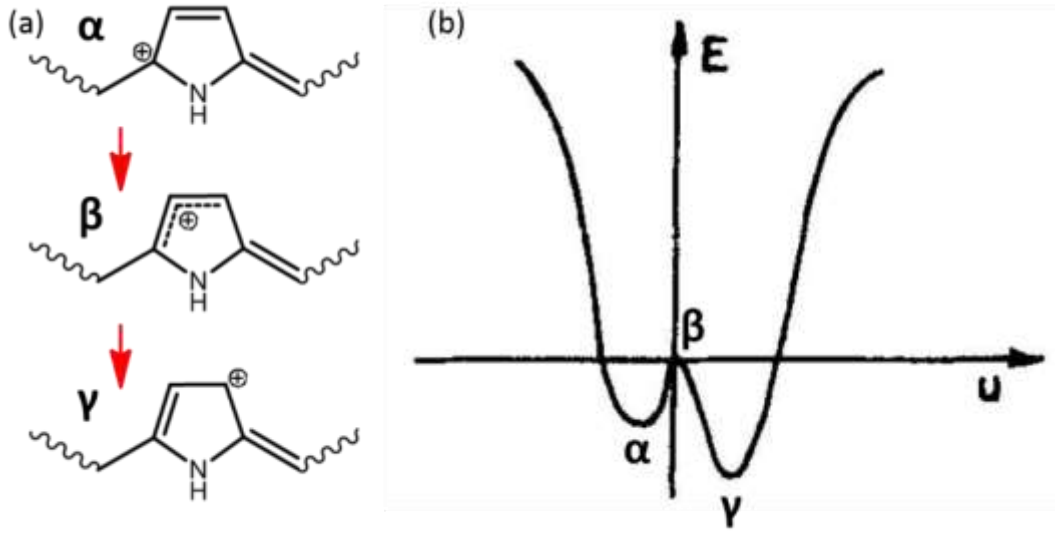

Figure 2-12 (a) A charge carrier defect (positive charge) moves along intra-molecular PPy chain and (b) corresponding energy variation. *E* – Energy; *u* – Distortion parameter. [133]

The electrochemical capacitance[19] of CP-based ES is formed from reversible redox reaction, switching between ground (insulating) state and charged (conductive) state, as shown in Figure 2-8. That is, when a positive potential is applied to the electrode, PPy lose electrons and transform to oxidized state, yielding polymeric salts with adsorbed anions at the electrode/electrolyte interface. When a negative potential is applied to the electrode, PPy obtain electrons and transform to neutral state, releasing anions to the bulk electrolyte.

2.7.2 Fabrication Methods

Various synthesis methods for fabrication of CPs have been investigated. CPs are conducting materials and can be regarded as cationic or anionic polymeric salts depending on n-type or p-type doping process. They can be polymerized by electrochemical deposition onto electrode from oxidation of monomer via applied potential. CPs can also be synthesized by typical chemical polymerization methods with proper oxidant. Commonly used are electrochemical polymerization(or deposition)[134, 135] and chemical polymerization (or precipitation)[136, 137], while they are also widely applied in fabricating metal oxide based ES [138, 139].Other synthesis methods such as emulsion polymerization[140], layer-by-layer assembly[141] and vapor deposition[142], have also been investigated recently.

2.7.3 Synthesis of Polypyrrole and Polypyrrole Based Composites

Among common heterocyclic polymers such as PAn, PPy, PTh and their derivatives, PPy [143]attract extensive attentions as ES active materials for the ease of polymer fabrication, high water solubility, high electrical conductivity, high capacitance, high resistance to degradation, high thermodynamic stability and low cost[39, 105]. PPy and PPy-based composite materials can be synthesized mainly by electrochemical deposition (polymerization) and chemical polymerization. In some cases, certain template materials are occupied in synthesis of CPs with ordered structures [144].

2.7.3.1 Electrochemical Synthesis

Electrochemical synthesis (polymerization) [130]has been long investigated and widely employed as the fabrication method for PPy films. The reasons include in-situ simultaneous deposition of polymer at electrode surface, ease and precise control of thickness, morphology and composition of synthesized film via such modifying parameters as deposition potential/current density, concentration of monomer/additive, properties of electrode/electrolyte, etc.

As shown in Figure 2-13, the steps involved in the electrochemical polymerization process include the oxidization of Py monomer[145] at electrode surface and the formation of polymer salts with incorporation of counter ions to maintain charge balance in the polymer backbone. According to the literature [146], the typical number of periodic units sharing one charge can range from 2.5 to 4.0 for oxidized state of PPy segment, which corresponds to a doping level of 0.25 to 0.4.

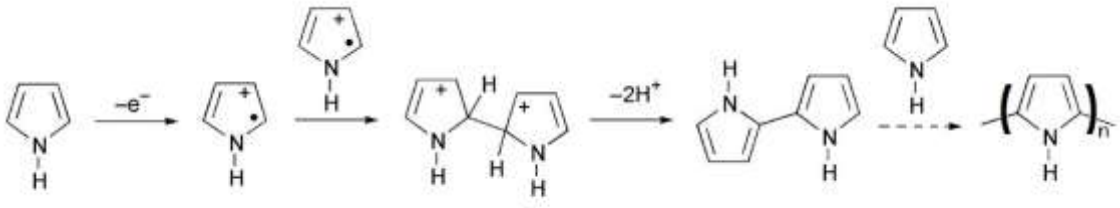

Figure 2-13 Mechanism of polymerization from Py monomer to PPy [145]

Various processes are available for electrochemical polymerization of deposited PPy films, i.e. potentiostatic (constant applied potential)[147], galvanostatic (constant applied current)[148], potentiodynamic [149] and pulse electro-deposition[150, 151], among which pulse electro-deposition is regarded as an ideal method towards fabricating uniform PPy

films with good surface morphology.

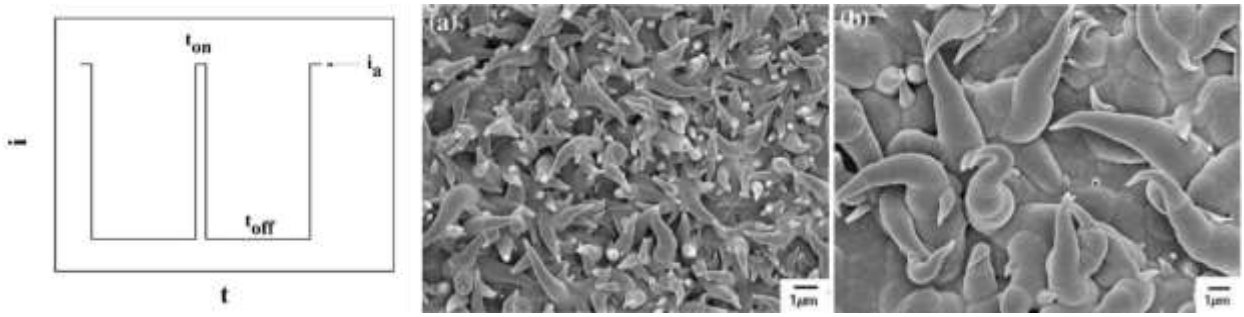

Figure 2-14(Left) Schematic diagram of mechanism of fabrication of PPy film via pulse electro-deposition. t_{on} – deposition time; t_{off} – rest time. (Right) SEM images of (a) PGM-PPy film and (b) GM-PPy film [152]

The morphology of synthesized PPy is greatly controlled by applied current [153]. During the synthesis of PPy films by oxidization, Py monomer is supplied by solution. With consumption at the electrode/electrolyte interface, there exists a concentration gradient at the interface, which drives diffusion of the monomer from solution to electrode surface. Because the diffusion is a relatively slow process compared to polymerization, microstructural defects across the film are not uniform because of presence of the monomer concentration gradient during the deposition [154]. However, when rest time periods are applied, i.e. so-called pulse electro-deposition, monomers have sufficient time to diffuse onto the IHP (Figure 2-4) and homogeneous PPy films can be produced[150]. As shown in Figure 2-14, the PPy film prepared by pulse galvanostatic method (PGM-PPy) has better homogeneous surface and increased porosity than the film by normal galvanostatic method (GM-PPy).

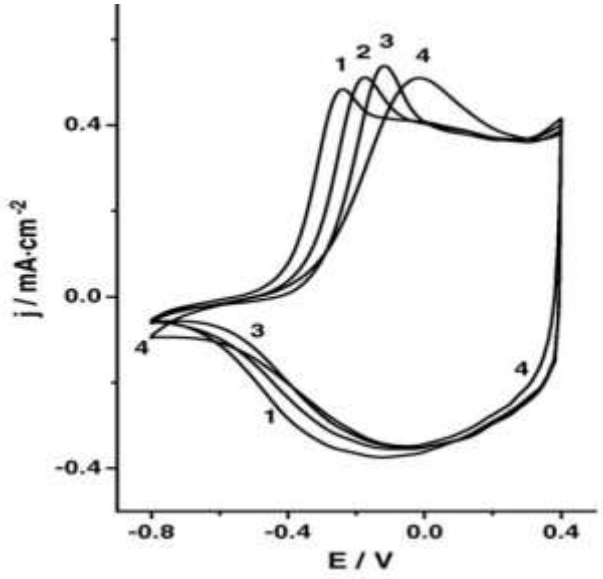

Figure 2-15 Cyclic voltammetry diagram of the PPy films at a scan rate of 5 mV s^{-1} measured in (1) $LiNO_3$, (2) LiCl, (3) LiBr and (4)$LiClO_4$ aqueous solution. [155]

The nature of counter ions (anionic dopants) is of particular importance in electrochemical behaviors of the synthesized PPy. Dopant anions, such as $Cl^-, Br^-, I^-, SO_4^{2-}, ClO_4^-$, $CF_3SO_3^-$, etc. have strong impact on the redox performance, film morphology, capacitance and electric conductivity. J. Tamm[155]compared the different anions ($Cl^-, Br^-, NO_3^-, ClO_4^-$) and revealed that the redox activity of PPy film is affected by size and mobility of the dopant anions in electrolyte, as shown in Figure 2-15.

Temperature also has a minor effect on the morphology and electric conductivity of PPy. At higher temperatures, the diffusions of monomer and additives are faster, leading to higher quality homogeneous PPy films. S.U. Rahman[156] investigated the temperature effect on Py electro-polymerization on mild substrate immersed in oxalic acid electrolyte. In alkaline medium, high temperature was favored for high quality films. In acidic medium, however, lower reaction temperature was favoured. Increased oscillations in electrode potential were observed at high temperature due to competition of iron dissolution and Py

oxidation.

The solvent for electrochemical deposition of CPs should undoubtedly be chemically inert to electrodes, monomer and other additives, which are used in fabricating the composite materials. PPy can be synthesized in aqueous solutions, while PTh can only be synthesized in organic solvents. In addition, Pan is usually synthesized in acidic aqueous solutions. Different solvents, including aqueous, organic and mixed solvents, were tried for PPy. D. Pletcher [157]found that the electric conductivity of PPy from aqueous solution was higher than that from aprotic solvent such as AN.

It should be pointed out that the electrochemical synthesis of PPy also faces great challenges in application. Firstly, it is difficult to separate film from electrode for further use. Direct use of the PPy deposited electrode decrease the whole capacitance due to incorporation of non-contributing component. Side reactions between the current-collector metal and other components could also occur. Secondly, although PPy has an acceptable level of electric conductivity initially, the conductivity decreases in electrochemical deposition. This is because as-synthesized PPy layer decreases the rate of charge transfer, preventing film from growing thicker and making mass production of the films difficult. Thirdly, it is also difficult to further modify and/or functionalize the synthesized PPy film. Fourthly, electrochemical synthesized PPy thick film showed swelling during cycling, which resulted in adhesion (to current collector) loss, increased impedance and poor cycling stability, as discussed in previous researches [158] of our group.

2.7.3.2 Chemical Synthesis

The chemical synthesis of PPy[159] has been investigated for decades. The mechanism of chemical polymerization of Py is quite similar to that of electrochemical polymerization. The major difference is the presence of chemical oxidants in the chemical synthesis. Its advantages include ease for mass production, high material loading of electrode, and options to modify CP backbone covalently, which make the chemical synthesis promising in industrial application.

As discussed previously, solvent and dopant, as well as temperature, are important factors in the electrochemical synthesis of PPy. These factors are also important in the chemical synthesis of PPy. The nature of oxidant greatly affects the morphology and electrochemical properties of PPy in the chemical synthesis [130]. According to literatures, common oxidants for CPs are peroxydisulfate anions ($S_2O_8^{2-}$), ferric cations (Fe^{3+}) and copper cations (Cu^{2+}) [160, 161]. In acidic conditions, other oxidants, i.e. ferrous cations (Fe^{2+}) [162], permanganate (MnO_4^-) [163] , dichromate($Cr_2O_7^{2-}$)[164], can also be involved in chemical synthesis of CPs. Together with incorporated additives (dopants), these oxidants determine the electric conductivity of PPy, as listed in Table 2-8. Although PPy synthesized with ferric cations give high conductivity, it might be partly contributed by the high level of iron cation residue in the PPy powder. These cations would escape from the PPy matrix after several C-D cycles, leading to a reduction in capacitance. As a result, ammonium persulfate is a preferable choice for chemical polymerization of PPy and is employed in this research.

Typical processes for chemical polymerization of CP powders include emulsion

polymerization, layer-by-layer assembly and solution polymerization. For example, Q. Wang [165]used ultrasonically initiated in-situ emulsion polymerization of n-butyl acrylate (BA) and methyl methacrylate (MMA) and prepared CP-encapsulated CNT, as shown in Figure 2-16. J. Joo [166] fabricated PPy/montmorillonite composites via emulsion polymerization with dodecylbenzenesulfonic acid (DBSA) as dopant. A typical layer-by-layer assembly method is alternating dipping substrate in monomer solution and oxidant solution. It is proven to be effective in preparation of thin-film PPy[141].

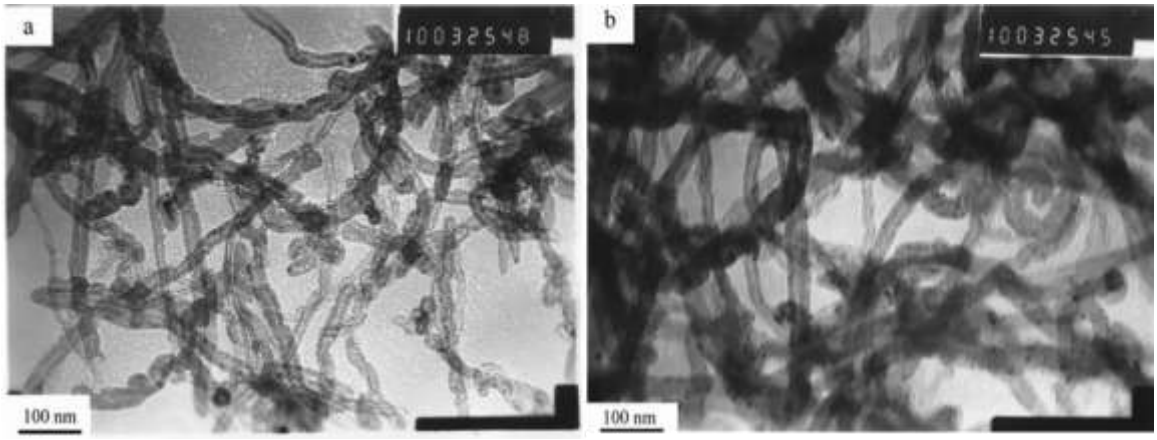

Figure 2-16 TEM images of (a) raw MWCNTs and (b) PBA-encapsulated MWCNTs after Soxhlet extraction for 72 h with acetone.[165]

The nature of dopant is particularly important in ES performance[39].The introduction of mild dopants increases CP's conductivity; however, strong dopants also induce irreversible degradation through introducing new functional groups to the polymer backbone, resulting in loss of π-conjugation [131].As shown in Table. 2-8, with variation of dopant additives, the conductivity of PPy synthesized differs in three magnitudes. As reported by G. Wallace's group[167], aromatic dopants promote preferred orientation of Py ring parallel to the current collector or growth surface and resulted in enhanced PPy

conductivity. In addition, ion exchange between electrolyte and PPy may bring about the replacements of dopants in PPy matrix by anions from electrolyte, resulting in swelling of bulky PPy and reduction in specific capacitance, especially when the dopant molecule is small. In contrast, the use of large dopant molecules in PPy offer the advantage of their reduced movement during ion exchange, reduced PPy swelling and enhanced cycling stability[168].

Table 2-8 Common oxidants for chemical synthesis of PPy [161]

Yield and conductivity of PPy samples prepared under various conditions [a]

Oxidant (mol dm^{-3})	Additive (mol dm^{-3})	Yield (g)	Conductivity (S cm^{-1})
$(NH_4)_2S_2O_8$ (0.1)		1.36	4.42
$(NH_4)_2S_2O_8$ (0.1)	NaDBS (0.0225)	2.01	0.570
$(NH_4)_2S_2O_8$ (0.1)	NaANS (0.024)	1.91	0.221
$Fe_2(SO_4)_3$ (0.1)		1.28	1.33
$Fe_2(SO_4)_3$ (0.05) $(NH_4)_2S_2O_8$ (0.05)	NaDBS (0.0225)	2.46	20.4
$Fe_2(SO_4)_3$ (0.1)	NaDBS (0.0225)	2.44	26.1
$Fe_2(SO_4)_3$ (0.1)	NaANS (0.024)	2.65	15.7
$Fe_2(SO_4)_3$ (0.1)	NaAS (0.022)	2.24	40.7

[a] Polymerization time, 60 min; polymerization temperature, 25 °C; pyrrole monomer concentration, 0.375 mol dm^{-3}; solvent, 200 dm^3 of deionized water; NaDBS, sodium dodecylbenzenesulfonate; NaANS, sodium alkylnaphthalenesulfonate; NaAS, sodium alkylsulfonate.

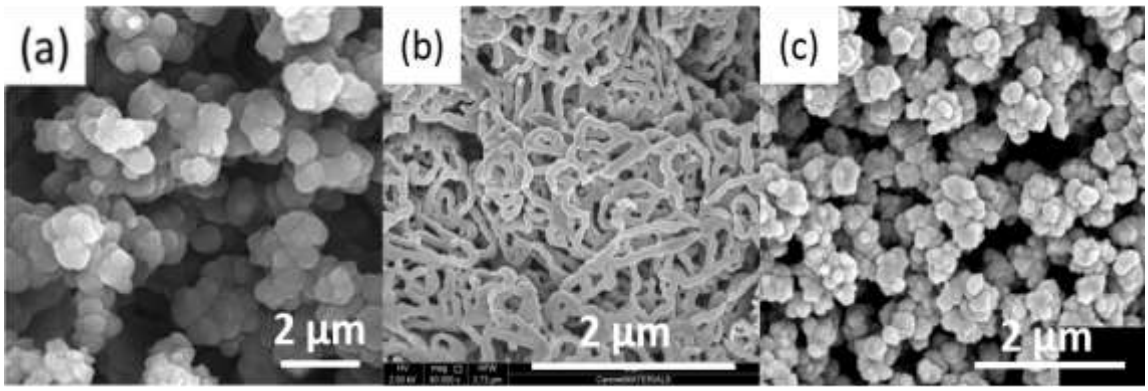

Figure 2-17 SEM images of (a) PPy powder without dopant [169], (b) PPy powder with CTAB as dopant [170], and (c) PPy powder with CHR as dopant [171].

As also discussed in many other literatures [169, 172], dopant anions have significant influence on the micro-morphology of PPy, including variations PPy size and shape (Figure 2-17), which have great impact on the electrochemical performance. Particularly, anionic dopants with several charged groups tend to link to different polymer chains, benefiting inter-chain mobility of charge carriers (mainly polaron and bipolaron) and increasing the bulky conductivity. However, as mentioned above in the PPy synthesis, dopants occupying different anionic groups, such as $–SO_3^-$, $-COO^-$ and phosphate anions, have been reported individually without a fundamental comparative study on their difference performance as dopants.

3 Objectives

The overall objective of this thesis work is to develop advanced electrodes for electrochemical supercapacitor (ES). The specific tasks include

- Dopants: develop advanced anionic dopants and investigate influences of the dopant structures on PPy.
- Chemical synthesis: develop advanced PPy powders of controlled morphology through chemical synthesis, potential for mass production.
- Electrodes: deposit PPy on high-porosity current collectors, achieving high mass loading and advanced electrochemical properties.
- Advanced active materials: incorporate MWCNT with good dispersing agent /multifunctional dopant and fabricate advanced PPy/MWCNT composite materials for ES application with improved morphology and enhanced electrochemical behaviors.

4 Approach and Methodology

4.1 Approach

PPy powders were fabricated by chemical synthesis of Py monomer at the presence of dopant anions, with ammonium peroxydisulfate ($(NH_4)_2S_2O_8$, APS) as oxidant. The product was fabricated as electrochemical materials for ES electrode and studied in aspect of morphology and electrochemical behaviors.

MWCNTs were incorporated to fabricate composite MWCNTs/PPy materials as mechanical reinforcement for excellent electric conductivity that allows fast charge/discharge (high power density). The composite materials were fabricated by chemical synthesis of Py monomer at the presence of dopant anions and MWCNTs suspension, with APS as oxidant. Similarly, the product was studied physically and electrochemically.

4.2 Methodology

4.2.1 Advanced Polyaromatic Dopants for PPy Synthesis

According to the discussion of chemical polymerization of PPy Chapter 2, several conclusions could be achieved.

- Anionic dopants have significant effects on morphology (size & shape) and electrochemical properties of PPy.
- Anionic dopants with several charged groups act as inter-chain linkage, resulting in improved PPy stability and enhanced electronic conductivity.

- Large-size anionic dopants benefit reduced PPy swelling and improved PPy stability.
- Aromatic anionic dopants promote preferred orientation of Py ring and resulted in enhanced PPy conductivity.

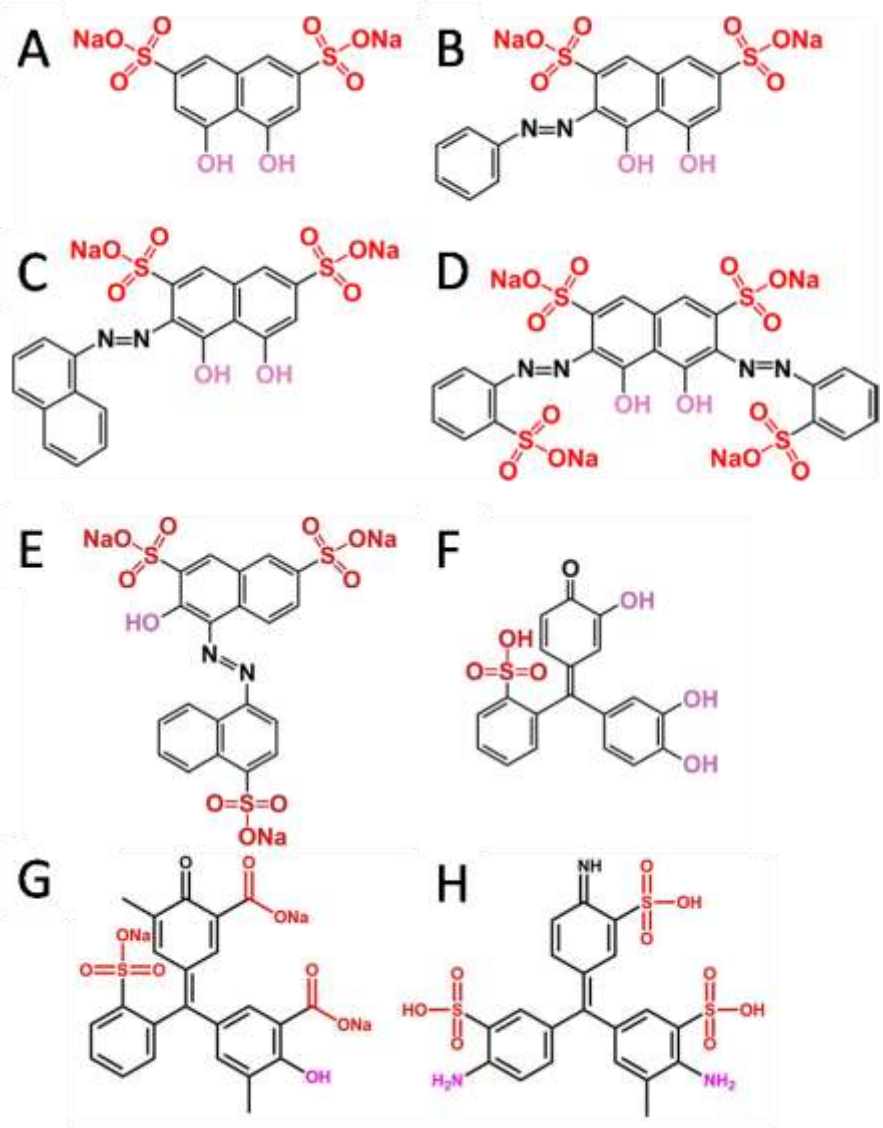

Figure 4-1 Molecular structures of dopants used in this research. (A) CHR, (B) CHR-P, (C) CHR-N, (D) CHR-BS, (E) amaranth, (F) PV, (G) ECR and (H) AF.

As a result, large polyaromatic dopants with several charged groups are expected to benefit PPy with enhanced electrochemical performances. In my research, chromotropic acid disodium salt (CHR) families, including chromotropic acid disodium salt (CHR), 2-(phenylazo)chromotropic acid disodium salt (CHR-P), 2-(1-naphthyldiazenyl)chromotropic acid disodium salt (CHR-N) and 2,7-Bis(2-sulfophenylazo)chromotropic acid tetrasodium salt(CHR-BS), with their molecular structures shown below in Figure 4-1(A-D), were employed as anionic dopants for PPy synthesis.

As shown in Figure 4-1, the CHR families are anionic dopants which can be used for PPy synthesis. They contains large aromatic structures and have good solubility in water; they differ each other in molecular weight/size and charge group numbers. As a result, the analysis of electron microscopy data and electrochemical performance of corresponding PPy potentially provide an insight into the influence of dopant structure, size and charge on the PPy morphology and electrochemical performance of PPy electrodes.

Besides the CHR families, other polyaromatic dopants, such as amaranth, pyrocatechol violet (PV), eriochrome cyanine R (ECR) and acid fuchsin (AF) are also employed in this research for in-depth investigation of dopants for advanced PPy based ES.

High mass loadings of PPy on current collectors are of critical importance for the fabrication of ES. Previous studies show that severe deduction in conductivity and capacitance are observed when thick layer of PPy is electrochemically synthesized on electrode substrate. In this research, PPy is chemically polymerized and tested in high mass loadings.

4.2.2 Advanced PPy/MWCNT Composite Materials

The conductivity of PPy in ES, as mentioned above, could be enhanced by the use of large aromatic anionic dopants with several charged groups. In addition, the conductivity of PPy could also be based on the development of MWCNTs/PPy composite materials. However, the major problem in utilizing MWCNT for the fabrication of MWCNTs reinforced PPy is poor dispersion of MWCNT. Early reports shows that treatment of acids will introduce charged groups to the surface of MWCNT and result in better dispersing performance. Nevertheless, the functionalized surface will definitely introduce defects on the MWCNT sidewalls and sacrifice the conductivity.

In this research, anionic surfactant could be used for preparation of stable MWCNTs dispersion. It is found that π-π stacking and electrostatic adsorption between aromatic anionic dopants and the sidewalls of MWCNTs, which avoids MWCNT aggregation and provides mono-dispersed MWCNT for good uniformity of downstream PPy coating. High quality MWCNTs dispersion (stable for 3 months) is achieved by using anionic surfactants in this research, without sacrificing loss of conductivity of MWCNTs. A group of aromatic dopants for PPy based ES meet the requirement of good dispersant of MWCNT, indicating that such dopants, which could be named as multifunctional dopants, are capable of preparing MWCNT dispersion and PPy synthesis. In this research, PV, ECR and AF are used as potential multifunctional dopants.

5 Experimental Procedures

5.1 Materials Preparation

All chemicals involved in this research were listed below in Table 5.1.

Table 5-1 Chemicals involved in fabrication of PPy and PPy based composite materials electrode for advanced ES application.

Category	Chemical Name	Source
Monomer	Pyrrole (**Py**) (> 98%)	Sigma Aldrich (Canada)
Oxidant	Ammonium peroxydisulfate (**APS**)	Sigma Aldrich (Canada)
Dopant	Chromotropic acid disodium salt (**CHR**)	Alfa Aesar (USA)
	2-(phenylazo)chromotropic acid disodium salt (**CHR-P**)	Sigma Aldrich (Canada)
	2-(1-naphthyldiazenyl)chromotropic acid disodium salt (**CHR-N**)	Sigma Aldrich (Canada)
	2,7-Bis(2-sulfophenylazo)chromotropic acid tetrasodium salt (**CHR-BS**)	Alfa Aesar (USA)
	Amaranth	Sigma Aldrich (Canada)
Multi-functional dopant	Pyrocatechol violet (**PV**)	Sigma Aldrich (Canada)
	Eriochrome cyanine R (**ECR**)	Sigma Aldrich (Canada)
	Acid fuchsin (**AF**)	Sigma Aldrich (Canada)
Additive	Multi-walled carbon nanotubes (**MWCNTs**)	Bayer Inc. (Canada)
Electrolyte salt	Sodium sulfate (**Na_2SO_4**)	Sigma Aldrich (Canada)
Current collector	Nickel foam (porosity ~95%)	Vale (Canada)

5.2 Chemical Synthesis of PPy Powder and PPy/CNT Composite Materials

For chemical synthesis of PPy powders (see Figure 5-1(a)), Py monomer (0.05 M in final solution) was dissolved in deionized water with different dopant (0.005M in final solution). The solution was cooled down to 4 ℃by an ice-water bath and mechanical agitated for 15 min. After aqueous APS solution (0.15 M in final solution, excessive amount) was dropped in the system, the reaction was processed with ultra-sonication (or magnetic stirring) for 2 hrs and the temperature was kept at 4 ℃ during the procedures. PPy precipitates were vacuum filtered and thoroughly washed with efficient deionized water, and then dried at 60 ℃ for 24 hrs in air. The final bulks were grinded into fine powders and stored in a box dryer.

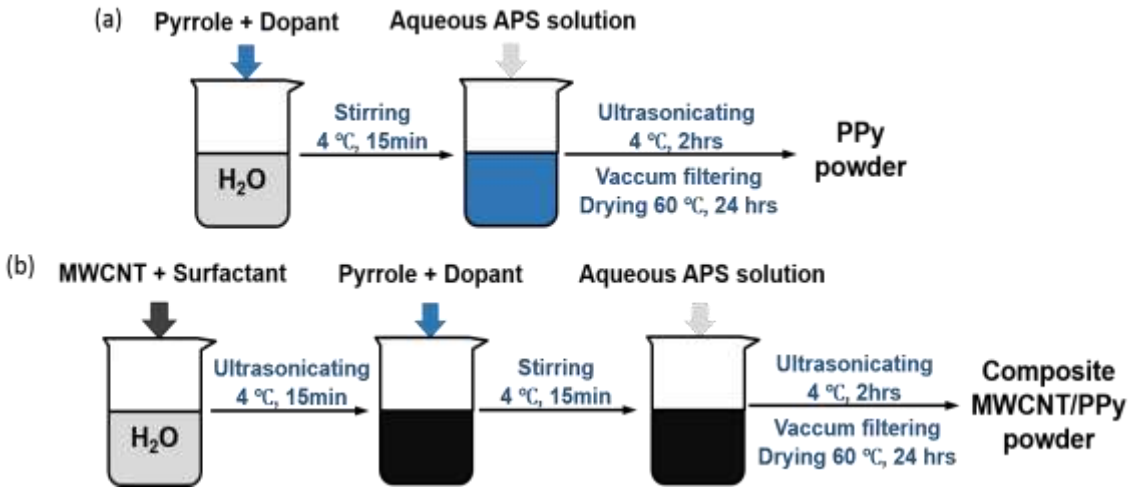

Figure 5-1 Schematic diagram of chemical synthesis of (a) PPy powder and (b) PPy/MWCNT composite materials.

For chemical synthesis of PPy/MWCNT composite materials (see Figure 5-1(b)), certain amount (determined by the PPy/MWCNT mass ratio in the composite product) of MWCNT with different surfactant (or multifunctional dopant) was added to deionized

water. Homogeneous suspension of MWCNT was obtained via 15 min ultrasonication, followed by addition of Py monomer (0.05 M in final solution) and corresponding dopant. The following steps were similar to those of synthesis of PPy powder.

5.3 Fabrication of Devices

To prepare the test electrode for electrochemical test, 1.0×1.5 cm^2 rectangle Nickel foam (Ni-foam) with active area of 1.0 cm^2 was impregnated by certain amount of PPy or PPy based composites slurry, which was prepared with active materials and ethanol. After heat treated at 60 ℃ for 24 hrs to evaporate the solvent, the infiltrated foam was then pressed to 30 % of the initial thickness, and fabricated into test electrode with incorporation of essential copper wires and insulated boxing materials, as shown in Figure 5-2(a). In different investigations, the mass loading of the test electrode varied in the range of 18-40 mg cm^{-2}, depending on the density or porosity of active materials.

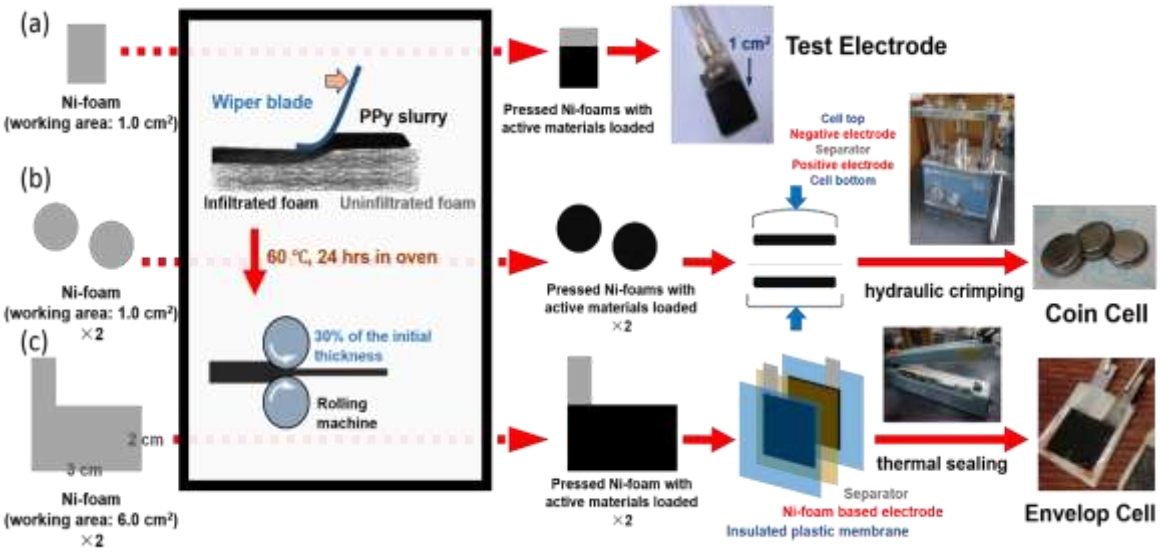

Figure 5-2 Schematic diagram of fabrication of (a) the test electrode, (b) coin cell device and (c) envelope cell device.

In this study, coin cell and envelope cell were utilized as device for practical applicability test. Coin cell device (see Figure 5-2(b)) was prepared from two pressed Ni-foams with active materials loaded on one side of the foam. After thoroughly infiltrated with 0.5 M or saturated sodium sulfate aqueous electrolyte, the two electrodes was loaded into a special mold with a commercial porous separator between and sealed together with a hydraulic crimping machine (MSK-110, MTI Corporation, USA). The preparation process of envelope cell device was similar to that of coin cell, except for the incorporation of ultra-thin plastic membrane as boxing materials, rather than coin cell mold (see Figure 5-2(c)). Compared to traditional coin cell, the design of envelop cell allowed higher mass & capacitance loading, designable electrode area & shape and smaller volume in size, making it promising as energy storage device.

5.4 Characterization

5.4.1 Morphology Characterization

The morphology of PPy powders and PPy/MWCNT composite materials was investigated using a JEOL JSM-7000F Scanning Electron Microscope (SEM) under magnification in the range of 10,000-80,000X (highest magnification was not always available for limited electric conductivity of samples), and Osiris field emission transmission electron microscope (TEM/STEM) with various detectors, i.e. high angle annular dark field (HAADF), electron energy loss spectroscopy (EELS), and energy dispersive X-ray spectroscopy (EDS).

5.4.2 Electrochemical Characterization

The electrochemical behaviors of the test electrodes were investigated using Potentiostat (PATSTAT 2273, Princeton Applied Research), controlled by computer software of PowerSuite, or VersaStat, controlled by corresponding software. Electrochemical investigations of the single test electrode were carried out using a standard three electrode electrochemical cell, with 0.5 M sodium sulfate aqueous solution as electrolyte (deaerated by 99.995% nitrogen gas flow before and during test), platinum gauze as counter electrode and a standard calomel electrode (SCE) as reference electrode.

For comparison, Cyclic Voltammetry (CV) results were obtained from a voltage window from -0.5 to 0.4 V vs. SCE, at scan rates of 2-100 mV s^{-1}. The specific capacitance (SC) was calculated by dividing half the integrated area of the CV curve (=amount of charge gained in charging process + amount of charge released in discharging process) by the mass m (or working area S) and the width of potential window ΔV, as shown below:

$$C_m = \frac{Q}{m\Delta V} = \frac{t}{m\Delta V}\bar{I} = \frac{1}{m} * \frac{1}{\Delta V/t} * \frac{1}{2(V_2 - V_1)} \int_{V_1}^{V_2} I(V)\delta V \cdots\cdots (5\text{-}1)$$

Rearranged into:

$$C_m = \frac{1}{2mv\Delta V} \int_{V_1}^{V_2} I(V)\delta V \text{ , } C_S = \frac{1}{2Sv\Delta V} \int_{V_1}^{V_2} I(V)\delta V \cdots\cdots\cdots (5\text{-}2)$$

Where C_m (C_s) are mass (area) normalized capacitance, respectively; v is the potential variation rate; V_1 and V_2 are two ends of potential window, so $\Delta V = V_2 - V_1$.

Electrochemical Impedance Spectroscopy (EIS) was applied in this research. The alternating current (AC) complex impedance Z*=Z'-*i*Z" was analyzed in the frequency range of 10 mHz -100 kHz at the amplitude of the AC signal of 5 mV. The complex capacitance [173] C*=C'-*i*C" was calculated from the impedance data as:

$$C_S' = \frac{Z''}{\omega S|Z|^2}, C_S'' = \frac{Z'}{\omega S|Z|^2} \quad \text{(5-3)}$$

Where $|Z^*|^2 = (Z')^2 + (Z'')^2$; ω=2π*f*, and *f* is the frequency of AC power supply.

The charge-discharge (C-D) behavior of the two electrode cells (coin cells and envelope cells) was investigated using battery analyzers (BST8-MA & BST8-3, MTI Corporation, USA). The SC of two electrode cells during galvanostatic cycles was calculated as:

$$C_m = \frac{It_d}{m\Delta V}, C_S = \frac{It_d}{S\Delta V} \quad \text{(5-4)}$$

Where t_d is the time of discharge process. To draw the Ragone Plot, the corresponding energy density and power density can be calculated according to Equation 2-3 and 2-4.

6 Results and Discussion

6.1 Characterization of Chemical Polymerization of PPy Doped with Chromotrope Family

In order to understand the influence of dopant structure, size and charge on the PPy morphology and electrochemical performance of PPy electrodes, chromotrope families, including CHR, CHR-P, CHR-N and CHR-BS are investigated as anionic dopants for chemical polymerization of PPy.

The chemical polymerization of PPy with chromotrope family as dopant is accomplished in process shown in Figure 5-1(a).

6.1.1 Morphology Characterization

The morphologies of chemically polymerized PPy from 0.05 M Py solutions with chromotrope family as dopants were characterized by SEM, as shown in Figure 6-1. The chemical structures of corresponding dopants are depicted in Figure 4-1(A-D).

It was found from the SEM images that the morphologies of PPy powders, prepared by chemical synthesis, are greatly influenced by the dopants. The size of primary PPy particles prepared using CHR was in the range of 50-150 nm. The corresponding powders showed severe agglomeration of such primary particles, shown in Figure 4-1(A). Comparatively, the SEM images of PPy powders doped with CHR-P and CHR-N showed smaller size of the primary particles; however, the particle agglomeration still forms. The SEM image of sample prepared using CHR-BS showed non-agglomerated particles, with

average size lower than 50 nm.

In summary, the PPy powders showed sphere structures with diameters in the range of ~20-150 nm, indicating chemical polymerization with chromotrope family as dopants a promising method for fabrication of PPy nano-particles. PPy powders prepared using dopant with large size and more charges revealed small particle size and poor tendency to agglomerate. It is possible that anionic dopant with larger size/aromatic structures and charge provides enhanced dispersion of PPy particles during chemical synthesis.

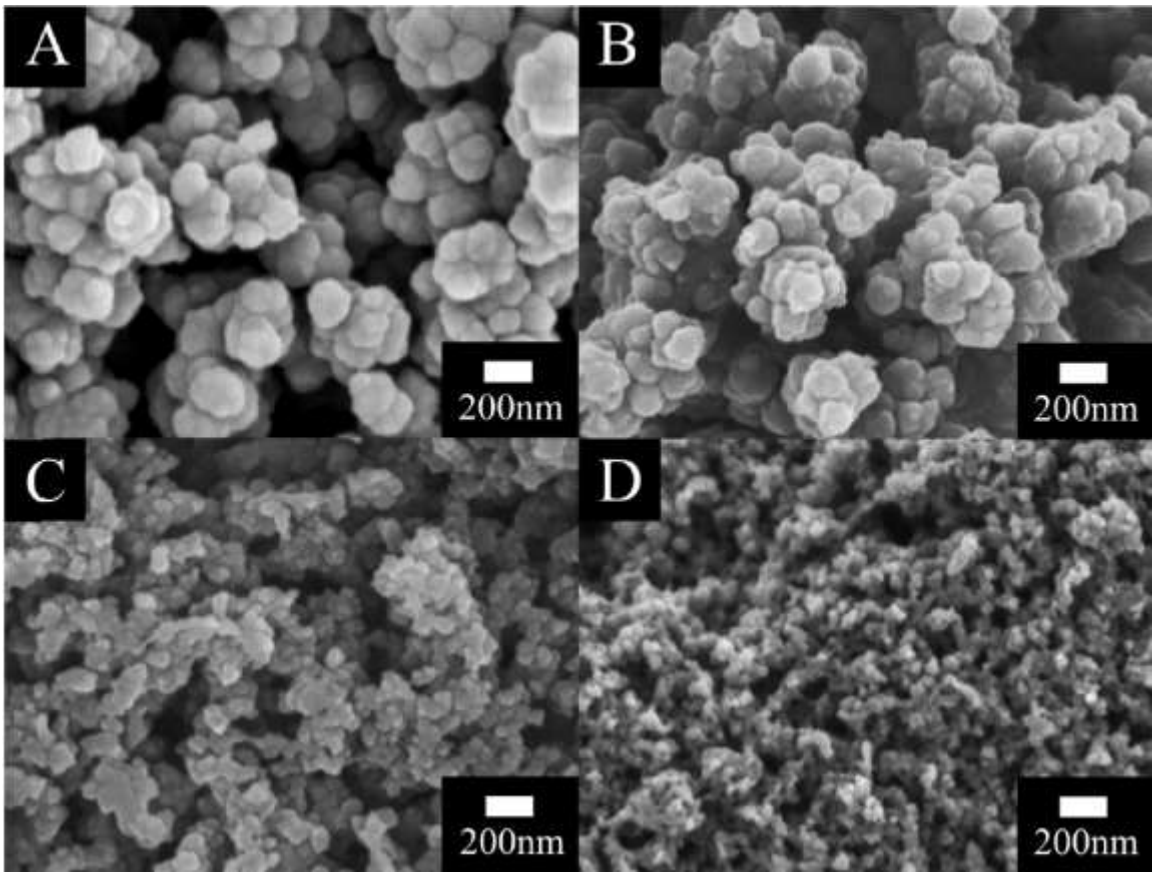

Figure 6-1 SEM images of PPy powders doped with (A) CHR, (B) CHR-P, (C) CHR-N and (D) CHR-BS. [171]

6.1.2 CV and Capacitance of PPy Doped with Chromotrope Family

The Cyclic Voltammetry (CV) tests were carried out according to the descriptions in Chapter 5.4.2 and depicted below in Figure 6-2.

As mentioned in Chapter 4.2.1, though high SC and low impedance have been accomplished in earlier researches with thin PPy film, it is important to fabricate ES electrode with > 10 mg cm^{-2} active material loading for practical applications [174]. In this research, ES electrodes with 20-40 mg cm^{-2} PPy loading were prepared and investigated. The CV cycles were obtained from single PPy electrode with mass loading of 30 mg cm^{-2} and depicted in Figure 6-2.

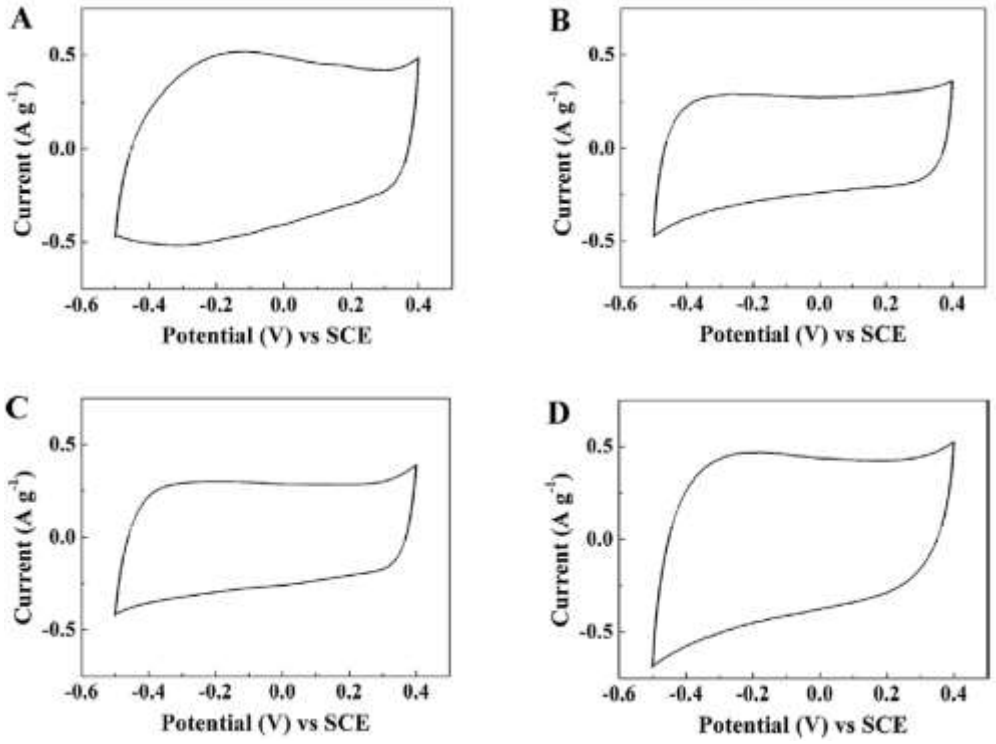

Figure 6-2 CVs of PPy electrodes, prepared using dopant (A) CHR, (B) CHR-P, (C) CHR-N and (D) CHR-BS, at mass loading of 30 mg cm^{-2} and scan rate of 2 mV s^{-1}. [171]

According to Equation 5-1, it is obvious that for an ideal capacitor, the capacitance value is constant, so the current value at different potential should be stable during CV scanning. The CV curve enclosed by individual charge and discharge curve showed nearly box shape, indicating good capacitive behavior of the prepared PPy electrode.

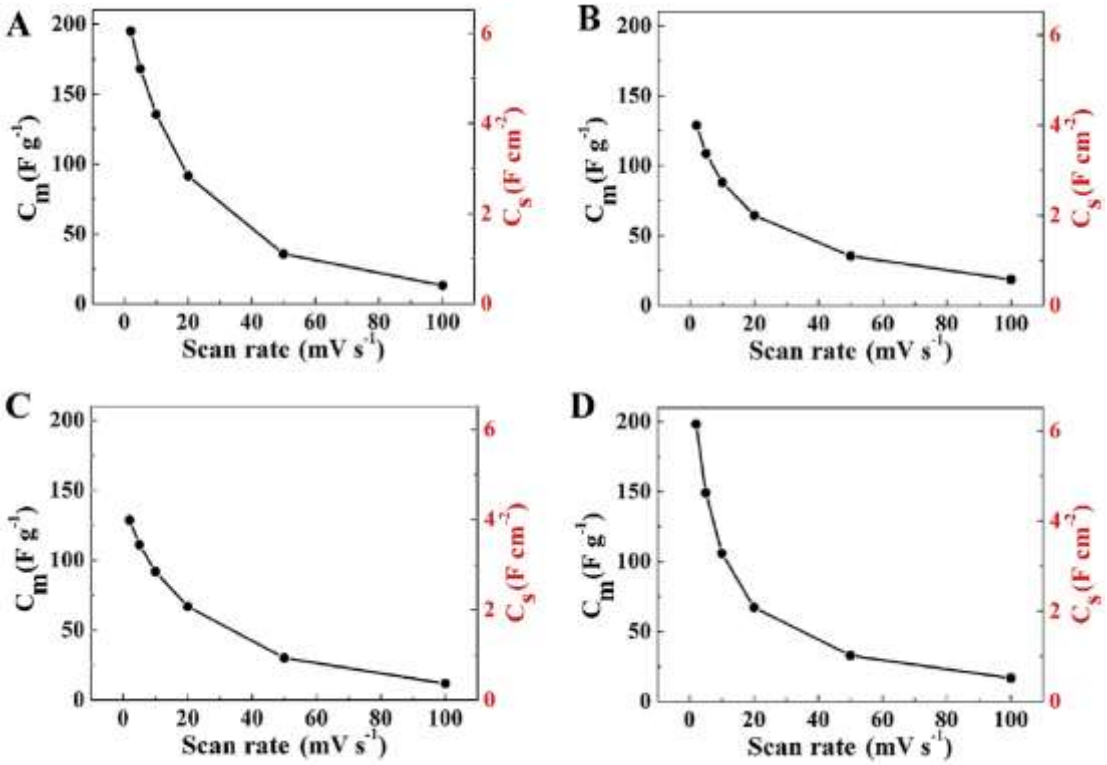

Figure 6-3 C_s and C_m vs. scan rate of PPy electrode, prepared using dopant (A) CHR, (B) CHR-P, (C) CHR-N and (D) CHR-BS, at mass loading of 30 mg cm^{-2}. [171]

The surface normalized capacitance C_s and mass normalized capacitance C_m were calculated from the same sample, according to Equation 5-2 and depicted in Figure 6-3. The C_m at a scan rate of 2 mV s^{-1} were found to be 195 F g^{-1}, 128.9 F g^{-1}, 128.6 F g^{-1}, 198.2 F g^{-1}, for PPy powders doped with CHR, CHR-P, CHR-N, CHR-BS, respectively.

As mentioned above, it is commonly reported that thick PPy layer with high mass

loading will lead to increased impedance and reduced capacitance. However, the C_m data in this research were comparable with the data for PPy thin film reported in earlier literature [175], indicating that the chemical synthesized PPy achieved the similar high capacitance behavior of electrochemical deposited PPy films. The PPy electrode had a relatively high mass loading of 30 mg cm^{-2}, which is two magnitudes higher than the thin PPy films (~0.3 mg cm^{-2}). As a result, the C_s values at a scan rate of 2 mV s^{-1}, were found to be as high as 5.9 F cm^{-1}, 3.9 F cm^{-1}, 3.9 F cm^{-1}, 6.0 F cm^{-1}, for PPy powders doped with CHR, CHR-P, CHR-N, CHR-BS, respectively. It is notable that few literatures have ever reported the achievement of C_s at 10^0 Fcm^{-1} level. The analysis of capacitance of PPy electrodes prepared using different dopants indicates that higher charge to mass ratio of CHR and CHR-BS contributed to high mobility of dopants in C-D cycles and allowed increased capacitance.

The EIS analysis provided an alternative to investigate the capacitance. The two parameters of the complex capacitance – real capacitance (C_s') and imaginary capacitance (C_s''), were obtained from the EIS data and depicted in Figure 6-4. At low frequency, the C_s' curves showed a continuous decrease and C_s'' showed an increase at first and then decrease, while at high frequency both C_s' and C_s'' for all the samples showed zero capacitance. At low frequency, the highest C_s data for PPy electrodes doped with CHR, CHR-P, CHR-N and CHR-BS were in the range of 1.55-1.75 F cm^{-2}, while the corresponding C_s'' curves showed no significant different in the low frequency capacitance.

At the same time scale, the real capacitance values derived from EIS data were much lower compared to the C_s data calculated from CVs (Figure 6-3). Such inconsistency in

capacitance can be illuminated by the different nature in capacitance testing of CV and EIS. It is often reported that low frequency AC capacitances of CPs are conventionally lower than the capacitance derived from CVs. It was suggested that some dopant anions can be immobile at low voltages in AC test and were not involved in the C-D cycles, but can become independent at higher voltages in CV test and contribute to the capacitance.

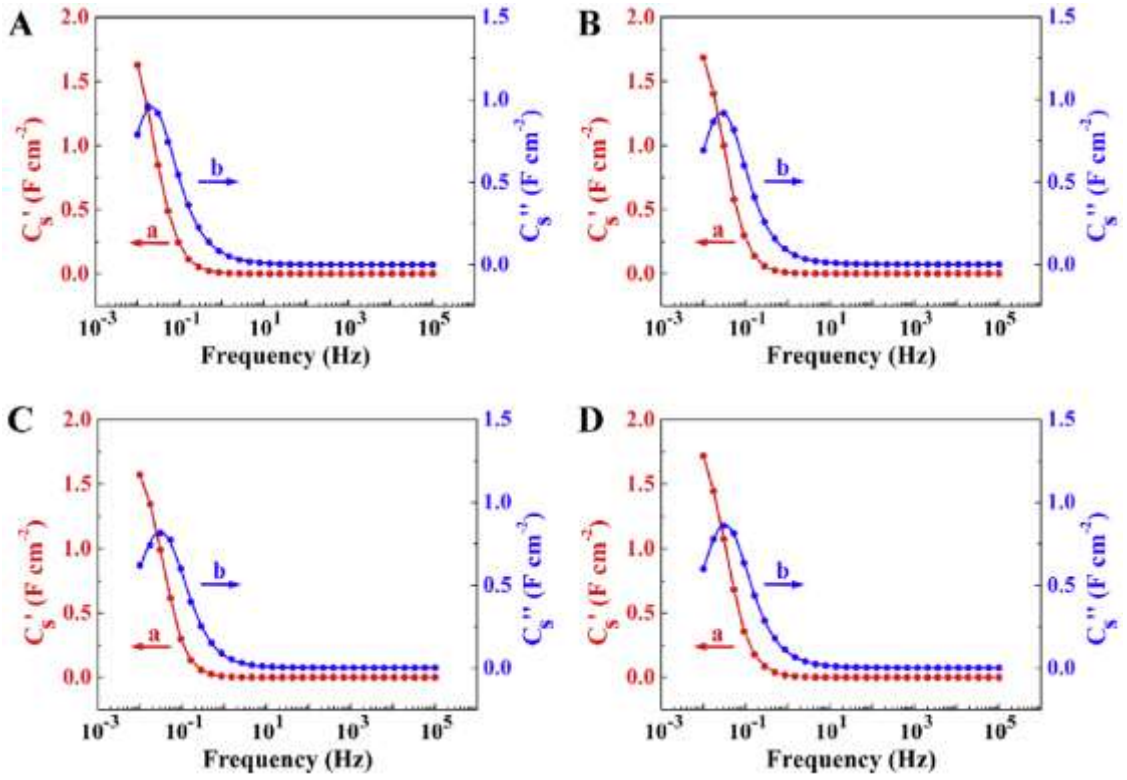

Figure 6-4 (a) C_s' and (b) C_s" vs. frequency of PPy electrodes prepared with (A) CHR, (B) CHR-P, (C) CHR-N and (D) CHR-BS, at mass loading of 30 mg cm^{-2}. [171]

Based on the previous C_m and C_s data (Figure 6-3), it was suggested that PPy powders, doped with CHR and CHR-BS, were promising active materials for advanced ES with high energy density. The dependence of capacitance on the mass loading were investigated and the data are depicted in Figure 6-5. It was found that the C_m values of both PPy powders

were relatively stable with PPy mass loading in the range of 20-40 mg cm^{-2}, indicating a desirable utilization of PPy materials even at a high mass loading of 40 mg cm^{-2}. As a result, the Cs values were found to increase in accordance with mass loading. The highest C_s of 6.9 mg cm^{-2} and 7.2 mg cm^{-2} were achieved from PPy powders prepared using CHR and CHR-BS, respectively.

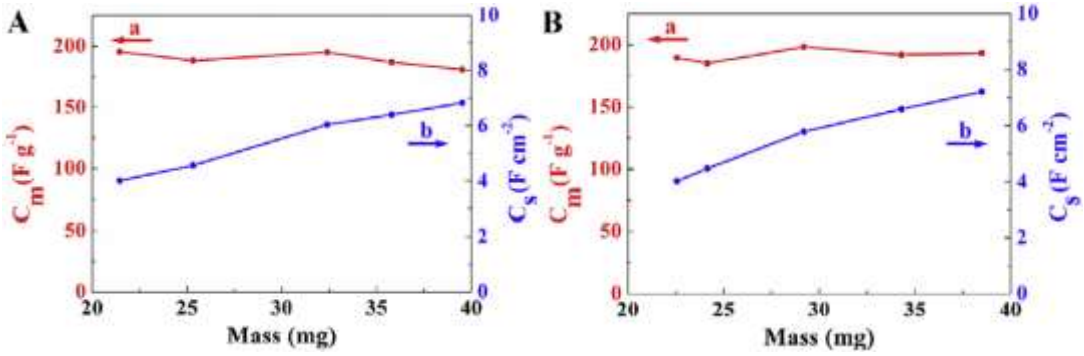

Figure 6-5 (a) C_m and (b) C_s vs. mass loading of PPy electrodes, prepared with (A) CHR, (B) CHR-BS, at a scan rate of 2 mV s^{-1}. [171]

6.1.3 Cycling Stability Test of PPy Doped with Chromotrope Family

Figure 6-6 compared the cycling stability of PPy electrodes prepared using CHR and CHR-BS, respectively. The figure was presented in the form of capacitance retention versus number of C-D cycles.

As mentioned above, good cycling stability is of critical importance for application of ES device. Earlier research reported severe capacitance reduction observed for PPy electrodes at high mass loading [174]. In this research, for the PPy electrode doped with CHR, the capacitance increased during the first 200 cycles and then gradually decreased to 100.4 % after 1000 cycle. For the PPy electrode doped with CHR-BS, a similar initial

increase in capacitance was observed during the first 200-300 cycles; however, it remained nearly constant during the following cycles, and finished with capacitance retention of 109.9 %. It is obvious that cycling stability is influenced by the nature of dopants.

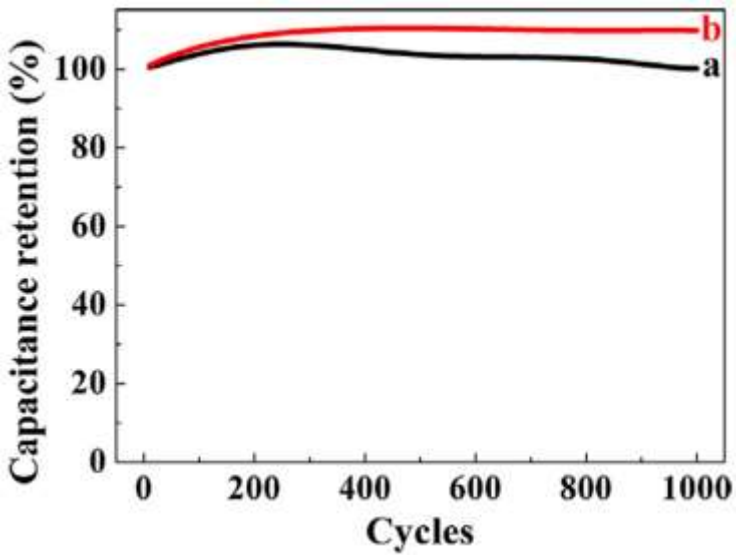

Figure 6-6 Capacitance retention vs. C-D cycle number for PPy electrode prepared with (a) CHR and (b) CHR-BS, for 1000 cycles at a scan rate of 50 mV s^{-1}. Values were derived from CV data. [171]

Although capacitance reduction was observed for PPy electrode doped with CHR in cycling test, the results showed that the capacitances of both the samples exceed 100 % after 1000 cycles, which is relatively good compared with previous investigations. The good capacitance stability was likely to result from the use of Ni foam as current collectors, which was supported the improved capacitance retention of Ni foam based PPy electrode prepared with CHR, compared to the thin-film PPy electrode with the same dopant [175]. In the previous research, plain Ni foil was used as current collector. The swelling and shrinking of thin-film PPy during C-D cycles led to poor mechanical stabilities, severe

detachment of active materials from current collectors and capacitance loss. In this research, Ni foam, which consists of micro-scale Ni matrix and has up to 95 % void space, was used as current collector. The micro-scale matrix supported impregnation of PPy powders, provided relatively good electrical conductivity between PPy and electrode base, and may help limit the swelling and shrinking of PPy, indicating Ni foam a promising current collector that could be used for fabrication of high-performance ES device.

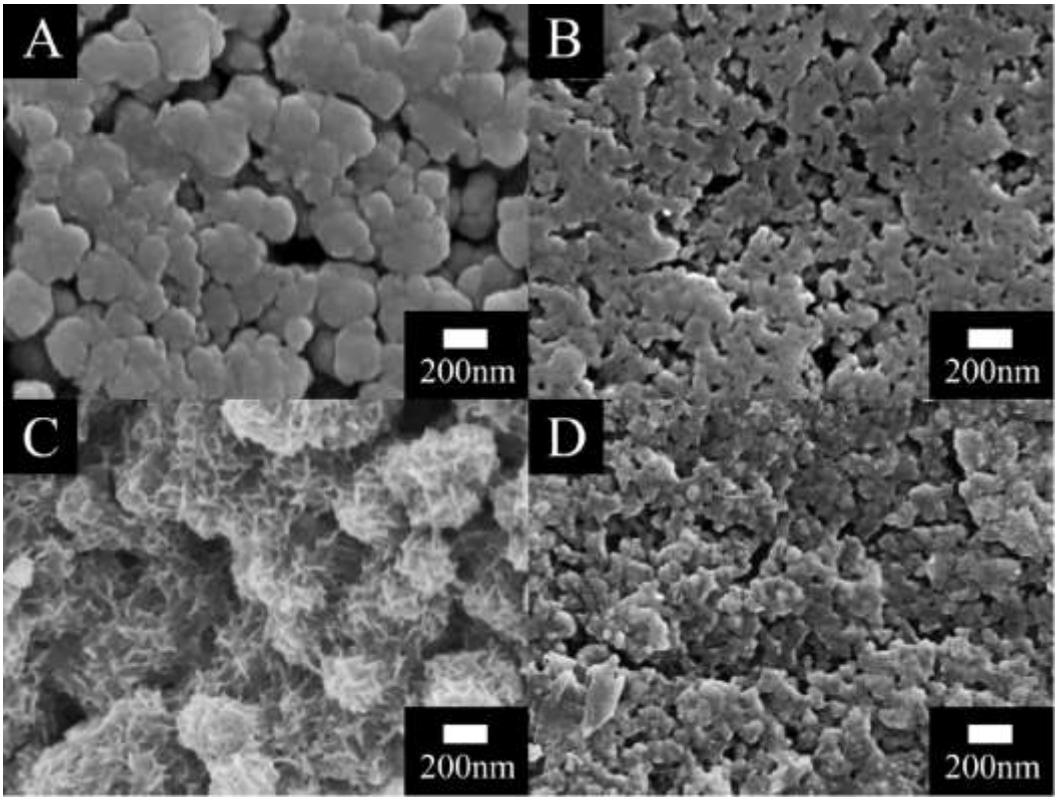

Figure 6-7 SEM images of PPy electrode doped with (A,C) CHR and (B,D) CHR-BS, scanned (A,B) before and (C,D) after cycling stability test. [171]

The SEM test of CHR and CHR-BS doped PPy electrodes before and after cycling tests, provided insights into the mechanisms of capacitance variation. The nanostructures of PPy powders doped with CHR and CHR-BS before test, shown in Figure 6-7(A,B), were

in accordance with the Figure 6-1(A,D). The PPy electrode, prepared with CHR, showed significant changes in surface morphology after 1000 C-D cycles. The increasing mesoporosity during cycling benefited ion exchange between anionic dopants and electrolyte anions, which led to a reduction of dopant content in active PPy materials and reduced capacitance, after 200 cycles (Figure 6-6(a)). For PPy electrode prepared with CHR-BS, the surface morphology after 1000 C-D cycles showed relatively small changes compared to the original sample.

Furthermore, the capacitance increase of both samples during the first hundreds of cycles (Figure 6-6) may be attributed to the variation in electrolyte infiltration into bulky PPy, which was likely to be enhanced by the microstructure change of PPy during the initial C-D cycles.

6.1.4 Device Test of PPy Doped with Chromotrope Family

The results presented above indicated that PPy electrode prepared with CHR-BS showed improved electrochemical performance compared to PPy electrode prepared with other three dopants in chromotrope family. As mentioned above, the improved electrochemical behaviors in microstructure and specific capacitance could be attributed to the high charge to mass ratio of CHR-BS.

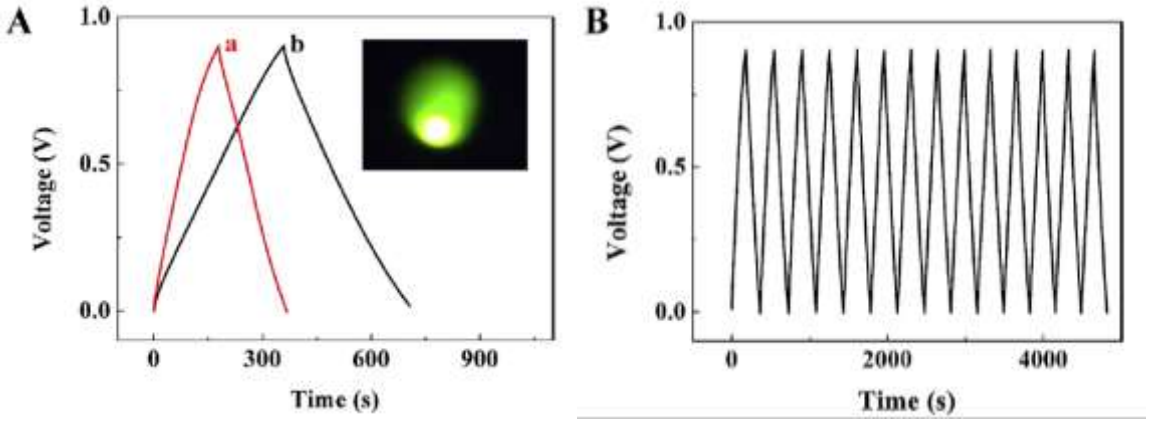

Figure 6-8 C-D cycle of a coin cell prepared with CHR-BS doped PPy powders at (A)(a) and (B) 0.5 A g^{-1}, and (A)(b) 0.2 A g^{-1}, inset (A) shows a 20 mA LED bulb powered by two coin cells. [171]

The PPy powder doped with CHR-BS was utilized to fabricate two-electrode coin cells. The C-D curves (Figure 6-8) showed nearly linear behavior at different current density and multiple-cycle test, indicating good capacitive performance of the PPy based ES.

The C-D behavior of the CHR-BS doped PPy based ES was further tested at different current densities, in the range of 0-0.7 A g^{-1}. The device capacitance was calculated from C-D data according to Equation 5.4, and depicted in Figure 6-9(A). The device C_m of PPy based ES was in the range of 55-62 F g^{-1}, at current density of 0-0.7 A g^{-1}. The C_m experienced a slight reduction with increasing current density, which can be attributed to the diffusion limitation of electrolyte in pores of the PPy bulk.

Figure 6-9(B) showed the cycling stability test result of the coin cell. The device capacitance showed a gradual decreasing trend with C-D cycles and relatively high capacitance retention of ~97 % was achieved at 1000 cycles, indicating the good stability

of ES prepared with CHR-BS doped PPy.

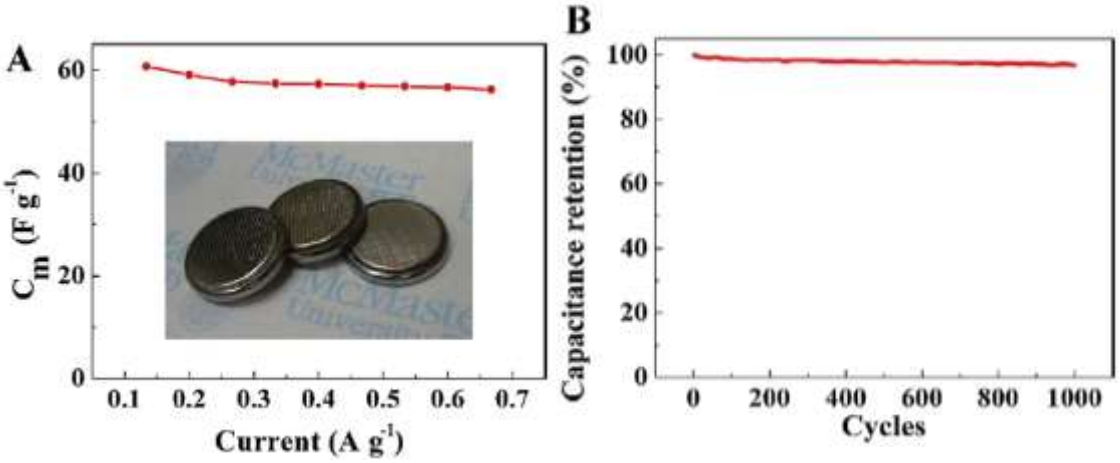

Figure 6-9 (A) C_m for coin cell based on CHR-BS doped PPy vs. current density, inset shows coin cells, (B) cycling stability test of the coin cell vs. C-D cycle number at current density of 0.7 A g^{-1}. [171]

6.1.5 Summary

In this research, CHR, CHR-P, CHR-N and CHR-BS were used as anionic dopants for chemical polymerization of PPy, which is used for fabrication of ES electrode. High SC was achieved at high PPy mass loadings; good capacitance retention in the range of 20-40 mg cm^{-2} showed promising application of PPy based ES electrode by using CHR and CHR-BS as dopants. The results suggested that PPy prepared with dopants of high charge/mass ratio and large molecular size benefited increased capacitance and improved cycling stability.

6.2 Chemical Polymerization of PPy/MWCNT Composite Doped with Amaranth

In the previous study, based on morphology and electrochemical analysis of CHR family based PPy electrode, we proposed a hypothesis that the dopant with high charge/mass ratio and large molecular size benefited increased capacitance and improved cycling stability. Moreover, though high SC was achieved for PPy based electrode at high mass loading and low scan rate (2 mV s^{-1}), severe capacitance reduction was observed with increasing scan rate, which critically limited the application of PPy based ES.

In this research, we used Amaranth (Figure 4.1(E)) as dopant for PPy synthesis. Similar to CHR-BS, Amaranth has relatively high charge/mass ratio and large molecular size, making it a promising anionic dopant for PPy synthesis. Moreover, the electroactive –N=N– group may help enhance the SC of the resultant PPy powders.

MWCNT was used in fabrication of PPy/MWCNT composite materials for ES application. As mentioned in Chapter 4.2.2, the use of MWCNT may increase the electrical conductivity of PPy electrode, which is important for good capacitance retention at high scan rate. However, MWCNT cannot form stable homogeneous dispersion in water, as shown in Figure 6-10(a) without additives, such as dispersant/surfactant. Experimental test showed that amaranth aqueous solution was not capable of dispersing MWCNT (Figure 6-10(b)(d)). In this research, pyrocatechol violet (PV), shown in Figure 4.1(F), act as dispersant for preparation of stable MWCNT dispersion, shown in Figure 6-10(c)(e).

In this research, amaranth and PV were used as dopant and MWCNT dispersant for chemical synthesis of PPy/MWCNT composite materials for ES use.

Figure 6-10 Dispersion performance test. (a) 1 g L^{-1} MWCNT in water, (b) 1 g L^{-1} amaranth aqueous solution, (c) 1 g L^{-1} PV aqueous solution, (d) 1 g L^{-1} MWCNT in 1 g L^{-1} amaranth aqueous solution, (e) 1 g L^{-1} MWCNT in 1 g L^{-1} PV aqueous solution, and (f) 1 g L^{-1} MWCNT in aqueous solution, containing 1 g L^{-1} amaranth and 1 g L^{-1} PV. [176]

6.2.1 Morphology Characterization

The microstructure of chemically polymerized PPy prepared with amaranth (Figure 5-1(a)) was characterized by SEM (Figure 6-11(A)). The size of the primary particles in the range of 30-50 nm was relatively small. However, agglomerations were mostly observed for such particles.

Figure 6-11(B) showed the SEM picture of PPy/MWCNT composite materials, prepared as shown in Figure 5-1(b). The microstructure analysis showed that PPy formed relatively uniform coating layer on the surface of mono-dispersed MWCNTs. It is suggested that mono-dispersed MWCNTs in aqueous solution and π-π interaction between

MWCNTs, and aromatic PPy and amaranth greatly promote the formation of uniform PPy/MWCNT composite nanowires.

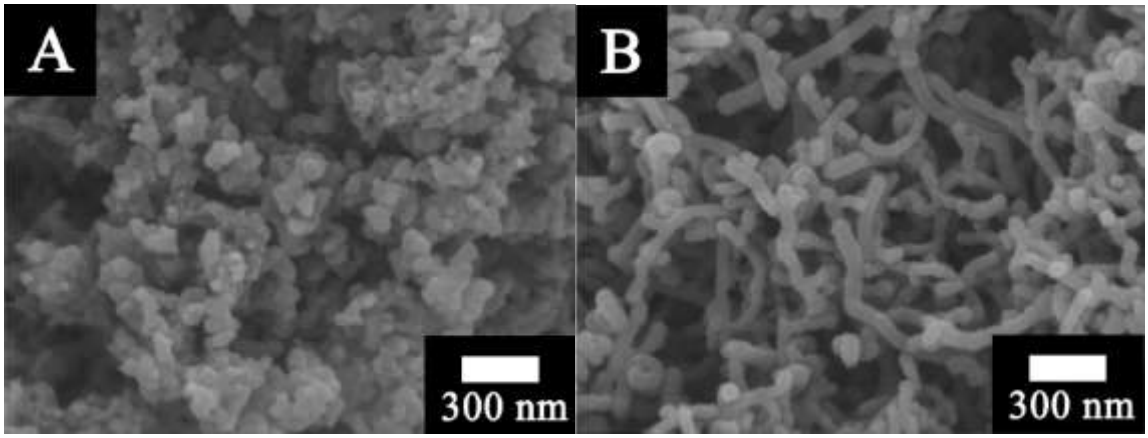

Figure 6-11 SEM figures of (A) PPy powder prepared with amaranth as dopant and (B) PPy/MWCNT composite materials with corresponding mass ratio of 7:3. [176]

Figure 6-12 Comparative sedimentation tests of (left) MWCNT and (right) PPy/MWCNT composite materials with PPy/MWCNT mass ratio of 7:3, at same concentration in aqueous solution. Pictures of samples (A) as prepared and (B) after a week. [176]

Figure 6-12 showed comparative sedimentation tests were carried out between MWCNT and the PPy/MWCNT composite materials in aqueous solutions. The observation

suggested that relatively stable MWCNT suspension could be prepared after PPy coating with amaranth dopant.

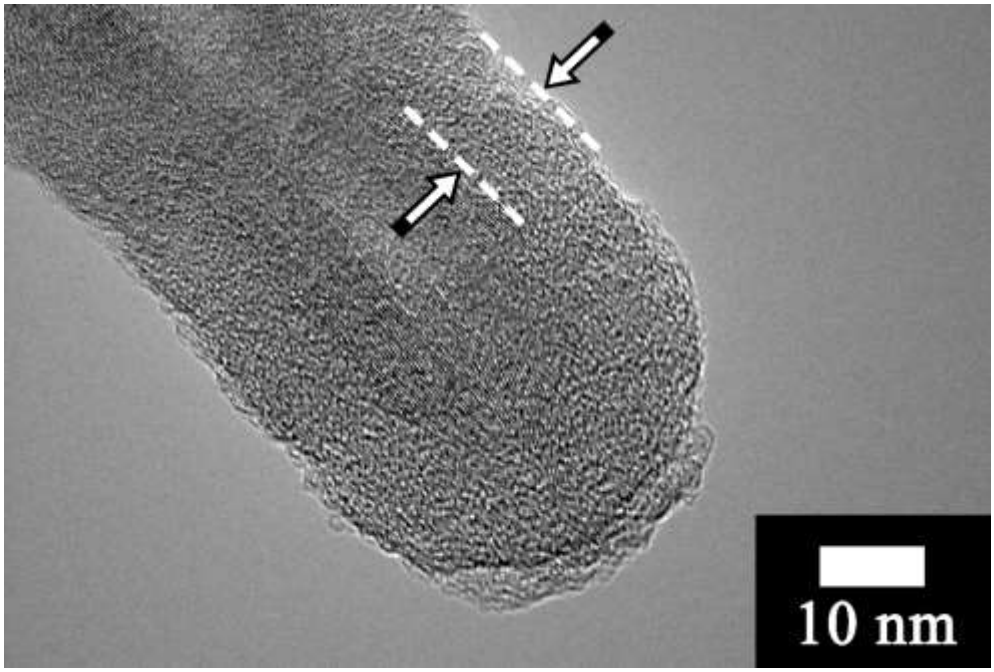

Figure 6-13 TEM image of PPy/MWCNT composite materials with PPy/MWCNT mass ratio of 7:3, arrows show PPy layer, coated outside MWCNT. [176]

In-depth investigation in microstructures of PPy/MWCNT was carried out by TEM testing, as shown in Figure 6-13 and Figure 6-14. The composite materials showed a MWCNT-PPy core-shell structures. TEM results indicated that the PPy layer was 10 nm in average, pointed out by arrows in Figure 6-13.

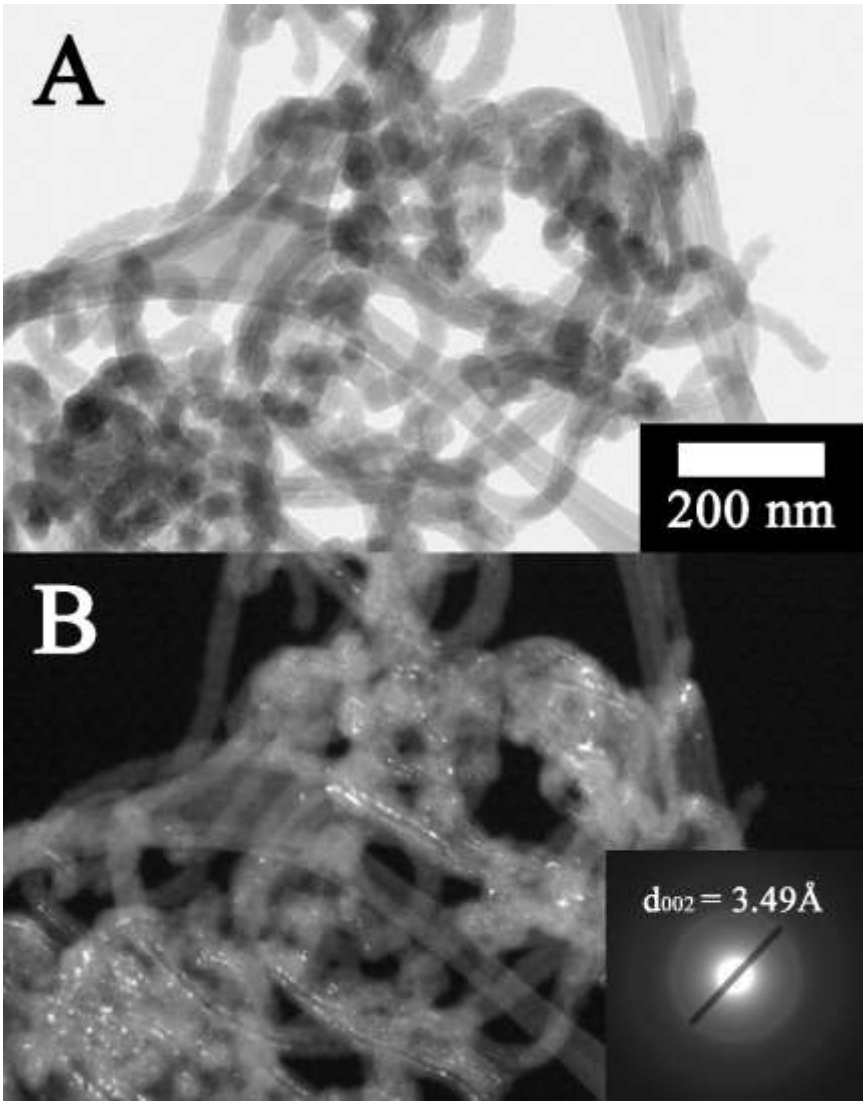

Figure 6-14 (A) The bright field image and (B) the dark field TEM image of the same area. Sample is PPy/MWCNT composite materials with PPy/MWCNT mass ratio of 7:3. The inset in B shows the selected area diffraction. [176]

The dark field image was obtained from TEM test. The interplanar d_{002} spacing measured from the diffraction data is 3.49 Å, which is in agreement with literature report [2***supporting2]. The TEM test results further supported the MWCNT-PPy core-shell structure of PPy/MWCNT composite materials.

6.2.2 CV and Capacitance of PPy and PPy/MWCNT Composite Materials Doped with Amaranth

The PPy powders with different amount of MWCNT addition were used for fabrication of ES electrodes. The Cyclic Voltammetry (CV) tests were carried out according to the descriptions in Chapter 5.4.2 and depicted below in Figure 6-15.

The active materials loading for electrode was ~29 mg cm^{-2}; the high mass electrode, as discussed in 4.2.1 and 6.1.2, was important for fabrication of ES for practical application. The results showed that ideal box shape CVs were observed for PPy electrode and PPy/MWCNT composite materials at a scan rate of 2 mV s^{-1}, shown in Figure 6-15(A). Such CVs showed that the use of amaranth as dopant promotes capacitive behavior for high mass loading electrode.

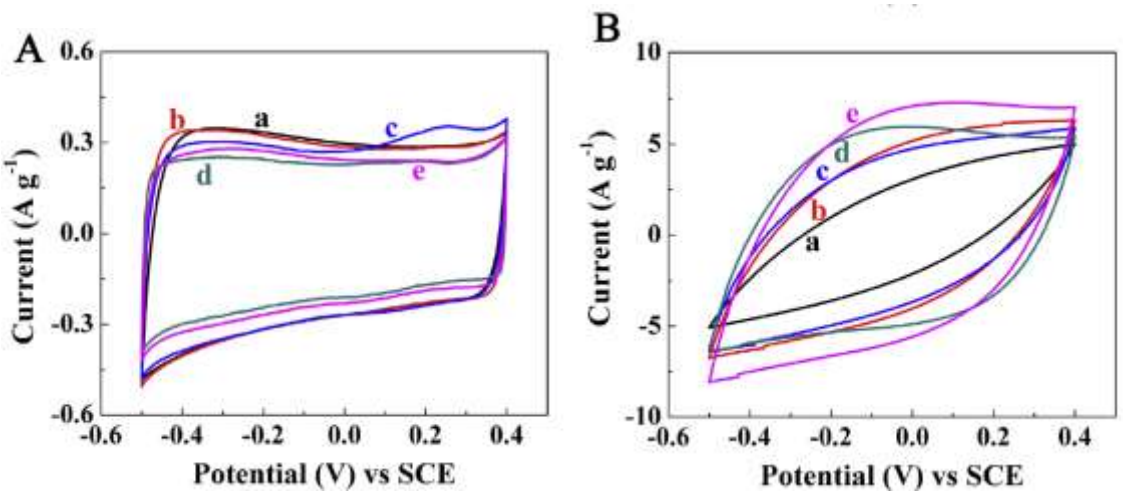

Figure 6-15 CVs of electrodes prepared with (a) PPy powders and PPy/MWCNT composite materials at PPy/MWCNT mass ratio of (b) 9:1, (c) 8:2, (d) 7:3 and (e) 6:4, at electrode mass loading of ~29 mg cm^{-2} and scan rate of (A) 2 mV s^{-1}, (B) 50 mV s^{-1}. [176]

However, the CVs at a high scan rate of 50 mV s-1 were quite different. The CV of pure PPy, shown in Figure 6-15B (a), showed a shallow leaf shape, deviating greatly from the ideal box shape. Comparatively, CV curves derived from PPy/MWCNT were relatively larger at the same scan rate, while the sample with PPy/MWCNT mass ratio of 7:3 held an approximately box shape, indicating the good capacitive behavior at high mass loading and high scan rate.

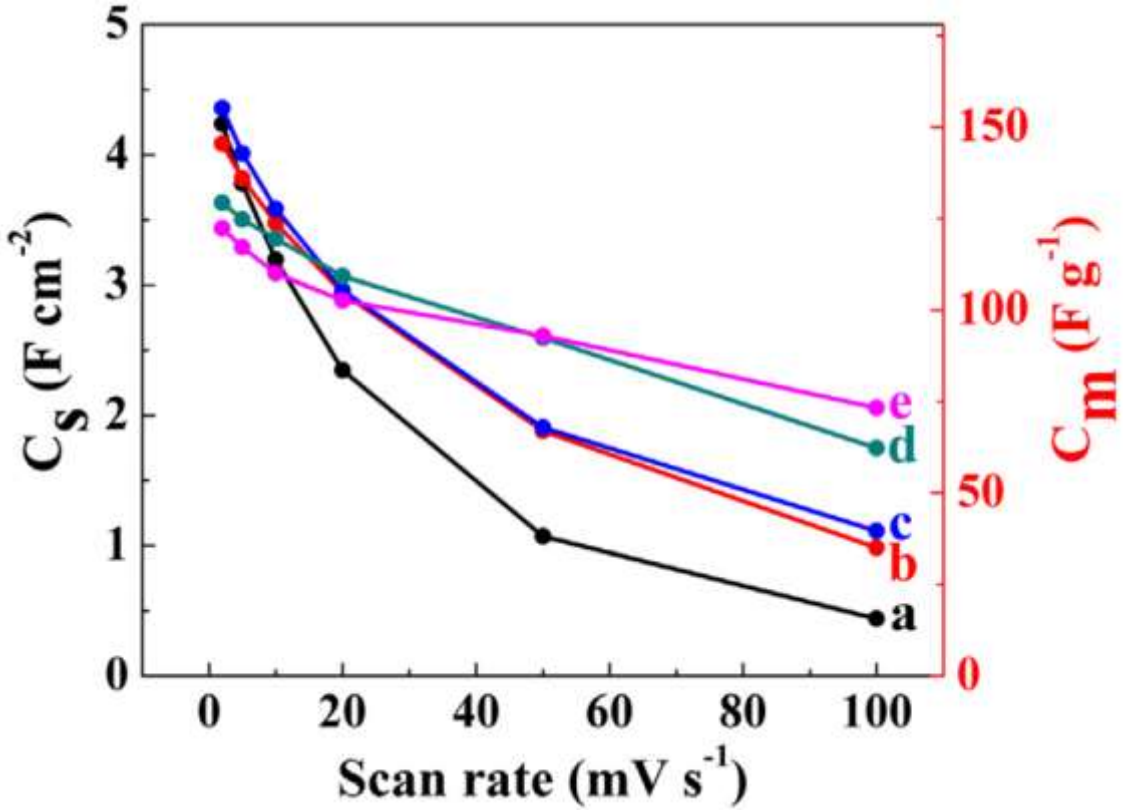

Figure 6-16 C_s and C_m vs. scan rate of ES electrode, prepared with (a) pure amaranth doped PPy and amaranth doped PPy/MWCNT composite materials at PPy/MWCNT mass ratio of (b) 9:1, (c) 8:2, (d) 7:3 and (e) 6:4, at electrode mass loading of ~29 mg cm^{-2} and scan rate of 2-100 mV s^{-1}. [176]

C_s and C_m were calculated based on CV data, according to Equation 5-2 and the results were depicted in Figure 6-16. The C_m of pure PPy electrode prepared using amaranth were 150.8 F g^{-1} (4.2 F cm^{-2}) at a scan rate of 2 mV s^{-1}; however, it dropped rapidly to 15.6 F g^{-1} (0.43 F cm^{-2}) at a scan rate of 100 mV s^{-1} (Figure 6-16(a)).

The PPy/MWCNT electrodes with PPy/MWCNT mass ratio of 9:1 and 8:2 showed high capacitance at low scan rate and approximately doubled capacitance at high scan rate (> 50 mV s^{-1}). The improved capacitance at high scan rate suggested that the addition of MWCNT benefited electrical conductivity, allowing improved capacitance at high scan rate. However, as mentioned in Table 2-2, it is notable that the theoretical capacitance of MWCNT in aqueous solutions can is in the range of 50-100 F g^{-1}, which is much lower than the PPy. As a result, partial substitution of PPy with MWCNT in the electrode materials will definitely result in decreased SC at low scan rate.

The SC of PPy/MWCNT electrode with PPy/MWCNT mass ratio of 7:3 was 129.3 F g^{-1} (3.6 F cm^{-2}) at 2 mV s^{-1}, which was comparably lower than the sample prepared with lower MWCNT content. In contrast, the higher MWCNT content further benefited the SC of composite materials at high scan rate, leading to a SC of 62.2 F g^{-1} (1.7 F cm^{-2}) at 100 mV s^{-1}, which was significantly higher than the pure PPy electrode.

The contribution of MWCNT to the electrical conductivity of PPy electrode was supported by the improved capacitance retention of PPy electrode vs. scan rate with increasing MWCNT content. The capacitance retention of PPy/MWCNT electrode with PPy/MWCNT mass ratio of 7:3 was 47.2 %, calculated from the SC data of 129.3 F g^{-1} to 62.2 F g^{-1}, at corresponding scan rate of 2 mV s^{-1} and 100 mV s^{-1}, respectively. In

comparison, the capacitance retention of pure PPy electrode was only 10.2 %, calculated from the SC data of 150.8 F g^{-1} to 15.6 F g^{-1}, at corresponding scan rate of 2 mV s^{-1} and 100 mV s^{-1}, respectively.

Moreover, the PPy/MWCNT electrode with PPy/MWCNT mass ratio of 6:4 showed reduced SC at scan rates lower than 50 mV s^{-1}, compared to the electrode with mass ratio of 7:3. It was concluded from the CV and CV derived SC data that, the mono-dispersed MWCNT, prepared with PV dispersant, allowed good SC of PPy electrode at high scan rates, which are of critical importance for practical applicability.

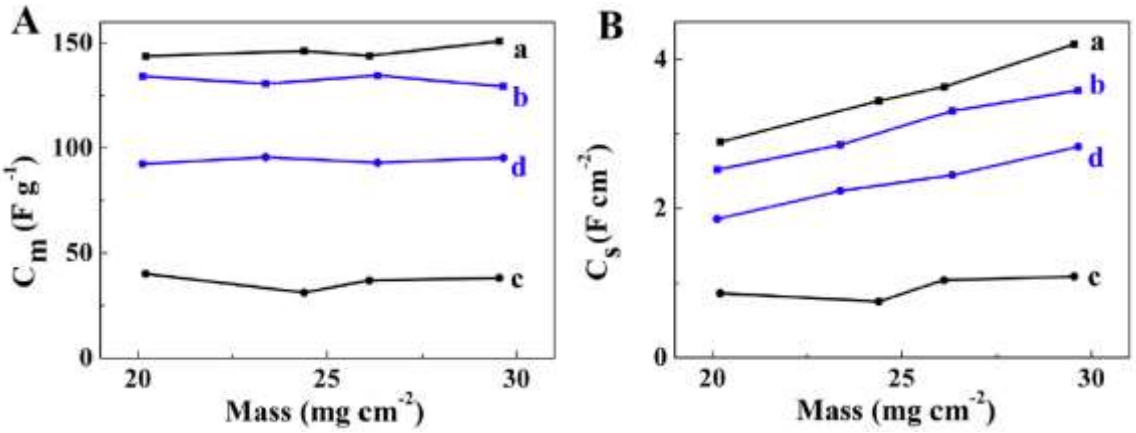

Figure 6-17 (A) C_m and (B) C_s vs. electrode mass loadings, at scan rates of (a,b) 2 mV s^{-1} and (c,d) 50 mV s^{-1}. Electrodes are prepared with (a,c) amaranth doped pure PPy electrode and (b,d) amaranth doped PPy/MWCNT composite materials with PPy/MWCNT mass ratio of 7:3. [176]

The previous results indicated that PPy/MWCNT composite materials with PPy/MWCNT mass ratio of 7:3 showed approximately ideal CV curve and high SC at both low and high scan rates. Figure 6-17 showed the comparison of SC between pure PPy electrodes and PPy/MWCNT (7:3) composite electrodes at a low scan rate (2 mV s^{-1}) and

a high scan rate (50 mV s^{-1}). The C_m and C_s of the composite electrodes were relatively lower than the pure PPy electrode at low scan rate (Figure A(a,b) and Figure B(a,b)); however, it showed significantly high value compared to the pure PPy electrode at high scan rate (Figure A(c,d) and Figure B(c,d)). Moreover, the C_m values of both samples showed relatively good stability with mass loading in the range of 20-30 mg cm^{-2}, indicating the good utilization of electrode materials, especially at high scan rate.

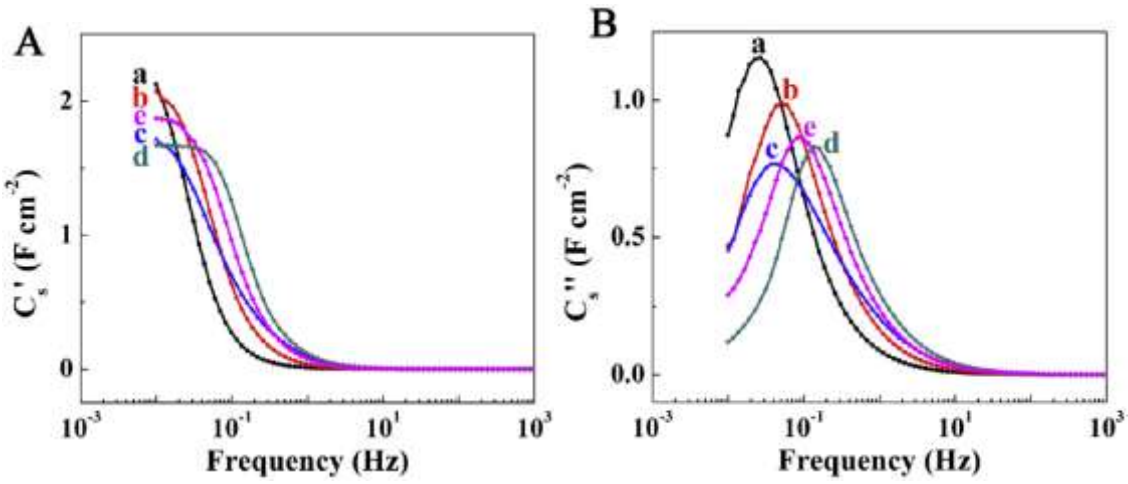

Figure 6-18 (A) C_s' and (B) C_s'' vs. frequency of PPy electrodes prepared with (a) amaranth doped pure PPy powders and amaranth doped PPy/MWCNT materials with PPy/MWCNT mass ratio of (b) 9:1, (c) 8:2, (d) 7:3 and (e) 6:4, at mass loading of ~29 mg cm^{-2}. [176]

Capacitance data derived from impedance test could be calculated based on Equation 5-3. Relaxation type dispersions were observed for the decreasing C_s' and corresponding maxima in C_s'' [170]. The real capacitance parameter C_s' data provided information about charge storage, while the imaginary capacitance parameter C_s'' offered additional information about active material behavior during C-D cycles.

From curve a to curve d in Figure 6-18(A), the C_s' data showed a decreasing trend, indicating that the increasing content of MWCNT led to reduced SC at low frequency, which is in accordance with the CV derived capacitance data. However, the PPy/MWCNT showed relatively better C_s' retention at higher frequency. The C_s' of PPy/MWCNT electrode with PPy/MWCNT mass ratio of 7:3 was higher than that of pure PPy electrode by one magnitude at a frequency of 0.1 Hz, indicating improved SC achieved at high testing frequency. The C_s'' maxima for samples from *a* to *e* shown in Figure 6-18(B), exhibited a mostly increasing trend in the values of corresponding frequencies (named relaxation frequency). The PPy/MWCNT electrode with PPy/MWCNT mass ratio of 7:3 showed highest relaxation frequency.

The CV curves and capacitances data derived from CV and impedance indicated that improved electrochemical performance was achieved by preparation of PPy/MWCNT composite materials, especially at high scan rate or at high testing frequency.

6.2.3 Device Test of PPy/MWCNT Composite Materials Doped with Amaranth

The PPy/MWCNT composite material was used for fabrication of ES device, including coin cells and envelop cells.

Figure 6-19 showed the C-D behavior of the coin cells at different current densities. The almost linear curves showed good capacitive behavior. The C-D cycles were symmetrical, indicating the energy released from the ES during discharging process, equalled in amounts to the energy obtained in the charging process, which showed its low energy loss during C-D cycles. Similar C-D characteristics were observed during envelop

cell testing. Figure 6-20 showed nearly linear C-D curves, indicating good capacitive behaviors.

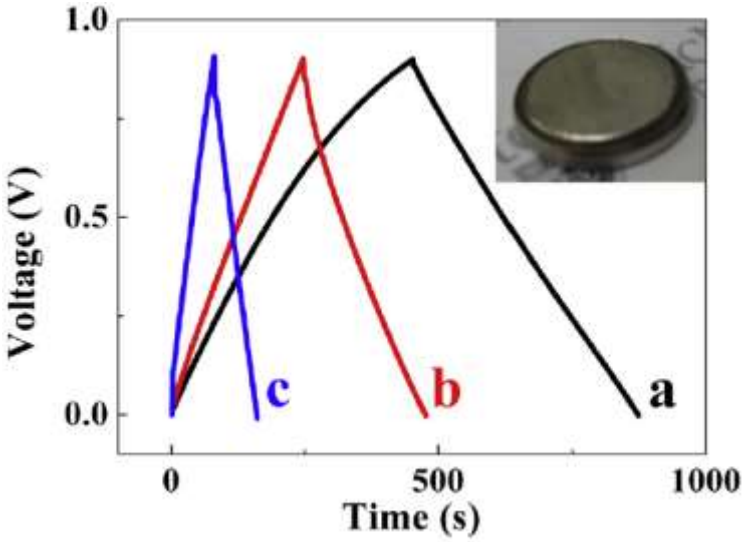

Equation 6-19 C-D cycles at a scan rate of (a) 2 mA, (b) 3 mA and (c) 9 mA for a coin cell, prepared with PPy/MWCNT electrode with PPy/MWCNT mass ratio of 7:3. Inset shows coin cell. [176]

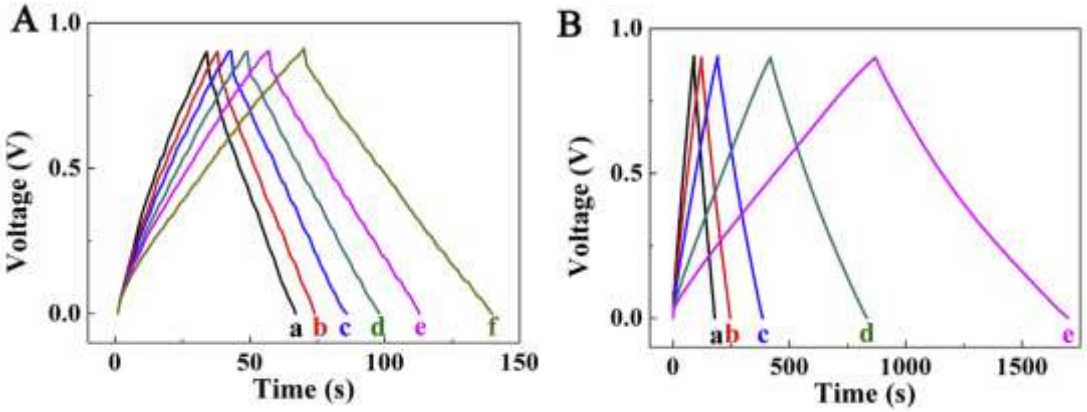

Figure 6-20 C-D cycles at a scan rate of (A): (a) 200, (b) 180, (c) 160, (d) 140, (e) 120, (f) 100; (B): (a) 80, (b) 60, (c) 40, (d) 20 and (e) 10 mA, for an envelope cell, prepared using the same materials as Figure 6-19. [176]

The cycling stability test of single PPy/MWCNT electrode and envelope cell were performed, with calculated capacitance retention shown in Figure 6-21. The capacitance retention of single electrode (Figure 6-21(a)) increased during the first 450 cycles and then decreased, with a maximum value of 106.97 %. The capacitance retention after 5000 cycles was found to be 101.2 %. The capacitance retention of envelop cell (Figure 6-21(b)) showed a gradual reduction in the stability test, achieving a 90.7 % after 5000 cycles. Such results indicated that the PPy/MWCNT composite materials prepared with amaranth allowed improved cycling stability of single electrode.

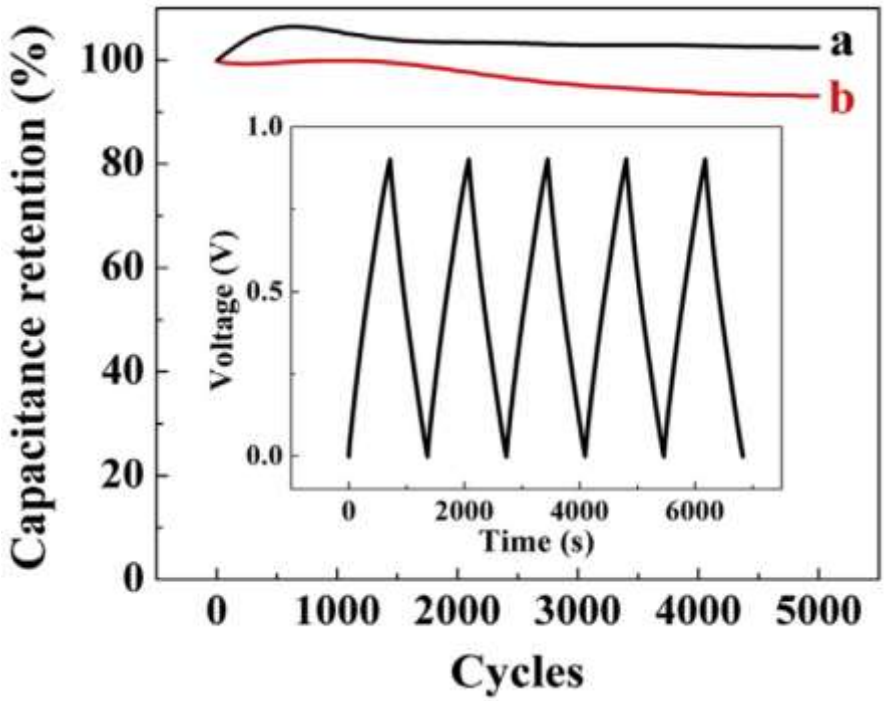

Figure 6-21 Cycling stability tests of (a) single electrode at a scan rate of 50 mV s^{-1}, and (b) envelop cell at a current density of 10 mA. PPy/MWCNT composite materials with PPy/MWCNT mass ratio of 7:3 were used for the fabrication of ES electrodes. Inset showed multi-cycles during stability test. [176]

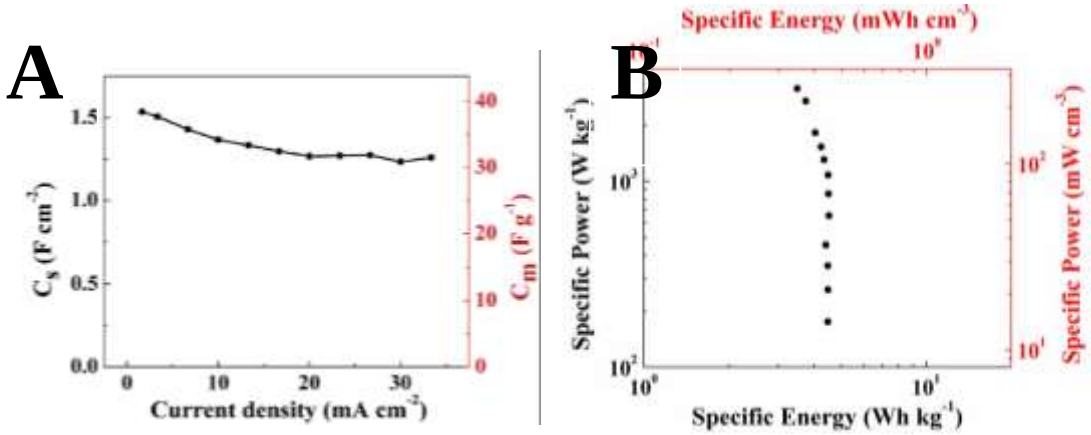

Figure 6-22 (A) C_s and C_m data vs. discharge current density and (B) corresponding Ragone plot. Data derived from C-D cycles (Figure 6-20) for envelop cells. [176]

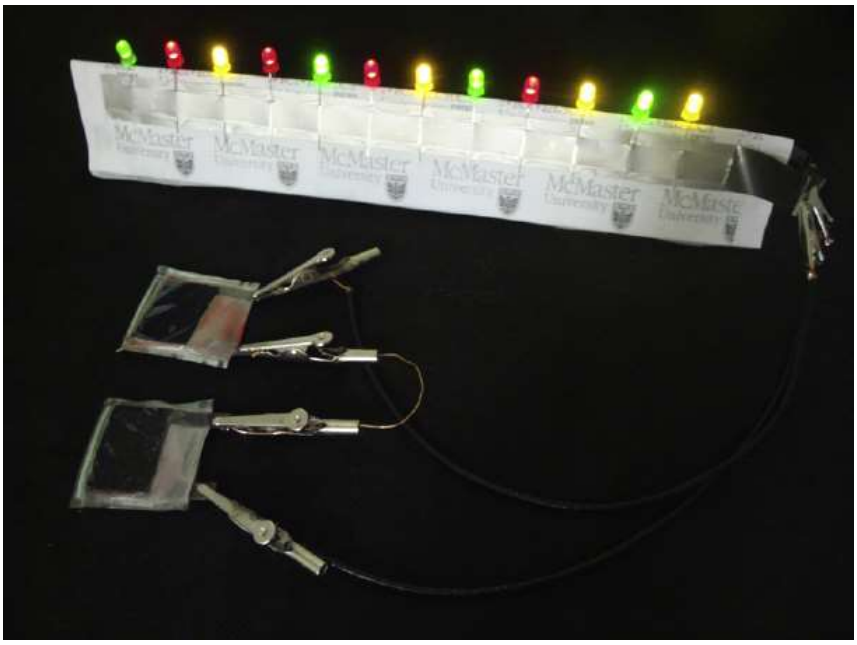

Figure 6-23 Twelve LED bulbs powered by two envelop cells in series. Electrode was prepared with PPy/MWCNT composite materials with PPy/MWCNT mass ratio of 7:3. [176]

The C_s and C_m data derived from C-D curves for envelop cells were shown in Figure 6-22(A). It was found that C_s in the range of 1.3-1.6 F cm^{-2} at discharge process was

achieved at current densities of 1-33 mA cm^{-2}. The Ragone plot (Figure 6-22(B)) showed the corresponding energy densities and power densities, indicating good electrochemical performance was achieved by PPy/MWCNT composite materials. Moreover, two envelop cells were used to power 12 LED bulbs (nominal current of 20 mA for individual bulb), as shown in Figure 6-23.

6.2.4 Summary

Advanced PPy/MWCNT composite materials were prepared in a one-step simple method using multi-aromatic amaranth as dopant and PV as MWCNT dispersant. The composite materials showed MWCNT-PPY core-shell structures, with PPy layer of 10 nm in thickness. The composite materials showed almost box shape in CV tests and high capacitance at a high mass loading of 20-30 mg cm^{-2}. Relatively good stability test indicated improved reliability in practical application. The fabrication of PPy/MWCNT composite materials showed approaches towards advanced ES electrode materials.

6.3 Chemical Polymerization of PPy/MWCNT Composite Doped with Multifunctional Dopants

In this research, multifunctional anions, including PV, ECR and AF (Figure 4.1(F-H)), were used as multifunctional dopants for advanced PPy based ES electrodes. Here, the term of "multifunctional" means that such anions can work both as multi-aromatic dopants for chemical synthesis of PPy powders, and as ideal dispersant MWCNT in solution (Figure 6-24).

6.3.1 Morphology Characterization

The PPy powders prepared with PV, ECR and AF, were prepared following process shown in Figure 5-1(a). The microstructures were characterized by SEM, shown in Figure 6-25(A-C). The sizes of the primary PPy particles doped with these multifunctional anions were mostly in the range of 30-100 nm, which is much smaller than the size of primary PPy particles prepared without dopants (Figure 2-17(a)). However, the primary particles formed agglomerates. The PPy powders prepared using AF as dopants showed relatively larger size of particle and agglomerate compared to PPy powdered prepared using PV and ECR.

Figure 6-24 Dispersion performance test. (a) 1 g L^{-1} MWCNT in water, (b) 1 g L^{-1} PV aqueous solution, (c) 1 g L^{-1} ECR aqueous solution, (d) 1 g L^{-1} AF aqueous solution, (e) 1 g L^{-1} MWCNT in 1 g L^{-1} PV aqueous solution, (f) 1 g L^{-1} MWCNT in 1 g L^{-1} ECR aqueous solution, and (g) 1 g L^{-1} MWCNT in 1 g L^{-1} AF aqueous solution. Suspensions (e-g) stable for 3 months. [177]

Figure 6-25(D-F) showed the SEM pictures of PPy/MWCNT composite materials,

prepared as shown in Figure 5-1(b) with dopants corresponding to Figure 6-25(A-C), respectively. The microstructure analysis indicated that PPy coating was formed on the surface of mono-dispersed MWCNTs. The diameter of PPy coated MWCNTs was found to be in the range of 25-60 nm, showing an increasing trend from samples prepared with PV to samples prepared with AF.

Among the three PPy/MWCNT composite materials, the powders prepared using ECR showed that almost all the PPy was utilized for MWCNT coatings. In contrast, the powders prepared using PV and AF showed that PPy agglomerates were observed, with size comparable to the sizes of pure PV and AF doped PPy powders.

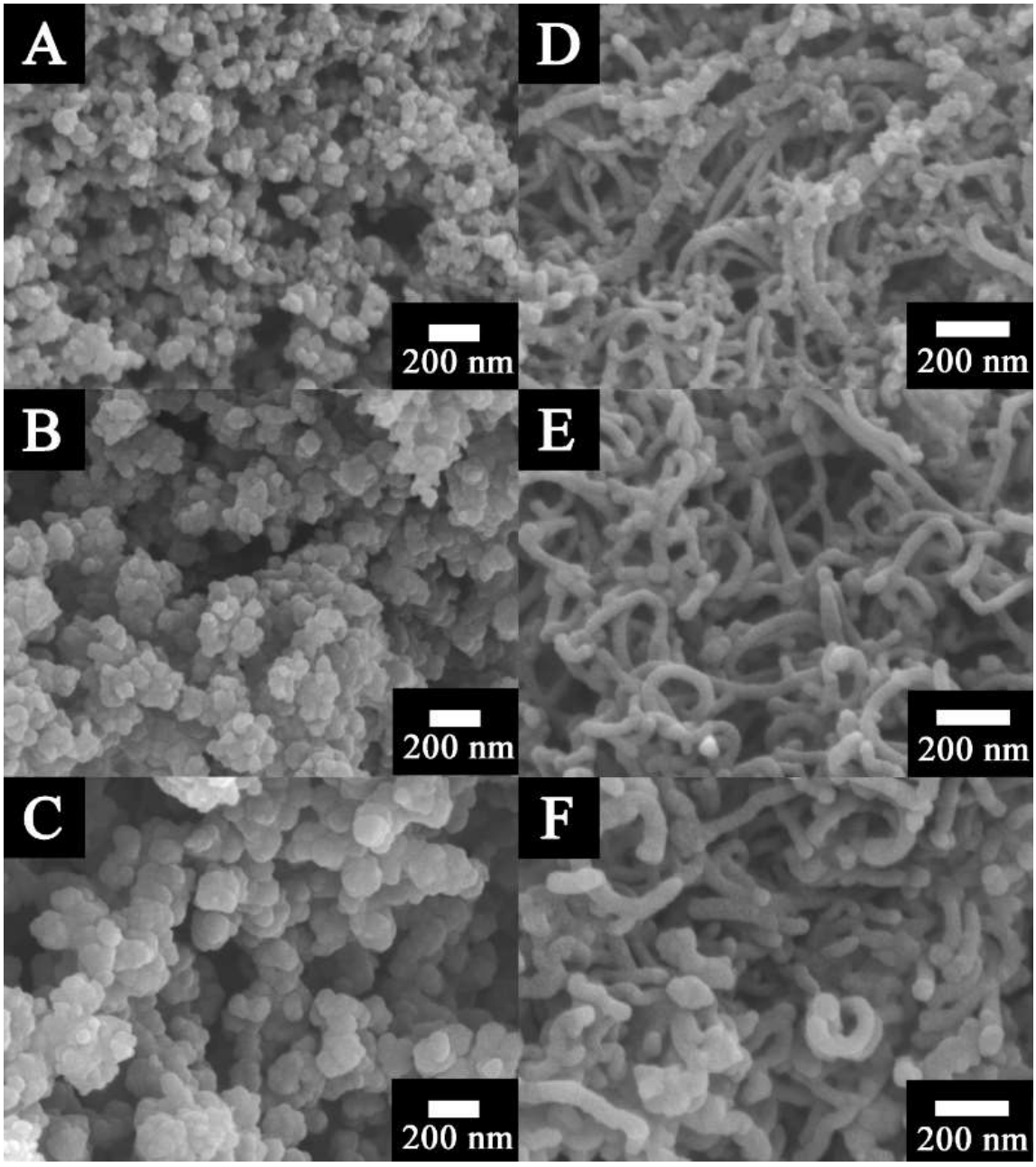

Figure 6-25 SEM images of pure PPy powders doped with (A) PV, (B) ECR and (C) AF; SEM images of PPy/MWCNT composite materials doped with (D) PV, (E) ECR and (F) AF, with PPy/MWCNT mass ratio of 7:3. [177]

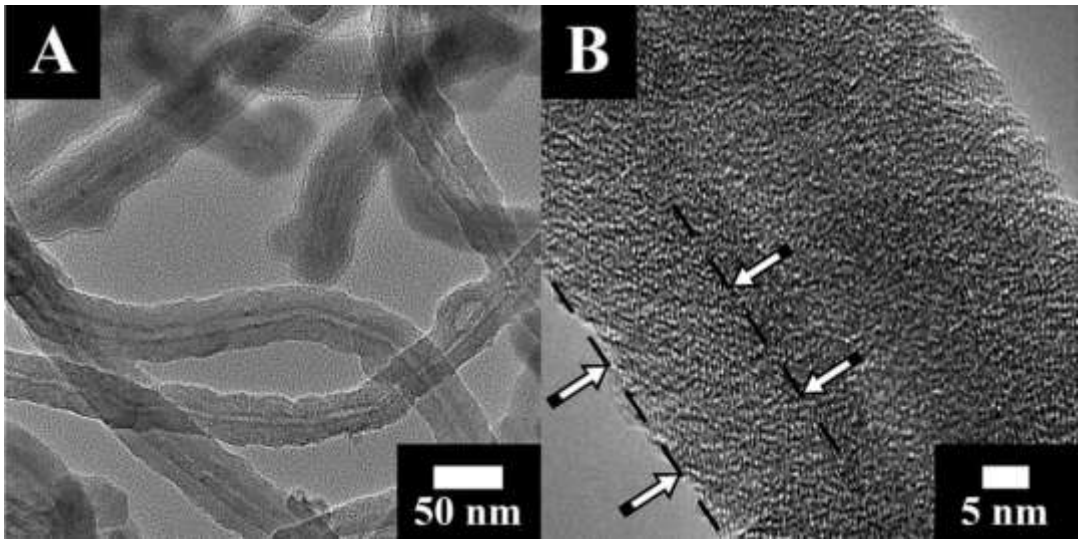

Figure 6-26 TEM images at (A) low magnification and (B) high magnification. Sample prepared from PPy/MWCNT composite materials doped with ECR. Arrows show PPy coatings. [177]

Figure 6-26 showed the TEM image of PPy/MWCNT composite materials with PPy/MWCNT mass ratio of 7:3, prepared with ECR, proving the MWCNT-PPy core-shell structures. It was found that relatively uniform PPy coating wrapped the mono-dispersed MWCNT. The PPy layer was ~15-16 nm in thickness, as pointed out by arrows in Figure 6-26(B). Such thickness was approximately 10 fold in value of literature data [178], indicating that enhanced SC was expected due to high capacitance of PPy compared to MWCNT.

The EELS and HAADF test results (Figure 6-27(A)) provide insights into the element distribution along a section vertical to a PPy/MWCNT composite nanowire.

It was found that the element distribution of nitrogen, as shown in Figure 6-27A (b), has a particular saddle shape, containing two maxima on both sides of the MWCNT. Such

shape was in agreement of the MWCNT-PPy core-shell structures for the composite materials. In theory, most nitrogen element in the PPy/MWCNT composite nanowire was contributed by PPy. Given uniform distribution of PPy molecules in PPy layers, the nitrogen distribution should be corresponding to the thickness (dashed lines in Figure 6-27(B)) of PPy in the direction of testing electron beam, which showed a saddle shape (integrated line in Figure 6-27(B)). As a result, such saddle shaped nitrogen distribution strongly proved the MWCNT-PPy core-shell structures.

For carbon distribution, the reduction of carbon derived from PPy layer in the middle was compensated by the high carbon content in MWCNT, leading to a maximum in the middle of element distribution, as shown in Figure 6-27A(a).

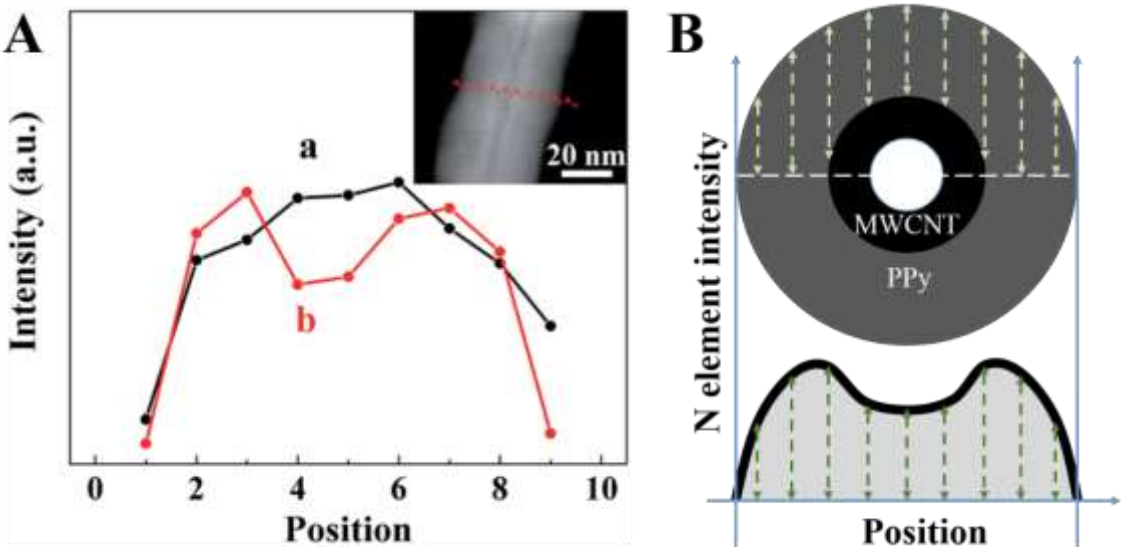

Figure 6-27 (A) Element distribution for (a) carbon and (b) nitrogen, obtained from EELS data along a section vertical to a PPy/MWCNT composite nanowire. (Inset) positions 1-9 points corresponded to positions (from left to right) of a region for

analysis. (B) Schematic figure of theoretical element distribution of nitrogen in MWCNT-PPy core-shell nanowire. [177]

6.3.2 CV and Capacitance of PPy and PPy/MWCNT Composite Materials with Multifunctional Dopants

The pure PPy powders and PPy/MWCNT composite materials prepared with PV, ECR and AF were used for fabrication of ES electrodes. The CV test were carried out based on the process described in Chapter 5.4.2 and results were depicted in Figure 6-28.

The active materials loading for electrodes was ~18 mg cm^{-2}; the high mass loading, as discussed above, was of significant importance for fabrication of ES device for practical use.

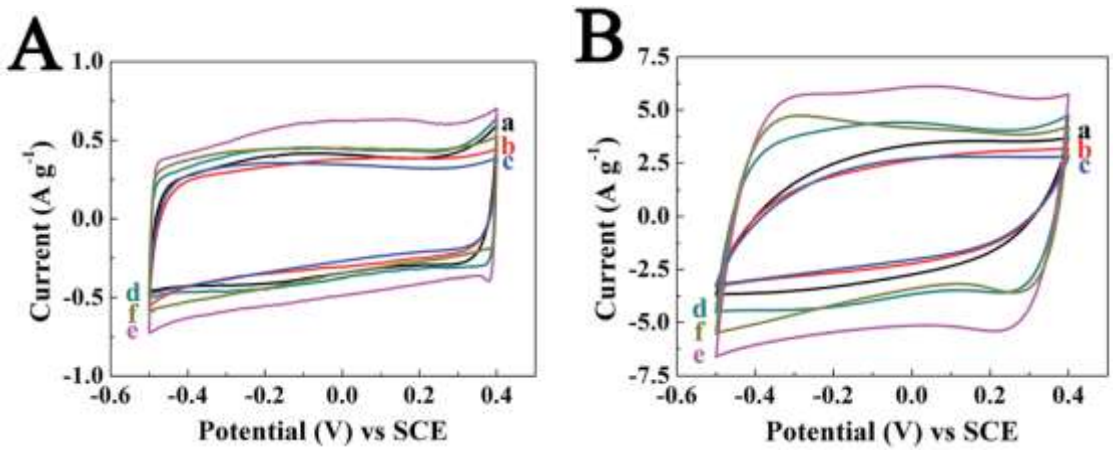

Figure 6-28 CVs at scan rates of (A) 2 mV s^{-1} and (B) 20 mV s^{-1}, for 18 mg cm^{-2} pure PPy electrodes, doped with (a) PV, (b) ECR, (c) AF, and 18 mg cm^{-2} PPy/MWCNT composite electrodes, doped with (d) PV, (e) ECR, (f) AF, with PPy/MWCNT mass ratio of 7:3. [177]

The CV curves showed nearly box shape and nearly similar area at a scan rate of 2 mV

s^{-1}, while PPy/MWCNT composite electrode prepared using ECR (Figure 6-28A (e)) showed much higher area than others. As discussed above, it indicated the good capacitive behavior of PPy prepared with multifunctional dopants PV, ECR and AF at low scan rate. However, the CV curves of pure PPy electrodes (Figure 6-28B (a-c)) deviated significantly from box shape at a scan rate of 20 mV s^{-1}. In contract, the PPY/MWCNT composite electrodes exhibited high stability in box shape CV curves, indicating good SC maintenance at high scan rate compared to corresponding pure PPy electrodes.

C_s and C_m were calculated based on CV data, according to Equation 5-2 and the results were depicted in Figure 6-29. The C_m of pure PPy electrode prepared using PV, ECR and AF reached as high as 213.9 F g^{-1} (3.81 F cm^{-2}), 192.1 F g^{-1} (3.42 F cm^{-2}) and 182.3 F g^{-1} (3.25 F cm^{-2}), respectively, at a scan rate of 2 mV s^{-1}; however, such high SCs dropped rapidly to 42.87 F g^{-1} (0.764 F cm^{-2}), 36.75 F g^{-1} (0.655 F cm^{-2}) and 29.07 F g^{-1} (0.518 F cm^{-2}), respectively, at a scan rate of 100 mV s^{-1}. Such severe reduction in SC, showed in Figure 6-29(a-c), resulted in a particularly poor capacitance retention of <20.0 %, with increasing scan rates from 2 mV s^{-1} to 100 mV s^{-1}.

The PPy/MWCNT composite electrodes prepared with PV, ECR and AF showed improved capacitance retention, as shown in Figure 6-29(d-f). The corresponding SCs were found to be 200.8 F g^{-1} (3.58 F cm^{-2}), 264.8 F g^{-1} (4.80 F cm^{-2}) and 199.8 F g^{-1} (3.58 F cm^{-2}), at a scan rate of 2 mV s^{-1}, while these values reduced to 110.8 F g^{-1} (1.98 F cm^{-2}), 134.3 F g^{-1} (2.43 F cm^{-2}) and 124.8 F g^{-1} (2.25 F cm^{-2}), at a scan rate of 100 mV s^{-1}, indicating a relatively small reduction compared to pure PPy electrode. According to the SC data, the capacitance retentions of PPy/MWCNT composite materials were found to be >50.7 %,

with increasing scan rates from 2 mV s^{-1} to 100 mV s^{-1}, which showed remarkably better capacitance stability at increasing scan rates compared to the pure PPy electrodes. It was notable that the high SC and good capacitance retention at high scan rates was achieved at high mass loading (~18 mg cm^{-2}), indicating PPy/MWCNT prepared using multifunctional dopants (especially ECR) as promising electrode materials for advanced ES.

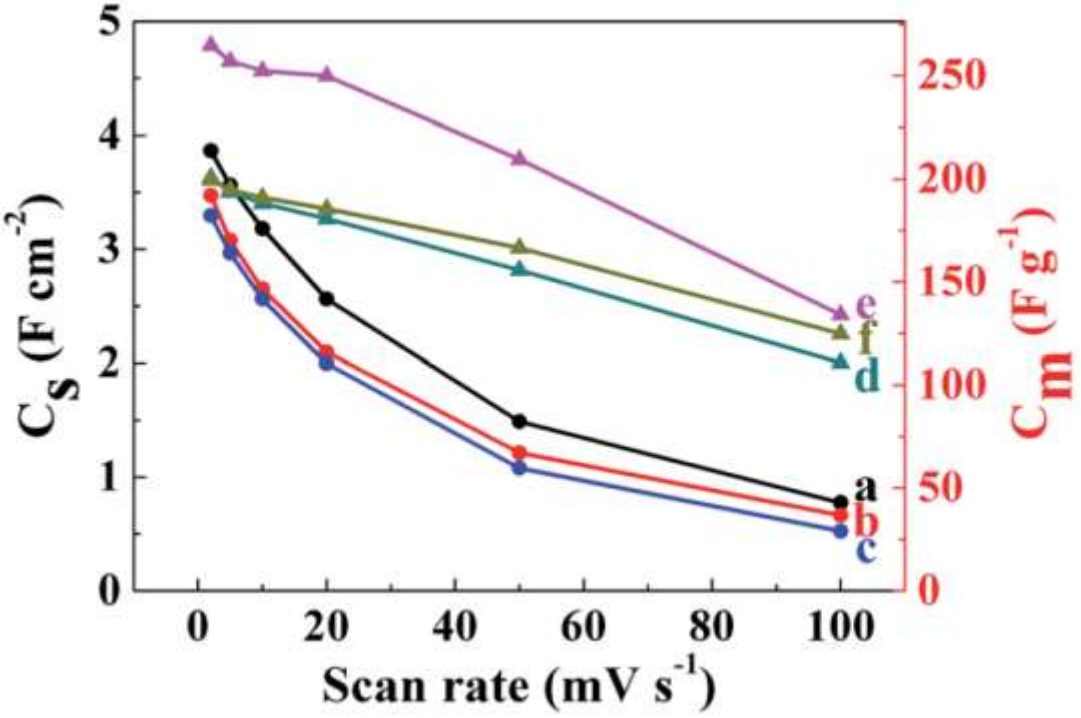

Figure 6-29 C_s and C_m vs. scan rate of ES electrode, prepared with pure PPy powders doped with (a) PV, (b) ECR, (c) AF, and PPy/MWCNT composite materials with PPy/MWCNT mass ratio of 7:3, doped with (d) PV, (e) ECR and (f) AF, at electrode mass loading of ~18 mg cm^{-2} and scan rate of 2-100 mV s^{-1}. [177]

Capacitance data derived from impedance test was calculated based on Equation 5-3 and depicted in Figure 6-30. Similar to the discussions in Chapter 6.2.2, relaxation type dispersions were observed for the decreasing C_s' and corresponding maxima in C_s'' [170].

From the C_s' data, it was obvious that PPy/MWCNT composite electrodes (Figure 6-30A (e-f)) showed higher values with increasing frequency, compared to pure PPy electrodes (Figure 6-30A (a-c)), indicating improved capacitance retention was achieved by fabrication of PPy/MWCNT materials. The relaxation frequencies (corresponding to the maxima in C_s" graph) of PPy/MWCNT composite electrodes were found to be approximately by one magnitude higher than those of PPy electrodes, indicating improved electrochemical behaviors, especially electrical conductivities of PPy/MWCNT composite materials.

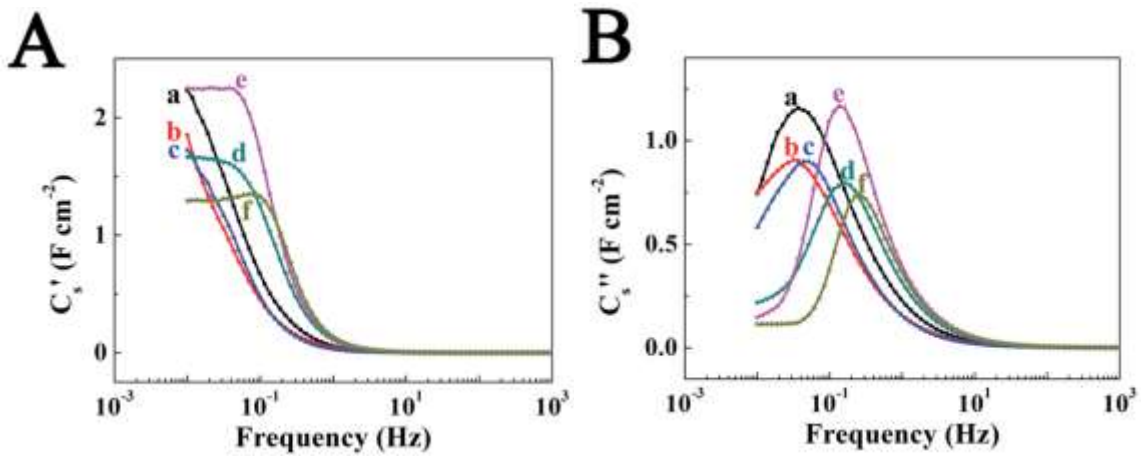

Figure 6-30 (A) C_s' and (B) C_s" vs. frequency of ES electrode, prepared with PPy powders doped with (a) PV, (b) ECR, (c) AF, and PPy/MWCNT composite materials with PPy/MWCNT mass ratio of 7:3, doped with (d) PV, (e) ECR and (f) AF, at electrode mass loading of ~18 mg cm^{-2}. [177]

6.3.3 Device Test of PPy/MWCNT Composite Materials with Multifunctional Dopants

According to microstructure analysis, and electrochemical analysis, including CV and impedance, the PPy/MWCNT composite materials prepared with multifunctional dopants, especially ECR, were found to have uniform microstructures and show promising electrochemical behaviors for fabrication of improved ES device.

Figure 6-31 showed the C-D behaviors of the envelope typed ES device at different current densities. As discussed in Chapter 6.2.3, the nearly linear curves and symmetrical shape in one C-D cycle showed god capacitive behaviors and high energy output/input ratio, indicating low energy loss during C-D cycles and good capacitive behaviors.

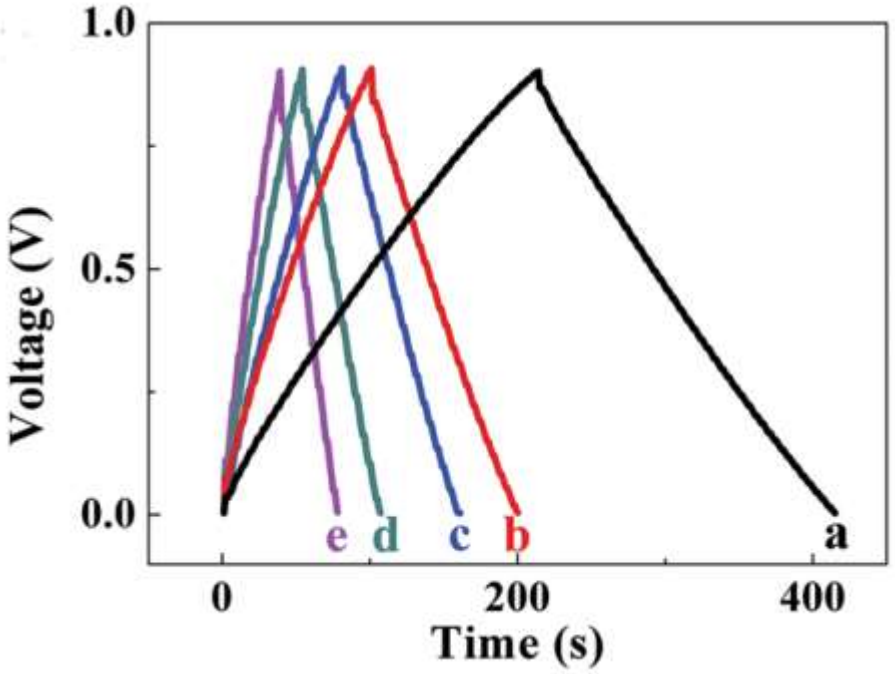

Figure 6-31 C-D cycles at a scan rate of (a) 4, (b) 8, (c) 10, (d) 15 and (e) 20 mA cm^{-2}, for ES device prepared with ECR doped PPy/MWCNT composite materials with mass ratio of 7:3. [177]

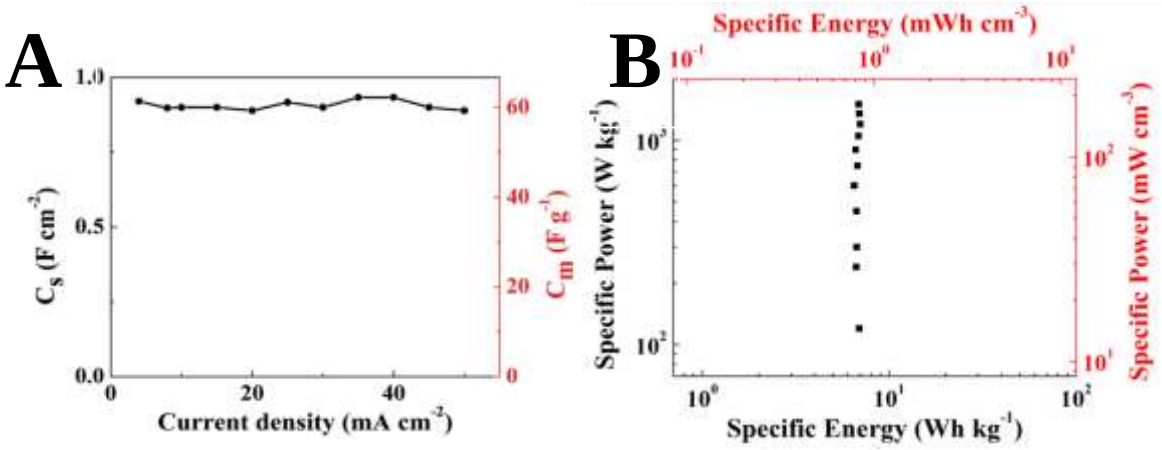

Figure 6-32 (A) C_s and C_m data vs. discharge current density and (B) corresponding Ragone plot. Data derived from C-D cycles (partially presented in Figure 6-31) for envelop cells. [177]

The C_s and C_m data derived from C-D curves for envelop cells, prepared with ECR doped PPy/MWCNT composite materials, were shown in Figure 6-32(A). It was found that SC of ~60 F g^{-1} (~0.9 F cm^{-2}) at discharge process was achieved at current densities of 1-50 mA cm^{-2}. The Ragone plot (Figure 6-32(B)) showed the corresponding energy densities and power densities, indicating good electrochemical performance was achieved by ECR doped PPy/MWCNT composite materials. In previous research [176], obvious reduction in energy density was observed at high power density (Figure 6-22(B)), which corresponded to diffusion limitation in C-D process. In this research, the energy density stayed quite stable with increasing power density, indicating that good stability in energy density of PPy/MWCNT composite materials.

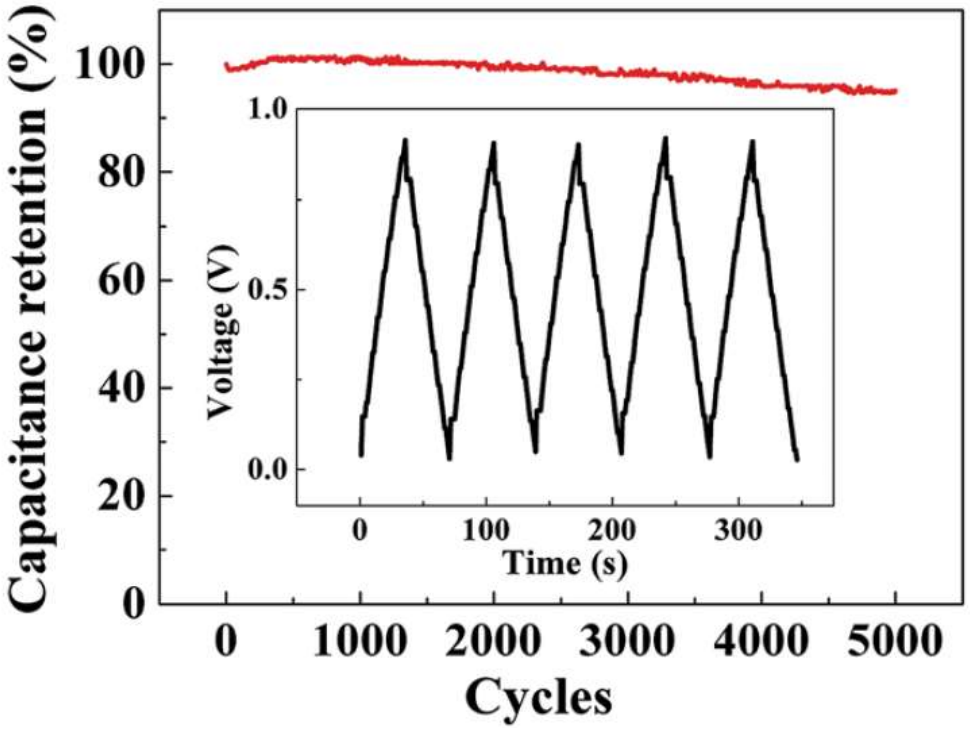

Figure 6-33 Cycling stability test of envelop cell, at a scan rate of 20 mA cm^{-2}. The inset showed multiple C-D cycles observed during cycling test. [177]

Figure 6-33 showed the cycling stability performance of ES device prepared with the same PPy/MWCNT composite materials. This test was carried out for a total cycles of 5000 and at current density of 20 mA cm^{-2}. The results indicated that the capacitance retention increased during the first 400 cycles and then experienced a gradual reduction. The capacitance retention value after 5000 cycles was 94.2 %, showing that the SC was relatively stable in long time use. Also, three of such ES devices were used to power 17 LED bulbs (nominal current of 20 mA for individual bulb), as shown in Figure 6-34.

Figure 6-34 Seventeen LED bulbs powered by three envelop cells in series. The ES cell had an effective area of 6 cm^2. Electrodes was prepared with ECR doped PPy/MWCNTs composite materials, with PPy/MWCNT mass ratio of 7:3. [177]

6.3.4 Summary

In this research, multifunctional anions including PV, ECR and AF were used as both dispersant for MWCNT dispersion and anionic dopant for chemical polymerization of PPy, in order to fabricate of PPy/MWCNT composite materials for ES use. The multifunctional dopants allowed formation of MWCNT-PPy core-shell structures; the PPy layer, coating uniformly on the surface of mono-dispersed MWCNT, was found to reach as high as ~15-16 nm in thickness. The electrochemical tests, including CVs, impedance and galvanostatic C-D cycles, indicated that PPy/MWCNT composite powders were promising electrode materials allowing increased SC, improved stability performance and potential practical applications.

7 Conclusions

The chemical polymerization of PPy and PPy/MWCNT prepared with different dopants, including CHR families (CHR, CHR-P, CHR-N and CHR-BS), amaranth, PV, ECR and AF, was carried out in experiments. Microstructure analysis and electrochemical tests, including CV, impedance and galvanostatic C-D cycles were used to characterize the products for applications as electrode materials for fabrication of advanced ES device.

The results suggested that anionic dopants had significant influence on microstructure and electrochemical performance of chemically-synthesized PPy powders. Particularly, this research strongly supported that large multi-charged dopants with high charge to mass ratio was beneficial for increased SC in a voltage window of -0.5 – +0.4 V vs. SCE, specifically at low scan rate. The use of multi-aromatic anionic dopants allowed the fabrication of ES electrode with improved stability. A maximum area normalized capacitance C_s of PPy powders was obtained as 7.2 F cm^{-2} with CHR-BS as dopant.

The PPy/MWCNT composite materials with advanced physical and chemical properties were successfully fabricated in a simple one-step chemical polymerization. The PPy/MWCNT composite materials showed different microstructures and electrochemical responds, with variations in PPy/MWCNT mass ratio and use of dopants. The PPy/MWCNT composite materials with mass ratio of 7:3 were proved to allow balanced capacitance at both high and low scan rates, and improved cyclic stability compared with previous researches. A maximum mass normalized capacitance of PPy/MWCNT material was calculated as 246.8 F g^{-1} with ECR as dopant.

Moreover, this research indicated that the used of high porosity current collectors (such as Ni foam with 95% porosity) allowed high active materials loading as high as 40 mg cm^{-2}, which was beneficial for practical application.

ES device, such as coin cells and envelope cells based on synthesized PPy and PPy/MWCNT products were fabricated for electrochemical testing. Good C-D cycles, cyclic stabilities and Ragone plot were achieved with use of multi-charged dopants, addition of MWCNT and Ni foam as current collector. The results indicated that PPy/MWCNT composite materials doped with multi-charged anions, especially with PPy/MWCNT mass ratio of 7:3, were promising electrode materials for advanced ES.

8 Contributions, Perspective and Recommendations for Future Research

8.1 Contributions

This work has made three major contributions to the ES techniques: theory development, high-performance polymer-based electrode for ES application and modules for industrialization of ES. These contributions are expanded in the following subsections.

8.1.1 Theory Development

A series of chemicals have been investigated and used as anionic dopants for PPy. Such dopants, most with anionic groups of $-COO^-$ or $-SO_3^-$, show significant influence on the micromorphology and electrochemical behaviors of synthesized PPy.

Prior to the publication of this thesis, however, none comprehensive investigation was focused on the mechanism of influence of dopant structure and charge on supercapacitive properties of PPy electrode. *"Are there any requirements in molar mass/molecular size/side groups, for high-efficiency dopant for PPy based supercapacitive materials? Moreover, which is the preferred anionic group for advanced dopants, sulfonic acid group, carboxylic acid group, phosphoric acid group or a specific combination of them?"* Provided certain answers to these questions, we can make in-depth understanding of the nature of relationship between dopant and CP materials, as well as manually design and synthesize desirable anionic dopants for CP-based supercapacitive materials.

In this work, we demonstrated experimental work (Chapter 6.1) with fundamental theoretical analysis. The regular dependence of SC, cyclic stability & microstructures of PPy electrode on charge number, charge to mass ratio and molecular size inspired the strong relationship between them. The values of SC showed 35.1% in difference between powders prepared using CHR-N and CHR-BS dopants [171]. With referring to previous works[175] and this work, we can come to a comprehensive conclusion *–multi-charged aromatic dopant with high charge/mass ratio, high molar mass and large molecular size gives high specific capacitance and ideal microstructure with smaller particle size of PPy for practical applicability.*

8.1.2 High-Performance Polymer-Based Electrode for ES Applications

Prior to the publication of this thesis, poor specific capacitance (or energy density) retention at increasing scan rate (or power density) was among the major obstacles for the applicability of CP based ES, as well as poor cyclic stability (low efficient cycles for energy input/output). The incorporation of high-conductivity carbon reinforcement, including AC, CNT and graphene, was recently regarded as an efficient method to improve conductivity of bulky materials, as well as to achieve better mechanical properties.

In this work, stable CNT aqueous suspension was prepared with addition of high-efficient aromatic dispersant (Chapter 6.2) or multifunctional dopant (Chapter 6.3). Dispersants and anionic dopants were adsorbed onto surface of CNT and provided

dispersion. Py monomer was concentrated at CNT/solvent interface via π-π interaction with graphene layer of CNT or electrostatic adsorption with anionic dopant. When oxidant (APS) was added to the system, Py monomer polymerized into large molecules and tightly coated onto CNT, forming controllable core-shell nanowires with the microstructure greatly influenced by anionic dopant. In our investigation, the PPy coated MWCNT composite nanowires showed high cyclic stability (mechanical stability) and high capacitance retention vs. scan rate (conductivity of bulky electrode and electrolyte matrix), which is important to meet the limiting factor for application of polymer based ES.

8.1.3 Modules Development for Industrialization of ES

Prior to the publication of this thesis, electrochemical deposition was widely investigated as effective approach towards high-quality supercapacitive electrode, for uniform polymer coating on current collector and ease of processability. However, as mentioned in Chapter 7, the thin film with mass loadings of 10^{-3}-1 mg cm^{-2} was miles away from industrialization, even though the mass normalized capacitance of active materials in some articles may reached up to 10^3 F g^{-1}.

In this work, high material loadings of 18-40 mg cm^{-2} were achieved via infiltration of active materials into high-porosity Ni current collector. The small particle size and high porosity of active materials provided high SSA for fast charge-discharge and benefited easy infiltration of electrolyte into bulky materials. This helped the bulky active material

maintain high capacitance and high conductivity at high mass loading, while a severe decrease in electronic conductivity was mostly observed for electrodeposited CP films for ES.

Besides, in this work the envelope cell (Figure 9-1) was designed and investigated as promising module for industrialization of ES. The volumetric active material loading of an envelope cell reached as high as 241.9 mg cm^{-3} and active material/current collector mass ratio reached 0.42, when individual PPy electrode had mass loading of 30 mg cm^{-2}. Such high material loading and high active material/current collector greatly allowed high energy density and benefited commercialization of PPy based ES.

Figure 9-1 (LEFT) PPy/MWCNT composite material based envelope ES cells. (Right) The thickness of envelope ES cell is 1.24 mm. [176]

8.2 Perspective

Research in CP based ES has focused on the development of ES systems supporting high energy density, high power density, high effective C-D cycles and environmental friendliness. Conventional CPs, including PAn, PPy, PTh and their derivatives, are under wide investigation for active materials for ES because good specific capacitance, ease of processability and low cost.

The limiting factors that restrict CP based ES from vast application are poor electrode stability (low effective cycles), severe reduction in energy density with increased power density, etc. Compared to EDLS materials, the swelling and shrinking of pseudo-capacitive CPs during charge-discharge process leads to loss of materials and poor mechanical stability, which greatly shortens the lifetime of CP based ES. For CPs of low specific surface area, the bulky materials that are far from the electrode/electrolyte interface are not provided with enough time to be charged and discharged and do not contribute to the whole energy stored during high charge-discharge rate (high power density). In our scientific development of CP based ES, we are targeting on fabricating CP based ES with high electrode stability and good energy density retention.

As mentioned in the Introduction part, an effective approach towards high energy density and power density is to broaden voltage window of ES devices, referring to Equation 2-3 and 2-4. As the thermodynamic decomposition of water prevents high voltage window of aqueous electrolyte, an attractive idea is to make use of organic electrolyte instead. With proper organic solvent and certain electrolytic salts, the voltage window could reach up to 4.0 V. However, the toxicity and recycling problem are still waiting to be solved

before wide application of organic-electrolyte ES. Though recent reports highlight increasing applications of ES based energy storage devices, including HEV and EV, there are still miles to go before the vast industrialization of ES devices, especially those based on CP materials. We believe however that PPy based ES devices can be further developed for industrialization.

8.3 Recommendation for Future Research

8.3.1 All-Solid-State ES

Various aqueous and organic electrolytes are used in fabricating all kinds of ES devices. Liquid electrolytes, however, are not convenient for application in certain circumstances. The possibility of electrolyte leakage may undoubtedly lead to reduction in specific capacitance, poor electrochemical performances, and even contamination to nearby circuits. The idea of all-solid-state ES[49] was most recently proposed and the approach was based on the incorporation of gel electrolyte. Commonly, an effective way towards gel electrolyte is adding polyvinyl alcohol (PVA) into aqueous solutions, “fixing” water molecules via the formation of 3-D hydrophilic polymer networks. However, the inevitable increase in system resistance calls for advanced systems for all-solid-state ES device, which is of significance for the development of ES and deserves further investigation.

8.3.2 Advanced Materials for ES Devices

As stated in the Introduction part, the relative poor mechanical behaviors of CPs based ES electrode restrict the effective cycles in application. Besides incorporation of

reinforcement materials, an alternative method towards high-stability CP based ES electrode is the modification of polymeric materials, including group modification of monomer [179], fabrication of copolymers [180, 181] and fabrication of polymer blends with unique structures [182]. For instance, a variety of Py derivatives [179] can be synthesized via group modification. The new CPs and copolymers have different microstructures and show developed electrochemical properties[183]. The poly(pyrrole derivatives) deserve further investigation for application as active materials for ES.

The specific capacitances (SCs) of CPs based ES are relatively high compared to EDLS devices, i.e. the theoretical SC of PPy is 620 F g^{-1}, compared to ~100 F g^{-1} of MWCNT. Higher energy density and miniaturization, however, is an eternal target for energy storage device. It is always an attractive idea for each supercapacitor engineer to develop active materials that allow even higher SCs.

Currently high attentions [101, 102] are drawn to hybridization of high specific capacitance of metal oxides (nitrides/sulfides) and high conductivity of CPs or carbon materials. Due to their advantages in high SC, it is widely convinced that comprehensive researches on the composite materials, i.e. metal oxides (nitrides/sulfides) particles with matrix of CPs or carbon materials, illuminate approaches towards advanced ES allowing high energy density, high power density and high effective cycles. However, it still remains as a problem to discover an easy and economic approach towards high-quality composite materials with ideal scale of dispersion and essential stability.

REFERENCE

[1] A. Burke, "Ultracapacitors: why, how, and where is the technology," *Journal of Power Sources,* vol. 91, pp. 37-50, Nov 2000.

[2] X. Du, X. Hao, Z. Wang, X. Ma, G. Guan, A. Abuliti*, et al.*, "Highly stable polypyrrole film prepared by unipolar pulse electro-polymerization method as electrode for electrochemical supercapacitor," *Synthetic Metals,* vol. 175, pp. 138-145, 7/1/ 2013.

[3] P. F. Ribeiro, B. K. Johnson, M. L. Crow, A. Arsoy, and Y. L. Liu, "Energy storage systems for advanced power applications," *Proceedings of the Ieee,* vol. 89, pp. 1744-1756, Dec 2001.

[4] J. R. Miller, "A Brief History of Supercapacitors," *Batteries & Energy Storage Technology,* pp. 61-78, 2007.

[5] "NanoMarkets forecasts supercapacitor market to reach $3B in 2016; decrease in transportation market share," *Green Car Congress,* 2010.

[6] W. S. Broecker, "Climatic Change Are We On The Brink of A Pronounced Global Warming," *Science,* vol. 189, pp. 460-463, 1975.

[7] E. Pahlich, "Effect of Sulfur Di Oxide Pollution on Cellular Regulation A General Concept Of The Mode of Action Of Gaseous Air Contamination," *Atmospheric Environment,* vol. 9, pp. 261-264, 1975.

[8] R. J. Shephard, "Perspective on air pollution: the canadian scene," *Canadian family physician Medecin de famille canadien,* vol. 21, pp. 67-73, 1975 1975.

[9] C. W. J. Van Koppen, "The potential of renewable energy sources," *Resources and Conservation,* vol. 7, pp. 17-36, 1981.

[10] B. Sorensen, "Renewable Energy - A Technical Overview," *Energy Policy,* vol. 19, pp. 386-391, May 1991.

[11] S. Baron, "Solar-Energy - Will It Conserve Our Non-Renewable Resources," *Transactions of the American Nuclear Society,* vol. 30, pp. 9-10, 1978.

[12] B. Sorensen, "Energy and Resources: A plan is outlined according to which solar and wind energy would supply Denmark's needs by the year 2050," *Science,* vol. 189, pp. 255-60, 1975.

[13] S. P. Simonovic and L. M. Miloradov, "Potential hydroenergy production by optimization," *Journal of Water Resources Planning and Management-Asce,* vol. 114, pp. 101-107, Jan 1988.

[14] M. Balat and H. Balat, "Biogas as a Renewable Energy SourceA Review," *Energy Sources Part a-Recovery Utilization and Environmental Effects,* vol. 31, pp. 1280-1293, 2009.

[15] W. D. Harkins, "The neutron, the intermediate or compound nuclous, and the atomic bomb," *Science (New York, N.Y.),* vol. 103, pp. 289-302, 1946 Mar 1946.

[16] X. F. Zheng, C. X. Liu, Y. Y. Yan, and Q. Wang, "A review of thermoelectrics research - Recent developments and potentials for sustainable and renewable energy applications," *Renewable & Sustainable Energy Reviews,* vol. 32, pp. 486-503, Apr 2014.

[17] Z. Hameed, Y. S. Hong, Y. M. Cho, S. H. Ahn, and C. K. Song, "Condition monitoring and fault detection of wind turbines and related algorithms: A review," *Renewable & Sustainable Energy Reviews,* vol. 13, pp. 1-39, Jan 2009.

[18] M. T. Dunham and B. D. Iverson, "High-efficiency thermodynamic power cycles for concentrated solar power systems," *Renewable & Sustainable Energy Reviews,* vol. 30, pp. 758-770, Feb 2014.

[19] B. E. Conway, *Electrochemical Supercapacitors. Scientific Fundamentals and Technological Applications*. New York, Boston, Bordrecht, London, Moscow: Kluwer Academic/Plenum Publishers, 1999.

[20] R. J. Brodd, K. R. Bullock, R. A. Leising, R. L. Middaugh, J. R. Miller, and E. Takeuchi, "Batteries, 1977 to 2002," *Journal of the Electrochemical Society,* vol. 151, pp. K1-K11, Mar 2004.

[21] W. E. Winsche, K. C. Hoffman, and F. J. Salzano, "Hydrogen: Its Future Role in the Nation's Energy Economy," *Science (New York, N.Y.),* vol. 180, pp. 1325-32, 1973 Jun 1973.

[22] R. Burt, G. Birkett, and X. S. Zhao, "A review of molecular modelling of electric double layer capacitors," *Physical Chemistry Chemical Physics,* vol. 16, pp. 6519-6538, 2014.

[23] A. Du Pasquier, I. Plitz, J. Gural, S. Menocal, and G. Amatucci, "Characteristics and performance of 500 F asymmetric hybrid advanced supercapacitor prototypes," *Journal of Power Sources,* vol. 113, pp. 62-71, Jan 2003.

[24] D. V. Ragone, "Review of Battery Systems for Electrically Powered Vehicles," *SAE paper,* 1968.

[25] J. Garche, C. Dyer, P. Moseley, Z. Ogumi, D. Rand, and B. Scrosati, *Encyclopedia of Electrochemical Power Sources*. Amsterdam: Elsevier, 2009.

[26] H. Ibrahim, A. Ilinca, and J. Perron, "Energy storage systems - characteristics and comparisons," *Renewable and Sustainable Energy Reviews,* vol. 12, pp. 1221-50, 06/ 2008.

[27] P. Simon and Y. Gogotsi, "Materials for electrochemical capacitors," *Nature Materials,* vol. 7, pp. 845-54, 11/ 2008.

[28] X. Cai, M. Peng, X. Yu, Y. Fu, and D. Zou, "Flexible planar/fiber-architectured supercapacitors for wearable energy storage," *Journal of Materials Chemistry C,* vol. 2, pp. 1184-1200, Feb 21 2014.

[29] P. Coenen, F. Leemans, and G. Mulder, "Applying large electric double layer capacitor systems," *Journal of Applied Electrochemistry,* vol. 44, pp. 533-542, Apr 2014.

[30] K. Takizawa and K. Kondo, "A method for designing the power and capacitance of fuel cells and electric double-layer capacitors of hybrid railway vehicles," *Electrical Engineering in Japan,* vol. 184, pp. 47-54, Aug 2013.

[31] S. M. Rezvanizaniani, Z. C. Liu, Y. Chen, and J. Lee, "Review and recent advances in battery health monitoring and prognostics technologies for electric vehicle (EV) safety and mobility," *Journal of Power Sources,* vol. 256, pp. 110-124, Jun 2014.

[32] S. Keshishian, G. A. Turner, G. L. Paul, and C. J. Drummond, "Energy storage device, e.g. for hybrid electric vehicle, has resistors connected between power supply rails that are connected to respective terminals of serially connected supercapacitor cells," WO2004073001-A1; EP1593135-A1; JP2006517733-W; US2006194102-A1.

[33] I. Galkin, A. Stepanov, J. Laugis, and Ieee, *Outlook of usage of supercapacitors in uninterruptible power supplies*, 2006.

[34] M. Ippolito, "Energy regenerating device for recovering kinetic energy in motor vehicles, has supercapacitor battery with micro-electro-mechanical system type acceleration sensor having static acceleration in single or multi-axial configuration," EP1764256-A2; IT1360672-B.

[35] S. Nardecchia, D. Carriazo, M. L. Ferrer, M. C. Gutierrez, and F. del Monte, "Three dimensional macroporous architectures and aerogels built of carbon nanotubes and/or graphene: synthesis and applications," *Chemical Society Reviews,* vol. 42, pp. 794-830, 2013.

[36] M. A. Hannan, F. A. Azidin, and A. Mohamed, "Hybrid electric vehicles and their challenges: A review," *Renewable & Sustainable Energy Reviews,* vol. 29, pp. 135-150, Jan 2014.

[37] L. T. Lam and R. Louey, "Development of ultra-battery for hybrid-electric vehicle applications," *Journal of Power Sources,* vol. 158, pp. 1140-1148, Aug 25 2006.

[38] J. Y. Liang, J. L. Zhang, X. Zhang, S. F. Yuan, and C. L. Yin, "Energy management strategy for a parallel hybrid electric vehicle equipped with a battery/ultra-capacitor hybrid energy storage system," *Journal of Zhejiang University-Science A,* vol. 14, pp. 535-553, Aug 2013.

[39] G. Wang, L. Zhang, and J. Zhang, "A review of electrode materials for electrochemical supercapacitors," *Chemical Society Reviews,* vol. 41, pp. 797-828, 2012 2012.

[40] Y. Zhang, H. Feng, X. B. Wu, L. Z. Wang, A. Q. Zhang, T. C. Xia*, et al.*, "Progress of electrochemical capacitor electrode materials: A review," *International Journal of Hydrogen Energy,* vol. 34, pp. 4889-4899, Jun 2009.

[41] R. Liu, J. Duay, and S. B. Lee, "Heterogeneous nanostructured electrode materials for electrochemical energy storage," *Chemical Communications,* vol. 47, pp. 1384-1404, 2011.

[42] B. E. Conway, V. Birss, and J. Wojtowicz, "The role and utilization of pseudocapacitance for energy storage by supercapacitors," *Journal of Power Sources,* vol. 66, pp. 1-14, May-Jun 1997.

[43] A. G. Pandolfo and A. F. Hollenkamp, "Carbon properties and their role in supercapacitors," *Journal of Power Sources,* vol. 157, pp. 11-27, Jun 19 2006.

[44] K. Kordesch and J. Daniel-Ivad, *Advances in battery systems for energy storage*. Montreal: Ecole Polytechnique Montreal, 1997.

[45] G. A. Snook, P. Kao, and A. S. Best, "Conducting-polymer-based supercapacitor devices and electrodes," *Journal of Power Sources,* vol. 196, pp. 1-12, Jan 1 2011.

[46] B. E. Conway and W. G. Pell, "Double-layer and pseudocapacitance types of electrochemical capacitors and their applications to the development of hybrid devices," *Journal of Solid State Electrochemistry,* vol. 7, pp. 637-644, Sep 2003.

[47] C. Peng, S. Zhang, D. Jewell, and G. Z. Chen, "Carbon nanotube and conducting polymer composites for supercapacitors," *Progress in Natural Science-Materials International,* vol. 18, pp. 777-788, Jul 10 2008.

[48] M. A. Guerrero, E. Romero, F. Barrero, M. I. Milanes, and E. Gonzalez, "Supercapacitors: Alternative Energy Storage Systems," *Przeglad Elektrotechniczny,* vol. 85, pp. 188-195, 2009 2009.

[49] H. Gao, F. Xiao, C. B. Ching, and H. Duan, "Flexible all-solid-state asymmetric supercapacitors based on free-standing carbon nanotube/graphene and Mn3O4 nanoparticle/graphene paper electrodes," *ACS Applied Materials and Interfaces,* vol. 4, pp. 7020-7026, 2012.

[50] M. S. Hong, S. H. Lee, and S. W. Kim, "Use of KCl aqueous electrolyte for 2 V manganese oxide/activated carbon hybrid capacitor," *Electrochemical and Solid State Letters,* vol. 5, pp. A227-A230, Oct 2002.

[51] D. A. Evans, "High Energy Density Electrlyic-Electrochemical Hybrid Capacitor," Evans Company, East Providence, RI1994.

[52] E. Frackowiak, "Carbon materials for supercapacitor application," *Physical Chemistry Chemical Physics,* vol. 9, pp. 1774-1785, 2007 2007.

[53] P. Simon and A. Burke, "Nanostructured carbons: double-layer capacitance and more," *Electrochemical Society Interface,* vol. 17, pp. 38-43, 2008.

[54] P. Simon and Y. Gogotsi, "Charge storage mechanism in nanoporous carbons and its consequence for electrical double layer capacitors," *Philosophical Transactions of the Royal Society a-Mathematical Physical and Engineering Sciences,* vol. 368, pp. 3457-3467, Jul 2010.

[55] H. Aoki and T. Kariyado, "Pressure Effects and Orbital Characters in Cuprate and Carbon-Based Superconductors," *Journal of Superconductivity and Novel Magnetism,* vol. 27, pp. 995-1001, Apr 2014.

[56] H. Shi, "Activated carbons and double layer capacitance," *Electrochimica Acta,* vol. 41, pp. 1633-1639, Jun 1996.
[57] Y. Zhai, Y. Dou, D. Zhao, P. F. Fulvio, R. T. Mayes, and S. Dai, "Carbon Materials for Chemical Capacitive Energy Storage," *Advanced Materials,* vol. 23, pp. 4828-4850, Nov 9 2011.
[58] M. Inagaki, H. Konno, and O. Tanaike, "Carbon materials for electrochemical capacitors," *Journal of Power Sources,* vol. 195, pp. 7880-7903, Dec 15 2010.
[59] J. Eskusson, A. Janes, A. Kikas, L. Matisen, and E. Lust, "Physical and electrochemical characteristics of supercapacitors based on carbide derived carbon electrodes in aqueous electrolytes," *Journal of Power Sources,* vol. 196, pp. 4109-4116, 2011.
[60] C. R. Perez, S.-H. Yeon, J. Segalini, V. Presser, P.-L. Taberna, P. Simon*, et al.*, "Structure and electrochemical performance of carbide-derived carbon nanopowders," *Advanced Functional Materials,* vol. 23, pp. 1081-1089, 2013.
[61] F. Liu, A. Gutes, I. Laboriante, C. Carraro, and R. Maboudian, "Graphitization of n-type polycrystalline silicon carbide for on-chip supercapacitor application," *Applied Physics Letters,* vol. 99, 2011.
[62] C. Liu and H. M. Cheng, "Carbon nanotubes for clean energy applications," *Journal of Physics D-Applied Physics,* vol. 38, pp. R231-R252, Jul 2005.
[63] V. V. N. Obreja, "On the performance of supercapacitors with electrodes based on carbon nanotubes and carbon activated material - A review," *Physica E-Low-Dimensional Systems & Nanostructures,* vol. 40, pp. 2596-2605, May 2008.
[64] F. Wu and B. Xu, "Progress on the application of carbon nanotubes in supercapacitors," *New Carbon Materials,* vol. 21, pp. 176-184, Jun 2006.
[65] Z. Y. Cao and B. Q. Wei, "A perspective: carbon nanotube macro-films for energy storage," *Energy & Environmental Science,* vol. 6, pp. 3183-3201, Nov 2013.
[66] F. Chaopeng, K. Yafei, H. Zhongyuan, W. Xiao, Y. Yifan, C. Jinhua*, et al.*, "Supercapacitor based on graphene and ionic liquid electrolyte," *Journal of Solid State Electrochemistry,* vol. 15, pp. 2581-5, 12/ 2011.
[67] Y. Wang, Z. Q. Shi, Y. Huang, Y. F. Ma, C. Y. Wang, M. M. Chen*, et al.*, "Supercapacitor Devices Based on Graphene Materials," *Journal of Physical Chemistry C,* vol. 113, pp. 13103-13107, Jul 2009.
[68] X.-m. Chen, G.-h. Wu, Y.-q. Jiang, Y.-r. Wang, and X. Chen, "Graphene and graphene-based nanomaterials: the promising materials for bright future of electroanalytical chemistry," *Analyst,* vol. 136, pp. 4631-4640, 2011 2011.
[69] Y. Huang, J. Liang, and Y. Chen, "An Overview of the Applications of Graphene-Based Materials in Supercapacitors," *Small,* vol. 8, pp. 1805-1834, Jun 25 2012.
[70] M. F. El-Kady, V. Strong, S. Dubin, and R. B. Kaner, "Laser scribing of high-performance and flexible graphene-based electrochemical capacitors," *Science,* vol. 335, pp. 1326-30, 03/16 2012.
[71] L. L. Zhang and X. S. Zhao, "Carbon-based materials as supercapacitor electrodes," *Chemical Society Reviews,* vol. 38, pp. 2520-2531, 2009 2009.
[72] B. Jin, Q. Yan, and Y. Dou, "Materials for energy storage and conversion based on metal oxides," *Recent Patents on Materials Science,* vol. 5, pp. 199-212, 2012.
[73] Y. R. Ahn, C. R. Park, S. M. Jo, and D. Y. Kim, "Enhanced charge-discharge characteristics of Ru O2 supercapacitors on heat-treated Ti O2 nanorods," *Applied Physics Letters,* vol. 90, 2007.
[74] I.-H. Kim, J.-H. Kim, and K.-B. Kim, "Electrochemical characterization of electrochemically prepared ruthenium oxide/carbon nanotube electrode for supercapacitor application," *Electrochemical and Solid-State Letters,* vol. 8, pp. A369-A372, 2005.

[75] S. K. Mondal and N. Munichandraiah, "Anodic deposition of porous RuO2 on stainless steel for supercapacitor studies at high current densities," *Journal of Power Sources,* vol. 175, pp. 657-663, 2008.

[76] Y. Xie and D. Fu, "Supercapacitance of ruthenium oxide deposited on titania and titanium substrates," *Materials Chemistry and Physics,* vol. 122, pp. 23-29, 2010.

[77] K. Armstrong, T. M. Dinh, D. Pech, M. Brunet, J. Gaudet, and D. Guay, "Ruthenium oxide electrodeposition on titanium interdigitated microarrays for energy storage," in *2012 MRS Fall Meeting, November 25, 2012 - November 30, 2012*, Boston, MA, United states, 2013, pp. 265-270.

[78] J. M. Ko, L. Byung Jun, S. R. Sivakkumar, K. Jong Huy, J. Seong Mu, and K. Dong Young, "Carbon nanofibre/hydrous RuO2 nanocomposite electrodes for supercapacitors," *Journal of Power Sources,* vol. 168, pp. 546-52, 06/01 2007.

[79] I.-H. Kim, J.-H. Kim, Y.-H. Lee, and K.-B. Kim, "Synthesis and characterization of electrochemically prepared ruthenium oxide on carbon nanotube film substrate for supercapacitor applications," *Journal of the Electrochemical Society,* vol. 152, pp. A2170-A2178, 2005.

[80] Y. M. Chen, J. H. Cai, Y. S. Huang, K. Y. Lee, and D. S. Tsai, "Preparation and characterization of iridium dioxide-carbon nanotube nanocomposites for supercapacitors," *Nanotechnology,* vol. 22, 2011.

[81] C. Xu, F. Kang, B. Li, and H. Du, "Recent progress on manganese dioxide based supercapacitors," *Journal of Materials Research,* vol. 25, pp. 1421-1432, Aug 2010.

[82] W. Wei, X. Cui, W. Chen, and D. G. Ivey, "Manganese oxide-based materials as electrochemical supercapacitor electrodes," *Chemical Society Reviews,* vol. 40, pp. 1697-1721, 2011 2011.

[83] F.-J. Liu, T.-F. Hsu, and C.-H. Yang, "Construction of composite electrodes comprising manganese dioxide nanoparticles distributed in polyaniline-poly(4-styrene sulfonic acid-co-maleic acid) for electrochemical supercapacitor," *Journal of Power Sources,* vol. 191, pp. 678-683, 2009.

[84] P.-Y. Tang, Y.-Q. Zhao, Y.-M. Wang, and C.-L. Xu, "A metal-decorated nickel foam-inducing regulatable manganese dioxide nanosheet array architecture for high-performance supercapacitor applications," *Nanoscale,* vol. 5, pp. 8156-8163, 2013.

[85] J. Zhang, W. Chu, J. Jiang, and X. S. Zhao, "Synthesis, characterization and capacitive performance of hydrous manganese dioxide nanostructures," *Nanotechnology,* vol. 22, 2011.

[86] C.-Y. Chen, S.-C. Wang, Y.-H. Tien, W.-T. Tsai, and C.-K. Lin, "Hybrid manganese oxide films for supercapacitor application prepared by sol-gel technique," *Thin Solid Films,* vol. 518, pp. 1557-1560, 2009.

[87] S. Isber, E. Majdalani, M. Tabbal, T. Christidis, K. Zahraman, and B. Nsouli, "Study of manganese oxide thin films grown by pulsed laser deposition," *Thin Solid Films,* vol. 517, pp. 1592-1595, 2009.

[88] Y. Dongfang, "Pulsed laser deposition of vanadium-doped manganese oxide thin films for supercapacitor applications," *Journal of Power Sources,* vol. 228, pp. 89-96, 04/15 2013.

[89] C.-K. Lin, K.-H. Chuang, C.-Y. Lin, C.-Y. Tsay, and C.-Y. Chen, "Manganese oxide films prepared by sol-gel process for supercapacitor application," *Surface and Coatings Technology,* vol. 202, pp. 1272-1276, 2007.

[90] Y.-H. Lin, T.-Y. Wei, H.-C. Chien, and S.-Y. Lu, "Manganese oxide/carbon aerogel composite: An outstanding supercapacitor electrode material," *Advanced Energy Materials,* vol. 1, pp. 901-907, 2011.

[91] S. G. Kandalkar, D. S. Dhawale, C.-K. Kim, and C. D. Lokhande, "Chemical synthesis of cobalt oxide thin film electrode for supercapacitor application," *Synthetic Metals,* vol. 160, pp. 1299-1302, 2010.

[92] A. K. Mishra and S. Ramaprabhu, "Ultrahigh arsenic sorption using iron oxide-graphene nanocomposite supercapacitor assembly," *Journal of Applied Physics,* vol. 112, p. 104315 (6 pp.), 11/15 2012.

[93] B. Gao, C.-Z. Yuan, L.-H. Su, L. Chen, and X.-G. Zhang, "Nickel oxide coated on ultrasonically pretreated carbon nanotubes for supercapacitor," *Journal of Solid State Electrochemistry,* vol. 13, pp. 1251-1257, 2009.

[94] C. Jeng-Kuei, L. Ming-Tsung, H. Chiung-Hui, and T. Wen-Ta, "Physicochemical properties and electrochemical behavior of binary manganese-cobalt oxide electrodes for supercapacitor applications," *Materials Chemistry & Physics,* vol. 108, pp. 124-31, 03/15 2008.

[95] D. P. Cai, B. Liu, D. D. Wang, L. L. Wang, Y. Liu, H. Li*, et al.*, "Construction of unique NiCo2O4 nanowire@CoMoO4 nanoplate core/shell arrays on Ni foam for high areal capacitance supercapacitors," *Journal of Materials Chemistry A,* vol. 2, pp. 4954-4960, 2014.

[96] M. Zhi, C. Xiang, J. Li, M. Li, and N. Wu, "Nanostructured carbon-metal oxide composite electrodes for supercapacitors: A review," *Nanoscale,* vol. 5, pp. 72-88, 2013.

[97] Y. J. Ting, K. Lian, and N. Kherani, "Fabrication of Titanium Nitride and Molybdenum Nitride for Supercapacitor Electrode Application," in *Batteries and Energy Technology*. vol. 35, M. C. Smart, A. Manivannan, P. N. Kumta, and S. R. Narayan, Eds., ed Pennington: Electrochemical Society Inc, 2011, pp. 133-139.

[98] D. Choi and P. N. Kumta, "Chemically synthesized nanostructured VN for pseudocapacitor application," *Electrochemical and Solid-State Letters,* vol. 8, pp. A418-A422, 2005.

[99] D. Choi, G. E. Blomgren, and P. N. Kumta, "Fast and reversible surface redox reaction in nanocrystalline vanadium nitride supercapacitors," *Advanced Materials,* vol. 18, pp. 1178-1182, 2006.

[100] X. Zhou, C. Shang, L. Gu, S. Dong, X. Chen, P. Han*, et al.*, "Mesoporous coaxial titanium nitride-vanadium nitride fibers of core-shell structures for high-performance supercapacitors," *ACS Applied Materials and Interfaces,* vol. 3, pp. 3058-3063, 2011.

[101] X. Lu, T. Liu, T. Zhai, G. Wang, M. Yu, S. Xie*, et al.*, "Improving the cycling stability of metal-nitride supercapacitor electrodes with a thin carbon shell," *Advanced Energy Materials,* vol. 4, 2014.

[102] C.-Y. Chen, Z.-Y. Shih, Z. Yang, and H.-T. Chang, "Carbon nanotubes/cobalt sulfide composites as potential high-rate and high-efficiency supercapacitors," *Journal of Power Sources,* vol. 215, pp. 43-47, 2012.

[103] R. Ramachandran, S. Felix, M. Saranya, C. Santhosh, V. Velmurugan, B. P. C. Ragupathy*, et al.*, "Synthesis of cobalt sulfide-graphene (CoS/G) nanocomposites for supercapacitor applications," *IEEE Transactions on Nanotechnology,* vol. 12, pp. 985-990, 2013.

[104] C. K. Chiang, C. R. Fincher, Jr., Y. W. Park, A. J. Heeger, H. Shirakawa, E. J. Louis*, et al.*, "Electrical conductivity in doped polyacetylene," *Physical Review Letters,* vol. 39, pp. 1098-101, 10/24 1977.

[105] C. Arbizzani, M. Mastragostino, and L. Meneghello, "Polymer-based redox supercapacitors: a comparative study," *Electrochimica Acta,* vol. 41, pp. 21-26, 1996.

[106] D. P. Dubal, S. V. Patil, W. B. Kim, and C. D. Lokhande, "Supercapacitors based on electrochemically deposited polypyrrole nanobricks," *Materials Letters,* vol. 65, pp. 2628-31, 2011.

[107] C. A. Amarnath, C. Jin Ho, K. Doyoung, R. S. Mane, H. Sung-Hwan, and S. Daewon, "Electrochemical supercapacitor application of electroless surface polymerization of polyaniline nanostructures," *Materials Chemistry and Physics,* vol. 113, pp. 14-17, 01/15 2009.

[108] A. Laforgue, P. Simon, C. Sarrazin, and J. F. Fauvarque, "Polythiophene-based supercapacitors," in *21st International Power Sources Symposium, 10-12 May 1999*, Switzerland, 1999, pp. 142-8.

[109] S. Patra and N. Munichandraiah, "Supercapacitor studies of electrochemically deposited PEDOT on stainless steel substrate," *Journal of Applied Polymer Science,* vol. 106, pp. 1160-71, 10/15 2007.

[110] Y. Wang and I. Zhitomirsky, "Electrophoretic deposition of manganese dioxide - Multiwalled carbon nanotube composites for electrochemical supercapacitors," *Langmuir,* vol. 25, pp. 9684-9689, 2009.

[111] S. W. Lee, J. Kim, S. Chen, P. T. Hammond, and Y. Shao-Horn, "Carbon nanotube/manganese oxide ultrathin film electrodes for electrochemical capacitors," *ACS Nano,* vol. 4, pp. 3889-3896, 2010.

[112] W. Aming, W. Hailong, Z. Shengyi, M. Changjie, S. Jiming, N. Helin*, et al.*, "Controlled synthesis of nickel sulfide/graphene oxide nanocomposite for high-performance supercapacitor," *Applied Surface Science,* vol. 282, pp. 704-8, 10/01 2013.

[113] S. K. Mondal, K. Barai, and N. Munichandraiah, "High capacitance properties of polyaniline by electrochemical deposition on a porous carbon substrate," *Electrochimica Acta,* vol. 52, pp. 3258-3264, 2007.

[114] R. K. Sharma, A. C. Rastogi, and S. B. Desu, "Manganese oxide embedded polypyrrole nanocomposites for electrochemical supercapacitor," *Electrochimica Acta,* vol. 53, pp. 7690-7695, 2008.

[115] S. R. Sivakkumar, J. M. Ko, D. Y. Kim, B. C. Kim, and G. G. Wallace, "Performance evaluation of CNT/polypyrrole/MnO2 composite electrodes for electrochemical capacitors," *Electrochimica Acta,* vol. 52, pp. 7377-7385, 2007.

[116] C. Z. Meng, C. H. Liu, L. Z. Chen, C. H. Hu, and S. S. Fan, "Highly Flexible and All-Solid-State Paper like Polymer Supercapacitors," *Nano Letters,* vol. 10, pp. 4025-4031, Oct 2010.

[117] D. P. Dubal, S. H. Lee, J. G. Kim, W. B. Kim, and C. D. Lokhande, "Porous polypyrrole clusters prepared by electropolymerization for a high performance supercapacitor," *Journal of Materials Chemistry,* vol. 22, pp. 3044-3052, 2012.

[118] J.-H. Kim, A. K. Sharma, and Y.-S. Lee, "Synthesis of polypyrrole and carbon nano-fiber composite for the electrode of electrochemical capacitors," *Materials Letters,* vol. 60, pp. 1697-1701, 2006.

[119] Y. Hu, Y. Zhao, Y. Li, H. Li, H. Shao, and L. Qu, "Defective super-long carbon nanotubes and polypyrrole composite for high-performance supercapacitor electrodes," *Electrochimica Acta,* vol. 66, pp. 279-286, 2012.

[120] Y. Haijun, W. Jihuai, F. Leqing, H. Sancun, L. Jianming, and H. Miaoliang, "An efficient redox-mediated organic electrolyte for high-energy supercapacitor," *Journal of Power Sources,* vol. 248, pp. 1123-6, 02/15 2014.

[121] O. N. Kalugin, V. V. Chaban, V. V. Loskutov, and O. V. Prezhdo, "Uniform diffusion of acetonitrile inside carbon nanotubes favors supercapacitor performance," *Nano Letters,* vol. 8, pp. 2126-2130, 2008.

[122] H. Yamada, I. Moriguchi, and T. Kudo, "Electric double layer capacitance on hierarchical porous carbons in an organic electrolyte," *Journal of Power Sources,* vol. 175, pp. 651-656, 2008.
[123] P. W. Ruch, M. Hahn, F. Rosciano, M. Holzapfel, H. Kaiser, W. Scheifele*, et al.*, "In situ X-ray diffraction of the intercalation of (C2H5)4N+ and BF4- into graphite from acetonitrile and propylene carbonate based supercapacitor electrolytes," *Electrochimica Acta,* vol. 53, pp. 1074-1082, 2007.
[124] H. Kaneko, Y. Nogami, T. Ishiguro, H. Nishiyama, H. Ishimoto, A. Takahashi*, et al.*, "LOW-TEMPERATURE ELECTRICAL-CONDUCTIVITY OF HIGHLY CONDUCTING IODINE-DOPED POLYACETYLENE," *Synthetic Metals,* vol. 57, pp. 4888-4893, Apr 1993.
[125] J. L. Bredas and G. B. Street, "Polarons, bipolarons, and solitons in conducting polymers," *Accounts of Chemical Research,* vol. 18, pp. 309-315, 1985.
[126] S. Kivelson and A. J. Heeger, "Theory of the soliton-lattice to polaron-lattice transition in conducting polymers," *Synthetic Metals,* vol. 17, pp. 183-188, Jan 1987.
[127] D. Fichou, G. Horowitz, and F. Garnier, "Polaron and bipolaron formation on isolated-model thiophene oligomers in solution," *Synthetic Metals,* vol. 39, pp. 125-131, Oct-Nov 1990.
[128] D. Baeriswyl, "Conducting polymers - solitons or not," *Helvetica Physica Acta,* vol. 56, pp. 639-653, 1983 1983.
[129] A. J. Heeger, "Charge storage in conducting polymers - solitons, polarons, and bipolarons," *Polymer Journal,* vol. 17, pp. 201-208, 1985 1985.
[130] R. Ramya, R. Sivasubramanian, and M. V. Sangaranarayanan, "Conducting polymers-based electrochemical supercapacitors-Progress and prospects," *Electrochimica Acta,* vol. 101, pp. 109-129, Jul 2013.
[131] N. C. Billingham, P. D. Calvert, P. J. S. Foot, and F. Mohammad, "Stability and degradation of some electrically conducting polymers," *Polymer Degradation and Stability,* vol. 19, pp. 323-341, 1987.
[132] C. Pratt, "Conducting polymers," *Kingston University, London,* 1996.
[133] B. Malhotra, "Defects in conducting polymers," *Bulletin of Materials Science,* vol. 10, pp. 85-96, 1988/03/01 1988.
[134] J. Bargon, S. Mohmand, and R. J. Waltman, "Electrochemical synthesis of electrically conducting polymers from aromatic compounds," *IBM Journal of Research and Development,* vol. 27, pp. 330-41, 07/ 1983.
[135] D. E. Labaye, C. Jerome, V. M. Geskin, P. Louette, R. Lazzaroni, L. Martinot*, et al.*, "Full electrochemical synthesis of conducting polymer films chemically grafted to conducting surfaces," *Langmuir,* vol. 18, pp. 5222-5230, 2002.
[136] H. Chang, Y. Chunhe, and L. Yongfang, "Chemical synthesis of coral-like nanowires and nanowire networks of conducting polypyrrole," *Synthetic Metals,* vol. 139, pp. 539-45, 2003.
[137] P. Soudan, H. Hoang Anh, L. Breau, and D. Belanger, "Chemical synthesis and electrochemical properties of poly(cyano-substituted-diheteroareneethylene) as conducting polymers for electrochemical supercapacitors," *Journal of the Electrochemical Society,* vol. 148, pp. 775-82, 07/ 2001.
[138] J. Jiang and A. Kucernak, "Electrochemical supercapacitor material based on manganese oxide: preparation and characterization," *Electrochimica Acta,* vol. 47, pp. 2381-2386, 2002.
[139] J. Zhao, Z. Tao, J. Liang, and J. Chen, "Facile synthesis of nanoporous γ-MnO2 structures and their application in rechargeable Li-ion batteries," *Crystal Growth and Design,* vol. 8, pp. 2799-2805, 2008.

[140] H. S. Xia, G. H. Qiu, and Q. Wang, "Polymer/carbon nanotube composite emulsion prepared through ultrasonically assisted in situ emulsion polymerization," *Journal of Applied Polymer Science,* vol. 100, pp. 3123-3130, May 2006.

[141] R. van den Schoor, R. H. M. van de Leur, and J. H. W. de Wit, "Synthesis of a polypyrrole film on a non-conducting substrate; the influence of the oxidant and acid concentration," *Synthetic Metals,* vol. 99, pp. 17-20, Jan 1999.

[142] J. Jang and J. H. Oh, "A facile synthesis of polypyrrole nanotubes using a template-mediated vapor deposition polymerization and the conversion to carbon nanotubes," *Chemical Communications,* pp. 882-883, Apr 2004.

[143] T. V. Vernitskaya and O. N. Efimov, "Polypyrrole: A conducting polymer (synthesis, properties, and applications)," *Uspekhi Khimii,* vol. 66, pp. 489-505, 1997.

[144] L. J. Pan, H. Qiu, C. M. Dou, Y. Li, L. Pu, J. B. Xu*, et al.*, "Conducting Polymer Nanostructures: Template Synthesis and Applications in Energy Storage," *International Journal of Molecular Sciences,* vol. 11, pp. 2636-2657, Jul 2010.

[145] S. Sadki, P. Schottland, N. Brodie, and G. Sabouraud, "The mechanisms of pyrrole electropolymerization," *Chemical Society Reviews,* vol. 29, pp. 283-293, Sep 2000.

[146] P. C. Wang and J. Y. Yu, "Dopant-dependent variation in the distribution of polarons and bipolarons as charge-carriers in polypyrrole thin films synthesized by oxidative chemical polymerization," *Reactive & Functional Polymers,* vol. 72, pp. 311-316, May 2012.

[147] Y. S. Lim, Y. P. Tan, H. N. Lim, N. M. Huang, W. T. Tan, M. A. Yarmo*, et al.*, "Potentiostatically deposited polypyrrole/graphene decorated nano-manganese oxide ternary film for supercapacitors," *Ceramics International,* vol. 40, pp. 3855-3864, Apr 2014.

[148] J. I. Martins, L. Diblikova, M. Bazzaoui, and M. C. Nunes, "Polypyrrole Coating Doped with Dihydrogenophosphate Ion to Protect Aluminium Against Corrosion in Sodium Chloride Medium," *Journal of the Brazilian Chemical Society,* vol. 23, pp. 377-384, Mar 2012.

[149] A. G. Porras-Gutierrez, B. A. Frontana-Uribe, S. Gutierrez-Granados, S. Griveau, and F. Bedioui, "In situ characterization by cyclic voltammetry and conductance of composites based on polypyrrole, multi-walled carbon nanotubes and cobalt phthalocyanine," *Electrochimica Acta,* vol. 89, pp. 840-847, Feb 2013.

[150] R. K. Sharma, A. C. Rastogi, and S. B. Desu, "Pulse polymerized polypyrrole electrodes for high energy density electrochemical supercapacitor," *Electrochemistry Communications,* vol. 10, pp. 268-272, Feb 2008.

[151] H. Karami and A. R. Nezhad, "Investigation of Pulse-Electropolymerization of Conductive Polypyrrole Nanostructures," *International Journal of Electrochemical Science,* vol. 8, pp. 8905-8921, Jun 2013.

[152] J. Zhang, L. B. Kong, H. Li, Y. C. Luo, and L. Kang, "Synthesis of polypyrrole film by pulse galvanostatic method and its application as supercapacitor electrode materials," *Journal of Materials Science,* vol. 45, pp. 1947-1954, Apr 2010.

[153] K. West, T. Jacobsen, B. Zachauchristiansen, M. A. Careem, and S. Skaarup, "Electrochemical synthesis of polypyrrole - influence of current-density on structure," *Synthetic Metals,* vol. 55, pp. 1412-1417, Mar 1993.

[154] Y. P. Fang, J. W. Liu, D. J. Yu, J. P. Wicksted, K. Kalkan, C. O. Topal*, et al.*, "Self-supported supercapacitor membranes: Polypyrrole-coated carbon nanotube networks enabled by pulsed electrodeposition," *Journal of Power Sources,* vol. 195, pp. 674-679, Jan 2010.

[155] U. Johanson, A. Marandi, T. Tamm, and J. Tamm, "Comparative study of the behavior of anions in polypyrrole films," *Electrochimica Acta,* vol. 50, pp. 1523-1528, Feb 2005.

[156] S. U. Rahman and M. S. Ba-Shammakh, "Thermal effects on the process of electropolymerization of pyrrole on mild steel," *Synthetic Metals,* vol. 140, pp. 207-223, Feb 2004.
[157] S. Asavapiriyanont, G. K. Chandler, G. A. Gunawardena, and D. Pletcher, "The electrodeposition of polypyrrole films from aqueous-solutions," *Journal of Electroanalytical Chemistry,* vol. 177, pp. 229-244, 1984.
[158] K. Shi and I. Zhitomirsky, "Influence of current collector on capacitive behavior and cycling stability of Tiron doped polypyrrole electrodes," *Journal of Power Sources,* vol. 240, pp. 42-49, 2013.
[159] J. Li, H. Q. Xie, and Y. Li, "Fabrication of graphene oxide/polypyrrole nanowire composite for high performance supercapacitor electrodes," *Journal of Power Sources,* vol. 241, pp. 388-395, Nov 2013.
[160] S. Rapi, V. Bocchi, and G. P. Gardini, "Conducting polypyrrole by chemical synthesis in water," *Synthetic Metals,* vol. 24, pp. 217-221, May 1988.
[161] Y. Kudoh, "Properties of polypyrrole prepared by chemical polymerization using aqueous solution containing Fe-2(SO4)(3) and anionic surfactant," *Synthetic Metals,* vol. 79, pp. 17-22, Apr 1996.
[162] C. F. Zhou, S. Kumar, C. D. Doyle, and J. M. Tour, "Functionalized single wall carbon nanotubes treated with pyrrole for electrochemical supercapacitor membranes," *Chemistry of Materials,* vol. 17, pp. 1997-2002, Apr 2005.
[163] Z. H. Zhou, N. C. Cai, and Y. H. Zhou, "Capacitive of characteristics of manganese oxides and polyaniline composite thin film deposited on porous carbon," *Materials Chemistry and Physics,* vol. 94, pp. 371-375, Dec 2005.
[164] V. Khomenko, E. Frackowiak, and F. Beguin, "Determination of the specific capacitance of conducting polymer/nanotubes composite electrodes using different cell configurations," *Electrochimica Acta,* vol. 50, pp. 2499-2506, Apr 2005.
[165] H. S. Xia, Q. Wang, and G. H. Qiu, "Polymer-encapsulated carbon nanotubes prepared through ultrasonically initiated in situ emulsion polymerization," *Chemistry of Materials,* vol. 15, pp. 3879-3886, Oct 2003.
[166] S. H. Hong, B. H. Kim, J. Joo, J. W. Kim, and H. J. Choi, "Polypyrrole-montmorillonite nanocomposites synthesized by emulsion polymerization," *Current Applied Physics,* vol. 1, pp. 447-450, Dec 2001.
[167] B. Weng, R. Shepherd, J. Chen, and G. G. Wallace, "Gemini surfactant doped polypyrrole nanodispersions: an inkjet printable formulation," *Journal of Materials Chemistry,* vol. 21, pp. 1918-1924, 2011.
[168] Y. Yang, C. Wang, S. Ashraf, and G. G. Wallace, "Polypyrrole doped with redox-active poly (2-methoxyaniline-5-sulfonic acid) for lithium secondary batteries," *RSC Advances,* vol. 3, pp. 5447-5452, 2013.
[169] L. Qie, L. X. Yuan, W. X. Zhang, W. M. Chen, and Y. H. Huang, "Revisit of Polypyrrole as Cathode Material for Lithium-Ion Battery," *Journal of the Electrochemical Society,* vol. 159, pp. A1624-A1629, 2012.
[170] K. Y. Shi and I. Zhitomirsky, "Polypyrrole nanofiber-carbon nanotube electrodes for supercapacitors with high mass loading obtained using an organic dye as a co-dispersant," *Journal of Materials Chemistry A,* vol. 1, pp. 11614-11622, 2013.
[171] Y. L. Zhu and I. Zhitomirsky, "Influence of dopant structure and charge on supercapacitive behavior of polypyrrole electrodes with high mass loading," *Synthetic Metals,* vol. 185, pp. 126-132, Dec 2013.

[172] M. Han, Y. Chu, D. Han, and Y. Liu, "Fabrication and characterizations of oligopyrrole doped with dodecylbenzenesulfonic acid in reverse microemulsion," *Journal of Colloid and Interface Science,* vol. 296, pp. 110-117, 2006.

[173] K. Shi and I. Zhitomirsky, "Fabrication of Polypyrrole-Coated Carbon Nanotubes Using Oxidant-Surfactant Nanocrystals for Supercapacitor Electrodes with High Mass Loading and Enhanced Performance," *ACS Applied Materials & Interfaces,* vol. 5, pp. 13161-13170, 2014/01/12 2013.

[174] Y. Gogotsi and P. Simon, "True Performance Metrics in Electrochemical Energy Storage," *Science,* vol. 334, pp. 917-918, November 18, 2011 2011.

[175] D. K. Ariyanayagamkumarappa and I. Zhitomirsky, "Electropolymerization of polypyrrole films on stainless steel substrates for electrodes of electrochemical supercapacitors," *Synthetic Metals,* vol. 162, pp. 868-872, 2012.

[176] Y. Zhu, K. Shi, and I. Zhitomirsky, "Polypyrrole coated carbon nanotubes for supercapacitor devices with enhanced electrochemical performance," *Journal of Power Sources,* vol. 268, pp. 233-239, 2014.

[177] Y. Zhu, K. Shi, and I. Zhitomirsky, "Anionic dopant–dispersants for synthesis of polypyrrole coated carbon nanotubes and fabrication of supercapacitor electrodes with high active mass loading," *Journal of Materials Chemistry A,* vol. 2, pp. 14666-14673, 2014.

[178] T. Qian, X. Zhou, C. Yu, S. Wu, and J. Shen, "Highly dispersed carbon nanotube/polypyrrole core/shell composites with improved electrochemical capacitive performance," *J. Mater. Chem. A,* vol. 1, pp. 15230-15234, 2013.

[179] H. Carpio, E. Galeazzi, R. Greenhouse, A. Guzman, E. Velarde, Y. Antonio*, et al.*, "Synthesis of 1,2-dihydro-3h-pyrrolo 1,2-a pyrrole-1-carboxylic acids and homologous pyridine and azepine analogs thereof," *Canadian Journal of Chemistry-Revue Canadienne De Chimie,* vol. 60, pp. 2295-2312, 1982.

[180] S. Palaniappan, S. B. Sydulu, and P. Srinivas, "Synthesis of copolymer of aniline and pyrrole by inverted emulsion polymerization method for supercapacitor," *Journal of Applied Polymer Science,* vol. 115, pp. 1695-1701, 2010.

[181] J.-F. Lu, L. Wang, Q.-Y. Lai, H.-Y. Chu, and Y. Zhao, "Study of capacitive properties in supercapacitor for copolymer of aniline with m-phenylenediamine," *Journal of Solid State Electrochemistry,* vol. 13, pp. 1803-1810, 2009/12/01 2009.

[182] D. P. Dubal, S. V. Patil, G. S. Gund, and C. D. Lokhande, "Polyaniline–polypyrrole nanograined composite via electrostatic adsorption for high performance electrochemical supercapacitors," *Journal of Alloys and Compounds,* vol. 552, pp. 240-247, 3/5/ 2013.

[183] Y. W. Chen-Yang, J. L. Li, T. L. Wu, W. S. Wang, and T. F. Hon, "Electropolymerization and electrochemical properties of (N-hydroxyalkyl)pyrrole/pyrrole copolymers," *Electrochimica Acta,* vol. 49, pp. 2031-2040, May 2004.